

**NONLINEAR CONTROLLER SYNTHESIS FOR COMPLEX
CHEMICAL AND BIOCHEMICAL REACTION SYSTEMS**

BY

SOPHIE LEISING

A THESIS

SUBMITTED TO THE FACULTY OF

WORCESTER POLYTECHNIC INSTITUTE

IN PARTIAL FULFILLMENT OF THE REQUIREMENTS FOR THE DEGREE OF

MASTER OF SCIENCE

CHEMICAL ENGINEERING

APPROVED

NIKOLAOS KAZANTZIS , Ph.D., ADVISOR
ASSISTANT PROFESSOR OF CHEMICAL ENGINEERING
WORCESTER POLYTECHNIC INSTITUTE

DAVID DIBIASIO , Ph.D., HEAD OF DEPARTMENT
ASSOCIATE PROFESSOR OF CHEMICAL ENGINEERING
WORCESTER POLYTECHNIC INSTITUTE

SPRING 2005

TABLE OF CONTENTS

TABLE OF CONTENTS.....	2
LIST OF FIGURES.....	4
LIST OF TABLES.....	5
ACKNOWLEDGMENTS.....	6
ABSTRACT	7
1 INTRODUCTION TO NONLINEAR PROCESS CONTROL: THE CONTINUOUS-TIME AND IN DISCRETE-TIME CASES	8
2 NONLINEAR CONTROL TECHNIQUES FOR HIV CHEMOTHERAPY OPTIMIZATION	13
.....	13
2.1 PROBLEM OVERVIEW.....	13
2.2 CURRENT HIV DRUG CHEMOTHERAPY PROTOCOLS	15
2.2.1 <i>HIV life cycle</i>	15
2.2.2 <i>Currently administered antiretroviral drugs</i>	17
2.2.3 <i>HIV modeling</i>	19
2.2.4 <i>Side effects modeling</i>	23
2.2.5 <i>Side effect mechanisms</i>	23
2.2.5.1 <i>Mitochondrial toxicity</i>	23
2.2.5.2 <i>Lipodystrophy syndrome</i>	24
2.2.5.3 <i>Hypersensitivity</i>	24
2.2.5.4 <i>Bone marrow suppression</i>	24
2.2.6 <i>Model for side effects affecting the liver</i>	25
2.2.7 <i>Pharmacokinetics models</i>	26
2.3 OPTIMIZATION METHOD DESCRIPTION.....	29
2.3.1 <i>Lie derivatives</i>	30
2.3.2 <i>Relative degree</i>	30
2.3.3 <i>Description of the control law</i>	32
2.4 DERIVATION OF THE MODEL OPTIMIZATION EQUATIONS.....	36
2.4.1 <i>Optimization A</i>	36
2.4.2 <i>Optimization B</i>	37
2.5 SIMULATIONS	39
2.5.1 <i>Behavior of HIV model with therapy optimization</i>	40
2.5.1.1 <i>Influence of the parameters p and γ</i>	40
2.5.1.2 <i>Saturation function : $0 \leq u \leq 1$</i>	43
2.5.1.3 <i>Saturation function: $0.3 \leq u \leq 0.9$</i>	44
2.6 CONCLUSIONS	47
2.7 DISCUSSION.....	50
REFERENCES	52
NOMENCLATURE	54

3	NONLINEAR DIGITAL CONTROL SYSTEMS FOR COMPLEX CHEMICAL PROCESSES.....	56
3.1	INTRODUCTION.....	56
3.2	MATHEMATICAL PRELIMINARIES.....	58
3.2.1	<i>Euler discretization</i>	59
3.2.2	<i>Quadratic Lyapunov function</i>	60
3.2.3	<i>Zubov's method</i>	61
3.2.3.1	Existence and uniqueness of solution.....	62
3.2.3.2	Solution method.....	62
3.2.3.3	Local positive-definiteness of the solution $V(x)$	64
3.2.4	<i>Quadratic estimates of the stability region</i>	65
3.3	FORMULATION OF THE ENERGY-PREDICTIVE CONTROL PROBLEM AND DERIVATION OF THE CONTROL LAW.....	66
3.4	PROPERTIES OF THE CONTROL LAW.....	71
3.4.1	<i>Continuity property</i>	71
3.4.2	<i>Equilibrium properties of the closed-loop system</i>	71
3.4.3	<i>Local asymptotic stability of the closed-loop system</i>	72
3.4.4	<i>Enlargement of the stability region in closed-loop</i>	73
3.4.5	<i>Synthesis of a dynamic output feedback controller</i>	75
3.5	ILLUSTRATIVE EXAMPLE I: VAN DE VUSSE REACTION IN A CSTR.....	77
3.5.1	<i>Open-loop Responses</i>	79
3.5.2	<i>Estimation of the stability region size:</i>	81
3.5.3	<i>Closed-loop Responses: The effect of the controller parameters a^2 and p^2</i>	82
3.5.4	<i>Results obtained using Zubov's method</i>	86
3.6	ILLUSTRATIVE EXAMPLE II: A BIOLOGICAL REACTOR.....	89
3.6.1	<i>Open-loop Responses</i>	91
3.6.2	<i>Results obtained using Zubov's method</i>	92
3.7	CONCLUSIONS.....	96
	NOMENCLATURE.....	97
	REFERENCES.....	99
	APPENDICES.....	102
	MAPLE CODE FOR THE VAN DE VUSSE EXAMPLE.....	102
	MAPLE CODE FOR THE BIOLOGICAL REACTOR EXAMPLE.....	105

LIST OF FIGURES

FIGURE 1: BASIC CONCEPT OF MODEL PREDICTIVE CONTROL	10
FIGURE 2.1: HIV LIFE CYCLE	16
FIGURE 2.2 : HIV DYNAMICS WITH NO THERAPY APPLIED	22
FIGURE 2.3 : SIMULATION FOR NORMAL AZT TREATMENT REGIMEN	29
FIGURE 2.4: COMPARISON OF OPTIMIZATIONS A AND B FOR VARYING VALUES OF P AT γ =100.	41
FIGURE 2.5: COMPARISON OF OPTIMIZATIONS A AND B FOR VARYING VALUES OF γ AT P =200.	42
FIGURE 2.6: COMPARISON OF OPTIMIZATIONS A AND B FOR $0 \leq U \leq 1$	44
FIGURE 2.7: COMPARISON OF OPTIMIZATIONS A AND B FOR DIFFERENT SATURATION FUNCTIONS.	46
FIGURE 3.1 : ALTERNATIVE APPROACHES FOR THE DESIGN OF DIGITAL CONTROL SYSTEMS.	57
FIGURE 3.2: MODEL STATE FEEDBACK CONTROLLER	77
FIGURE 3.3. : OPEN-LOOP RESPONSE: CHECK FOR THE SAMPLING PERIOD OF THE DISCRETIZATION	80
FIGURE 3.4: VARIATION OF THE SIZE OF THE STABILITY REGION WITH R.	82
FIGURE 3.5: CLOSED-LOOP RESPONSES FOR DIFFERENT VALUES OF a^2 AND p^2	84
FIGURE 3.6: COMPARISON BETWEEN TWO CONTROLLERS: WITH AND WITHOUT INPUT CONSTRAINTS	85
FIGURE 3.7: INFLUENCE OF THE SATURATION FUNCTION ON THE PERFORMANCE CHARACTERISTICS.....	86
FIGURE 3.8: ESTIMATES OF THE STABILITY REGION AS R VARIES FOR THE 4 TH ORDER APPROXIMATION OF V	87
FIGURE 3.9: STABILITY REGION SIZE ESTIMATES FOR DIFFERENT ORDERS OF THE TAYLOR APPROXIMATION OF V	87
FIGURE 3.10: COMPARISON OF THE RESULTS OBTAINED FOR DIFFERENT ORDERS OF THE TAYLOR APPROXIMATION OF V	88
FIGURE 3.11: OPEN-LOOP RESPONSE: CHECK FOR THE SAMPLING PERIOD OF THE DISCRETIZATION	91
FIGURE 3.12: COMPARISON OF THE RESULTS OBTAINED FOR DIFFERENT TRUNCATION ORDERS OF THE TAYLOR SERIES APPROXIMATION OF V	94

LIST OF TABLES

TABLE 2.1 : LIST OF ANTIRETROVIRAL MEDICATIONS AND THEIR GENERIC AND TRADE NAMES.	18
TABLE 2.2: PARAMETERS USED FOR HIV DYNAMICS MODEL.....	21
TABLE 2.3: PARAMETERS USED FOR SIDE EFFECTS MODEL	25
TABLE 2.3: PARAMETERS USED FOR PHARMACOKINETICS MODEL.....	28
TABLE 3.1: NUMERICAL VALUES OF THE VAN DE VUSSE REACTION IN A CSTR	80
TABLE 3.2: NUMERICAL VALUES OF THE BIOREACTOR EXAMPLE.....	92

ACKNOWLEDGMENTS

In this section, I would like to thank all the people who were with me during my journey at Worcester Polytechnic Institute.

First of all, I would like to thank my advisor, Prof Nikolaos Kazantzis for his guidance, patience and enthusiasm concerning this work. I will always appreciate his continuous support and understanding throughout my stay at WPI.

Next I would like to thank all the faculty and staff from the Chemical Engineering Department at Worcester Polytechnic Institute, and especially Sandra Natale for the many chats we had about various things.

I also thank the Ecole Nationale Supérieure des Industries Chimiques (ENSIC), Nancy, FRANCE, for the opportunity which was given to me to pursue my degree abroad. This opportunity definitely changed my life.

I would also like to thank WPI in general and Prof Camesano for the financial supports.

I would like to thank all my friends at WPI. They helped me through this journey and I had an enjoyable time in Worcester with them.

Last but not least; I would like to thank my family: my parents, my sister, her husband and my lovely niece, and my husband. They have always been there for me and I want to thank them for all the love, trust, support, and encouragement. Their great influence made me who I am today. They also stood beside me for some of the big decisions that I had to make during my stay at WPI.

I had to face educational challenges as well as important life decisions, these last two years helped me into my transformation from a child to grown up person.

NONLINEAR CONTROLLER SYNTHESIS FOR COMPLEX CHEMICAL AND BIOCHEMICAL REACTION SYSTEMS

ABSTRACT

The present research study is comprised of two main parts.

The first part aims at the development of a systematic system-theoretic framework that allows the derivation of optimal chemotherapy protocols for HIV patients. The proposed framework is conceptually aligned with a notion of continuous-time model predictive control of nonlinear dynamical systems, and results in an optimal way to control viral replication, while maintaining low antiretroviral drug toxicity levels. This study is particularly important because it naturally integrates powerful system-theoretic techniques into a clinically challenging problem with worldwide implications, namely the one of developing chemotherapy patterns for HIV patients that are effective and do not induce adverse side-effects.

The second part introduces a new digital controller design methodology for nonlinear (bio)chemical processes, that reflects contemporary necessities in the practical implementation of advanced process control strategies via digital computer-based algorithms. The proposed methodology relies on the derivation of an accurate sampled-data representation of the process, and the subsequent formulation and solution to a nonlinear digital controller synthesis problem. In particular, for the latter two distinct approaches are followed that are both based on the methodological principles of Lyapunov design and rely on a short-horizon model-based prediction and optimization of the rate of “energy dissipation” of the system, as it is realized through the time derivative of an appropriately selected Lyapunov function. First, the Lyapunov function is computed by solving the discrete Lyapunov matrix equation. In the second approach however, it is computed by solving a Zubov-like functional equation based on the system’s drift vector field. Finally, two examples of a chemical and a biological reactor that both exhibit nonlinear behavior illustrate the main features of the proposed digital controller design method.

1 INTRODUCTION TO NONLINEAR PROCESS CONTROL: THE CONTINUOUS-TIME AND IN DISCRETE-TIME CASES

In the field of chemical engineering, most physical and chemical processes exhibit complex nonlinear behavior, as it is commonly the case for chemical or biochemical reactors, distillation columns, separation units, etc. Traditionally however, to control the operation of a chemical process system, a linear process model, obtained either through linearization or direct identification methods, is typically used as the basis for the development of the associated control law. (Corriou, 1996). As a result, new stringent performance requirements for tighter control imposed on the majority of processes, spawned extensive research efforts for the development of nonlinear process control strategies and algorithms that could directly cope with process complexity and nonlinearities. Among the different techniques currently available for nonlinear process control, the one whose main principles will be adopted in the present study, is a continuous-time model predictive approach, that leads to the explicit and analytical derivation of nonlinear control laws for open-loop stable, single-input single-output processes in the presence of input constraints (Soroush and Kravaris, 1996). The methodology developed by Soroush and Kravaris was even applicable for processes with deadtime, but here, we will only focus on the minimization of a quadratic performance index in the presence of input constraints and penalty on the controller action in the derivation of the model predictive control law. Please notice that one major contributor to the success of model predictive control is the ability to handle constraints (Bequette, 2003). As stated earlier, a key feature of the derived model predictive control law is that the intuitive optimization problem has an explicit analytical solution with interesting properties.

Model predictive control techniques are based on the explicit use of a process model for the prediction of the future trend of the process behavior, and the calculation of a sequence of controller actions, minimizing a desirable performance index over a certain time horizon (Soroush and Kravaris, 1996). Because of model errors or process

disturbances, there is a deterioration of the quality of the output prediction as the prediction horizon becomes larger. There is also a significant computational effort, needed to solve numerically the optimization problem online, especially for the case of large horizons. In view of these considerations, Soroush and Kravaris sought a simple output-prediction equation, that explicitly captures the effect of the manipulated variable u on the controlled variable y , while maintaining satisfactory accuracy in the nonlinear regime.

The first part of the thesis is the application of this methodology to an important societal problem. As the understanding of the biochemical and biological Human Immunodeficiency Virus (HIV) advances, researchers are able to develop better antiretroviral medications, which have substantially improved life expectancy for HIV infected patients. However, current anti-HIV drugs do not completely eradicate the virus, but slow its course thanks to long periods of treatment (*AIDSInfo*, 2004, Johns Hopkins University Division of Infectious Diseases and AIDS Service, 1999). Continuous administration of antiretroviral drugs leads to serious drug toxicity, resulting in forced therapy ceased, and consequent viral rebound (Carr and Cooper, 2000).

The problem of developing optimal chemotherapy protocols in the presence of side-effects and toxicity constraints is formulated and solved based on a continuous-time model predictive approach for nonlinear systems, similar in spirit to the one developed by Soroush and Kravaris.

This chapter is subdivided into sub-sections that first enable the reader to become familiar with the mechanism of HIV viral replication and drug therapy before simulating the optimal drug dosage dictated by the control law derived.

The second part of the thesis rests on the same theoretic ideas, but is developed in the discrete time domain, since the primary focus is the systematic development of a nonlinear digital controller synthesis method that can be algorithmically implemented in practice with the aid of a computer. It has to be pointed out that another interesting feature of model predictive control is that is inherently suitable for digital applications in the discrete-time domain (Bequette, 2003). Indeed, at each time step, k , the optimization

problem is solved. A quadratic objective function based on output predictions over a prediction horizon of P time steps is minimized by a selection of manipulated variables moves over a control horizon of M control moves, as shown on Figure 1.

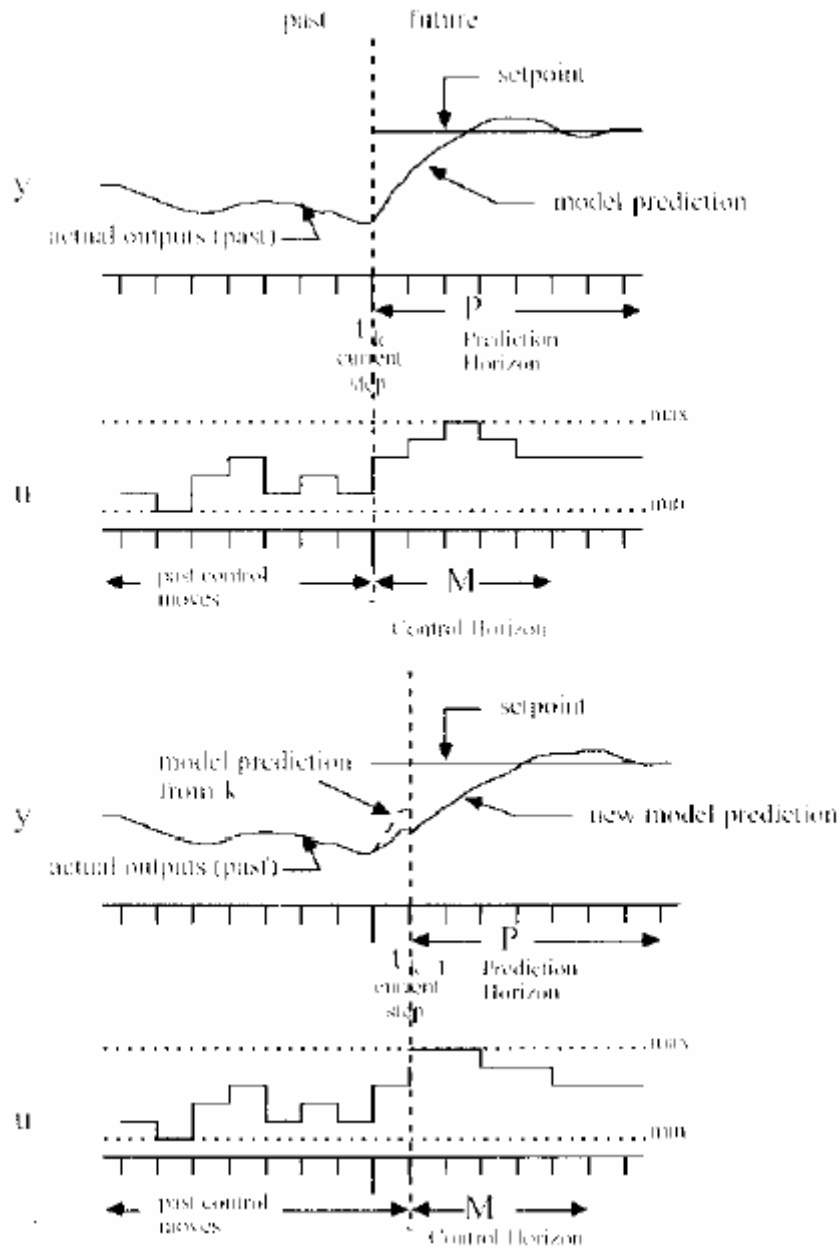


Figure 1: Basic concept of model predictive control

(from Process Control: modeling, design and simulation, B.W. Bequette, 2003)

After u_k is implemented, the measurement at the next time-step, y_{k+1} is obtained. Corrections for error can be performed, in case the measured output is different from the model predicted value. A new optimization problem is then solved, again (Bequette, 2003). However, models used for calculating the predicted values of the process outputs limit its applications to open-loop stable processes (Bequette, 2003).

The approach typically followed for the design of a digital controller is to obtain a discrete-time process model (sampled-data representation) from a continuous-time model, and then, synthesize a discrete-time controller (Franklin et al. ,1992, Soroush and Kravaris, 1992, Hernandez and Arkun, 1993). Due to the difficulty of exactly computing the matrix exponential that generates the exact discrete-time model, an approximate discrete-time process is chosen most of the time (Nešić, Teel and Kokotović, 1999). The discretization procedure should possess the following characteristics: simplicity, convergence (convergence of the approximate solution to the exact solution of the differential equation) and stability (avoidance of possible error propagation along the sequence of time steps). Standard numerical simulations methods like Euler or Runge-Kutta meet these criteria, as long as the time-step of the algorithm remains small compared to the fastest time constant of the original continuous-time process model. (Kazantzis and Kravaris, 1999)

Here we will use the Euler discretization method for the original continuous-time process model to get the approximate discrete-time process model. The popularity of Euler approximate discrete-time modeling techniques for digital controller design is primarily due to the fact that it is the simplest approximate model that preserves the structure of the continuous-time model (Nešić and Teel, 2004). This however requires fast sampling, which can eventually become a problem since it may lead to nonminimum-phase behavior in discrete-time. On the other end of the sampling spectrum, large sampling periods may arise in many industrial control problems as either a technical or physical limitation on the system under consideration (Kazantzis and Kravaris, 1999, Nešić and Teel, 2004).

In the present study, two approaches for the derivation of a nonlinear control law that can be digitally implemented are presented, both based on the methodological principles of Lyapunov design and relying on a short-horizon model-based prediction and optimization of the rate of “energy dissipation” of the system, as it is realized through the time derivative of an appropriately selected Lyapunov function. First, the Lyapunov function is computed by solving the discrete Lyapunov matrix equation (in a discrete-time analogy of Kazantzis and Kravaris, 1999). In the second approach, it is computed by solving a Zubov-like functional equation based on the system’s drift vector field (in a discrete-time analogy of Dubljević and Kazantzis, 2002). The latter becomes particularly important because it enhances convergence properties and accuracy, especially in the case of highly nonlinear systems, or large sampling periods due to inherent process limitations. Indeed, this objective can be attained by increasing the truncation order of the Taylor series expansion of the Lyapunov function solution to the above Zubov-like functional equation.

Finally, two examples of chemical reaction systems exhibiting nonlinear behavior are considered to illustrate the main aspects of the proposed approach.

2 NONLINEAR CONTROL TECHNIQUES FOR HIV CHEMOTHERAPY OPTIMIZATION

2.1 Problem overview

Currently, Highly Active AntiRetroviral Therapy (HAART) does not eradicate the HIV virus, but only slows the course of the disease by preventing virus replication. However, maintaining high drug dosages for long periods of time is not the best strategy. Prolonged periods of continuous drug therapy is rarely experienced by patients undergoing HAART. Furthermore, discontinuation of treatment is triggered by adverse side effects prompted by antiretroviral drug administration and a majority of patients well tolerates minor side effects (*AIDSInfo*, 2004). However, some side effects which have unbearable physical and psychological implications on a patient's life have been present in a small but significant percentage of patients. These conditions include, but are not limited to, lipodystrophy, insulin resistance (and in extreme cases, diabetes), osteopenia, lactic acidemia and other metabolic complications, as it will be discussed later (Carr and Cooper, 2000, Highleyman, 1998).

Quite a few strategies have been developed to deal with the aforementioned problem of drug toxicity. One of them is to treat particular side effects' symptoms with additional medications. This approach however, imposes the drug burden on patients.

Other types of strategies include the method of Structured Treatment Interruption (STI): a strategy based on periodic on-off HAART periods, as well as new schemes involving Therapeutic Drug level Monitoring (TDM) (Velez Vega, 2002).

The proposed approach developed here offers a systematic framework for the development of a comprehensive drug administration policy. This is realized through the formulation and solution of a chemotherapy optimization problem: maximization of the

benefits of therapy ($CD4^+$ T Cells count increases and viral load decrease) and minimization of its adverse effects.

The drug dosage optimization problem is formulated and solved in accordance to the methodology of a continuous-time model predictive control framework for nonlinear systems (Soroush and Kravaris ,1996).

By using an appropriate model for viral load, immune system response and side effects behavior, an optimized chemotherapy scheme is presented based on a quadratic output function (or map) which represents a maximization of the total number of healthy T cells and liver cells.

This formulation of the optimization problem enhances the requirements of rapid regulation of the output towards the attainment of the target values for T and liver cells, while also penalizing aggressive chemotherapy patterns.

The solution of this optimization problem consists of an expression for the “optimal” chemotherapy strategy.

At this point, it would be methodologically appropriate to provide some information about HIV and the currently implemented treatment strategies in clinical practice.

2.2 Current HIV drug chemotherapy protocols

The acquired immunodeficiency syndrome (AIDS) is the term given to the most advanced stages of HIV infection. HIV gradually kills T cells, and results in a weakened immune system. The individual is then subject to opportunistic infections caused by other viruses or bacteria, which by themselves result in aggravated illnesses that lead to death. (*AIDSInfo*, 2004).

2.2.1 HIV life cycle

The HIV mechanism of infection is complex, and what follows is a summary of the relevant literature, especially from the Johns Hopkins University Division of Infectious Diseases and AIDS Service (1999) and *AIDSInfo* (2004).

HIV begins its infection of a susceptible host cell by binding to the CD4 receptor on the host cell, and then fuses to the cell. CD4 is present on the surface of many lymphocytes, which are a critical part of the body's immune system.

Once fusion takes place, HIV enters the cell by injecting a single stranded RNA, which is converted into double stranded DNA by reverse transcription. An enzyme in HIV called reverse transcriptase is necessary to catalyze this conversion of viral RNA into DNA.

After entering the host's nucleus, this viral DNA can be integrated into the genetic material of the cell with the aid of the integrase enzyme.

Activation of the host cells results in the transcription of viral DNA into messenger RNA (mRNA), which is then translated into viral proteins. The new viral RNA forms the genetic material of the next generation of viruses.

The viral RNA and synthesized protein chains associate at the cell membrane and form an immature virus.

Following assembly at the cell surface, the virus then buds forth from the cell and is released to infect another cell, after having been rendered completely functional with the help of the protease enzyme, which cuts chains into specific proteins.

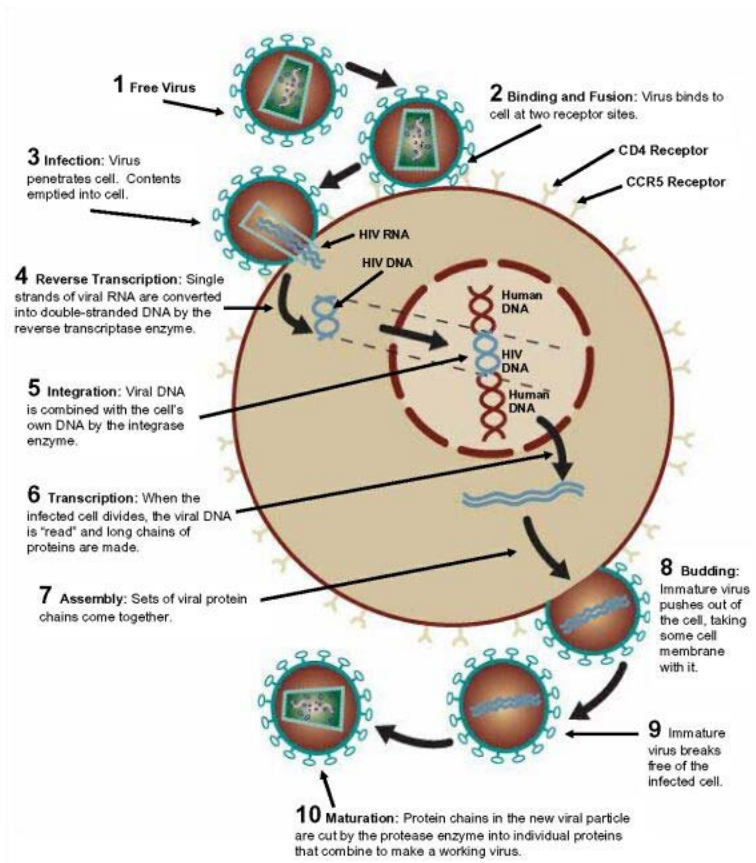


Figure 2.1: HIV life cycle

(from <http://www.aids.org/factSheets/400-HIV-Life-Cycle.html>)

2.2.2 Currently administered antiretroviral drugs

The understanding of the HIV lifecycle helped to develop medications that contain HIV infection. (AIDSInfo, 2004, Johns Hopkins University Division of Infectious Diseases and AIDS Service, 1999)

Anti-HIV medication approved by the U.S. Food and Drug Administration (FDA) are divided into four categories, depending on their particular mechanism of action against viral replication.

Nucleoside/Nucleotide Reverse Transcriptase Inhibitors (NRTIs) work by blocking the step, where the HIV genetic material is converted from RNA into DNA. Nucleoside Transcriptase Inhibitors are faulty versions of building blocks that HIV needs in order to produce more copies of itself. When HIV uses an NRTI instead of a normal building block, reproduction of the virus is stalled.

Nucleotide Reverse Transcriptase Inhibitors behave similar to Nucleoside Transcriptase Inhibitors. The difference between the two is their activation process: nucleosides require three phosphorylations for activation, while nucleotides require only two.

Non-Nucleoside Reverse Transcriptase Inhibitors (NNRTIs) bind to and disable reverse transcriptase, a protein that HIV needs to make more copies of itself.

Protease Inhibitors (PIs) bind to the protease and it result in the rupture of intracellular proteins, meaning that defective non-infectious virions are produced by the cells.

A new kind of drug is still in the experimental phase: Fusion Inhibitors are under study as a new way to block the fusion and attachment steps of HIV life cycle.

Table 2.1 : List of antiretroviral medications and their generic and trade names.

Nucleoside/ Nucleotide Reverse Transcriptase Inhibitors	<p>zidovudine/<i>Retrovir</i> (AZT, ZDV)</p> <p>didanosine/<i>Videx, Videx EC</i> (ddI)</p> <p>zalcitabine/<i>HIVID</i> (ddC)</p> <p>stavudine/<i>Zerit</i> (d4T)</p> <p>lamivudine/<i>Epivir</i> (3TC)</p> <p>abacavir/<i>Ziagen</i> (ABC)</p> <p>tenofovir DF/<i>Viread</i> (TDF)</p>
Protease Inhibitors	<p>indinavir/<i>Crixivan</i></p> <p>ritonavir/<i>Norvir</i></p> <p>saquinavir/<i>Invirase, Fortovase</i></p> <p>nelfinavir/<i>Viracept</i></p> <p>amprenavir/<i>Agenerase</i></p> <p>lopinavir/ritonavir, <i>Kaletra</i></p>
Non-Nucleoside Reverse Transcriptase Inhibitors	<p>nevirapine/<i>Viramune</i> (NVP)</p> <p>delavirdine/<i>Rescriptor</i> (DLV)</p> <p>efavirenz/<i>Sustiva</i> (EFV)</p>
Fusion Inhibitors	<p>enfuvirtide/<i>Fuzeon</i> (T-20)</p>

With current antiretroviral medications, HIV infection can be contained. However, a lot of research has still to be done before the AIDS epidemic is brought under control. One important goal is to design new, more potent medications that are easier to take and have fewer side effects. Also, a better understanding of the HIV infection mechanism could help create a vaccine. (Johns Hopkins University Division of Infectious Diseases and AIDS Service, 1999)

The recommended treatment for HIV is a combination of three or more drugs. In general taking less than three drugs is not recommended because the decrease in viral load would probably be only temporary. However, each HAART regimen is adapted to the individual patient. (*AIDSInfo*, 2004)

2.2.3 HIV modeling

As scientists increasingly enhance their understanding on the behavior of HIV, it became possible for the scientific community to propose a multitude of models characterized by various degrees of complexity and drugs taken (Perelson and Nelson, 1999).

In particular, the group by Perelson has developed through intensive research efforts a substantial body of work on how to model HIV dynamics.

There are two types of mechanisms which have proven successful in accounting for several features of HIV infection: target-cell limited models and immune control models. Briefly, target-cell models assume that viral replication is essentially limited by the amount of uninfected T cells and account for immune responses through a constant death rate of infected T cells. Immune response models are based on the natural response of cytotoxic T cells lymphocytes, which eliminate productively infected T cells prior to viral evacuation from the cell.

Target cell limited models are also commonly used.

The one which was chosen for the purpose of this study is a rather simple nonlinear model comprised of four nonlinear differential equations.

It was first developed by Perelson, Kirschner and DeBoer (1993) and was further improved/refined by Fister, Lenhart and McNally (1998). Recently, it has been slightly modified by Velez Vega (2002) in order to offer convenient units : *cell/day*.

In the model, the following notation was used:

- _ T represents uninfected $CD4^+$ T Cells
- _ T^* represents latently infected T cells
- _ T^{**} represents actively infected T cells
- _ V represents the viral load.

The control variable has been denoted u and represents the strength of drug dosage, so that when $u = 1$, chemotherapy is 100% effective and no infection takes place.

$$\begin{aligned}
 \frac{dT}{dt} &= \frac{sV_b}{1 + V/V_b} - \mu_T T + rT \left(1 - \frac{T + T^* + T^{**}}{T_{\max}} \right) - (1 - u(t)) \frac{K_1 VT}{V_b} \\
 \frac{dT^*}{dt} &= -\mu_T T^* - K_2 T^* + (1 - u(t)) \frac{K_1 VT}{V_b} \\
 \frac{dT^{**}}{dt} &= K_2 T^* - \mu_b T^{**} \\
 \frac{dV}{dt} &= N\mu_b T^{**} - \mu_v V - \frac{K_1 VT}{V_b}
 \end{aligned} \tag{2.1}$$

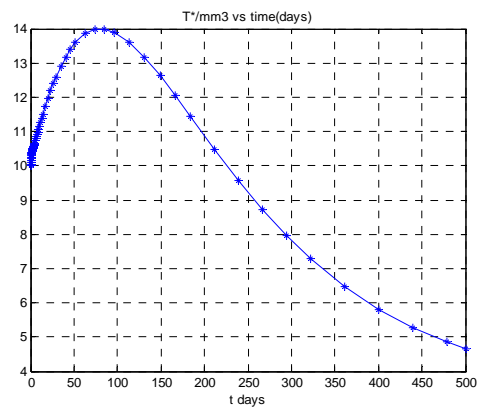
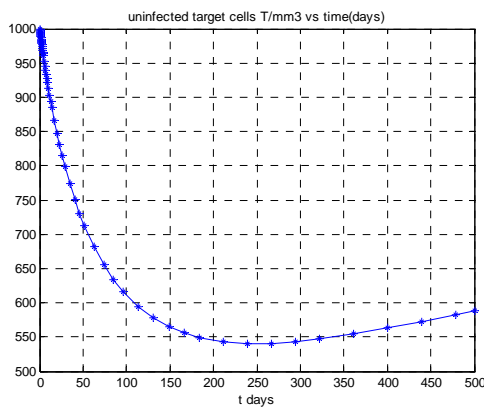
Table 2.2 illustrates the meaning and values of the parameters used in the model for HIV dynamics.

Table 2.2: parameters used for HIV dynamics model

Parameter	Value
μ_T : Death rate of T cells, unassociated with viral infection.	0.02 day^{-1}
μ_b : Death rate of T cells associated with viral induced cell lysis.	0.24 day^{-1}
μ_v : Death rate of V	2.4 day^{-1}
K_1 : Rate of T cell infection by virus	$2.4 \times 10^{-5} \text{ mm}^3 \cdot \text{day}^{-1}$
K_2 : Rate of T^* activation to T^{**}	$3 \times 10^{-3} \text{ day}^{-1}$
r : Rate of T cell growth	$3 \times 10^{-2} \text{ day}^{-1}$
N : Number of virions produced by T^{**}	1200
T_{max} : Maximum T cell level	1500 mm^{-3}
s : Source term for T	$10 \text{ day}^{-1} (\text{mm}^{-3})^2$
V_b : Blood volume	$5 \times 10^6 \text{ mm}^3$

Simulations were run for a period of 500 days without any therapy being applied. The results are given in Figure 2.2, and plotted as cell or virion density.

The initial conditions used are : $T(0) = 1000 V_b$ cells, $T^*(0) = 10 V_b$ cells, $T^{**}(0) = 0.1 V_b$ cells and $V(0) = 50 V_b$ virions.



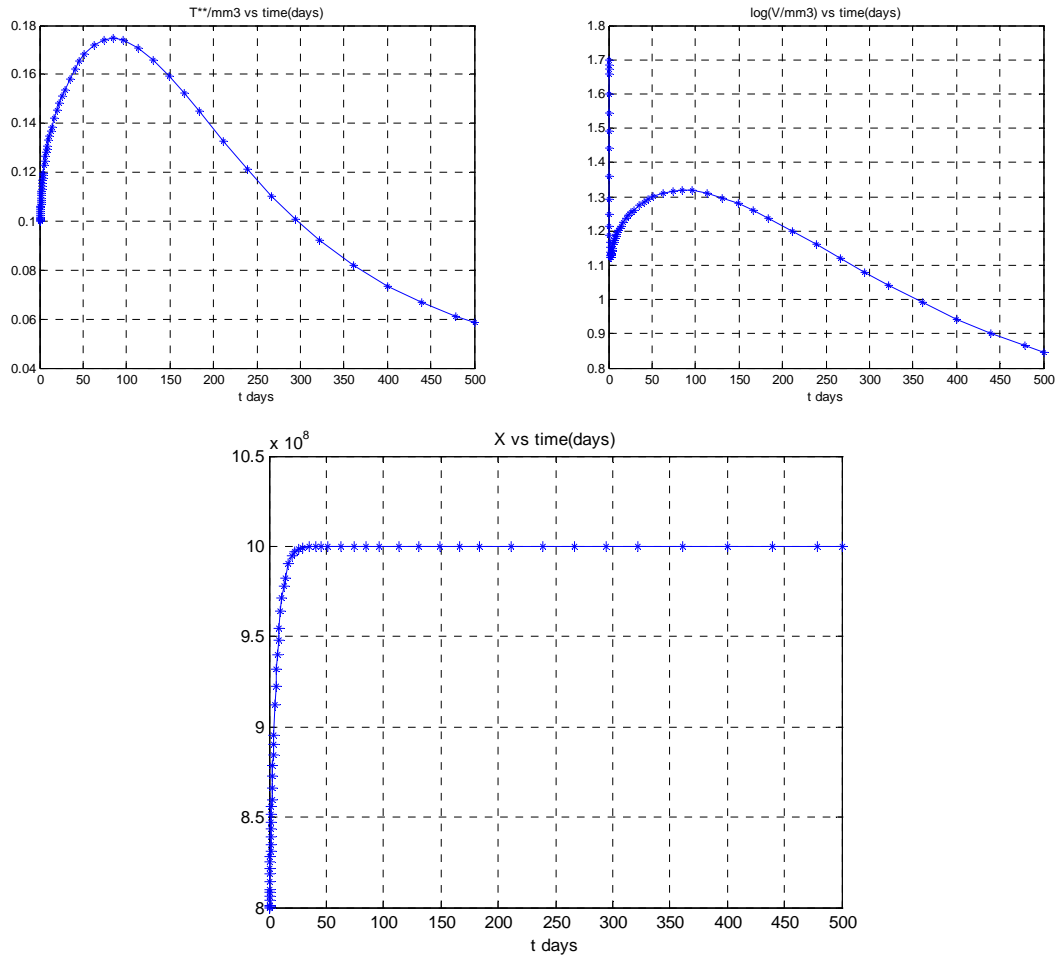


Figure 2.2 : HIV dynamics with no therapy applied

2.2.4 Side effects modeling

Nowadays, serious toxicity with antiretroviral drugs is a topic of high controversy in the treatment of HIV disease. Some of the negative side effects are serious, even life-threatening, but taking anti-HIV medications is necessary to control the reproduction of the virus, and thus slow the progression of the disease.

This section presents the ideas developed by Camilo Velez Vega in 2002, and does not intend to be exhaustive.

2.2.5 Side effect mechanisms

In this section, the hypothesis that natural HIV disease progression has an effect on the syndromes observed is not considered here.

Here are some of the most commonly observed drug toxicities, which have been summarized by Carr and Cooper (2000). Some complementary information coming from *AIDSInfo* has been added.

2.2.5.1 *Mitochondrial toxicity*

The major toxicities linked to NRTI and NtRTI therapy, especially over the long-term, are thought to be secondary to inhibition of mitochondrial DNA polymerase, resulting in impaired synthesis of mitochondrial enzymes that generate ATP. This results in myopathy, neuropathy, hepatic steatosis and lactic acidemia, pancreatitis and possibly peripheral lipodystrophy. A cause is probably because NRTIs and NtRTIs are typically administered in therapeutically inactive forms and need to be phosphorylated by cellular enzymes into their active forms. The management of mitochondrial toxicity is generally a cessation of the causative drug (Carr and Cooper, 2000).

2.2.5.2 *Lipodystrophy syndrome*

Body fat redistribution has been observed on patients who had been on long-term protease inhibitor therapy. The main clinical features are peripheral fat loss in the face and limbs, and central fat accumulation (the “buffalo hump”, fat accumulated at top of the back, and “protease paunch”, a pad of fat that develops behind the stomach muscles). Recently, lipodystrophy has been associated with low-grade lactic acidemia and liver dysfunction. The metabolic features include hypertriglyceridaemia, hypercholesterolaemia, insulin resistance, diabetes or lactic acidemia. Furthermore, these effects are linked to an increase in cardiovascular disease and the pathogenesis of the syndrome is unclear. One possibility is that PI inhibits lipogenesis. Moreover, there is no proven therapy for the lipodystrophy syndrome. (Project Inform, 1998, Carr and Cooper , 2000).

2.2.5.3 *Hypersensitivity*

Drug hypersensitivity usually manifests itself as an erythematous, maculopapular, pruritic and confluent rash. Fever can precede the rash. NNRTIs are common antiretroviral drugs that cause hypersensitivity, which is rare with NRTIs or PIs. Suggested causes include long duration and high doses of therapy, or degree of immunodeficiency. Usually, antiretroviral hypersensitivity resolves spontaneously, despite continuation of therapy (Carr and Cooper , 2000).

2.2.5.4 *Bone marrow suppression*

Bone marrow toxicity can be caused by several drugs (AZT and several anti-cancer drugs). This is particularly a problem since damage to the bone marrow

jeopardizes the ability to produce new blood cells. This can result in anemia, leucopenia, neutropenia and thrombocytopenia (Highleyman, 1998).

2.2.6 Model for side effects affecting the liver

All side antiretroviral drugs can cause side effects involving the liver (Highleyman, 1998).

It is assumed that drug toxicity for our model is caused by NRTI, and more specifically through AZT therapy, associated with mitochondrial toxicity.

Even though other organs can be similarly affected by drug therapy, it is only considered that liver dysfunction poses considerable limitations to the therapy implemented.

This syndrome progression is directly linked to the hepatic steatosis evolution: this will be modeled as a gradual liver cell dysfunction.

Also, a simple liver regeneration term is added to the model in order to account for liver regeneration when drug dosage is lowered or suspended (Velez Vega, 2002).

$$\frac{dX}{dt} = \underbrace{-k_{se} X C_{\max} \cdot u(t)}_{\text{liver cell depletion}} + \underbrace{(1-u(t)) \cdot k_r (X_{\max} - X)}_{\text{liver cell regeneration}} \quad (2.2)$$

$$\text{with } k_r = \frac{X_{\max}}{10(X_{\max} - X) + 5X_{\max}}$$

Table 2.3: parameters used for side effects model

Parameter	Value for AZT
C_{\max} : Maximum allowable drug concentration	600 mg .day ⁻¹
X_{\max} : Maximum number of liver cells	10 ⁹
k_{se} : Depletion rate	2.2831×10 ⁻⁶ mg ⁻¹

The rate constant k_{se} has been calculated such that for full chemotherapy, the amount of dysfunctional cells is 50% in 500days.

2.2.7 Pharmacokinetics models

In the majority of mathematical models available for HIV dynamics, the treatment effect is considered constant. However, the treatment effect changes over time, most probably because of pharmacokinetic variations, imperfect adherence, drug resistant mutations, etc. Dixit and Perelson (2004) developed a model for the treatment effect which combines drug pharmacokinetics and intracellular delays. The model they developed is a two compartment pharmacokinetic model:

- _ the blood compartment, which determines how much of the drug is absorbed from the gut to the blood.
- _ the cell compartment, which determines the intracellular drug concentrations, since, depending on the nature of the drug, they are either administered in active or inactive forms, and thus need to be transformed by cellular enzymes into their active forms.

However, for the sake of simplicity, a simpler one compartment model was used, so that the efficacy of the treatment using AZT is defined using plasma concentrations of the drug, as it was done by Y. Huang et al. (2003).

Their model assumes an one-compartment model with first-order absorption and elimination, and it also assumes that the pharmacokinetic parameters remain constant.

Considering $C_a(t)$ to be the apparent concentration in the absorption depot and $C(t)$ to be the plasma concentration at time t , the model can be expressed as follows:

For the non-steady state at a dosage time $t = t_l$:

$$\begin{aligned}
 C_a(t_l) &= C_a(t_{l-1}) \cdot \exp[-k_a \tau] + \frac{FD_l}{V_c} \\
 C(t_l) &= C(t_{l-1}) \cdot \exp[-k_e \tau] + C_a(t_{l-1}) \frac{k_a}{k_a - k_e} \times [\exp\{-k_e \tau\} - \exp\{-k_a \tau\}]
 \end{aligned}
 \tag{2.3}$$

For the steady state at a dosage time $t = t_l$:

$$\begin{aligned}
 C_a(t_l) &= \left(\frac{FD_l}{V_c} \right) \times (1 - \exp[-k_a \tau])^{-1} \\
 C(t_l) &= \left(\frac{FD_l}{V_c} \right) \frac{k_a}{k_a - k_e} \times \left[(1 - \exp[-k_e \tau])^{-1} - (1 - \exp[-k_a \tau])^{-1} \right]
 \end{aligned} \tag{2.4}$$

Between dosage times , $t_l < t < t_{l+1}$

$$C(t) = C(t_l) \exp[-k_e(t - t_l)] + C_a(t_l) \frac{k_a}{k_a - k_e} \times \{ \exp[-k_e(t - t_l)] - \exp[-k_a(t - t_l)] \} \tag{2.5}$$

with t_l , $l = 0, 1, 2, \dots$ are the times at which the dose is taken, and $C_a(t_0) = FD_0/V_c$ and $C(t_0) = 0$.

Y. Huang et al. (2003) also introduced the idea that the phenotype marker IC_{50} (which represents the 50% inhibitory concentration of the drug) changes over time due to the emergence of drug resistant mutations. They proposed the following simple function:

$$IC_{50}(t) = \begin{cases} I_0 + \frac{I_r - I_0}{t_r} \cdot t & \text{for } 0 < t < t_r \\ I_r & \text{for } t \geq t_r \end{cases} \tag{2.6}$$

The explanation of the different parameters is given in Table 2.3.

Table 2.3: Parameters used for pharmacokinetics model

Parameter	Value for Zidovudine(AZT)
D_l : doses	200 mg
k_a : absorption rate	0.5 h^{-1}
k_e : elimination rate	$k_e = C_l/V_c = 1 \text{ h}^{-1}$
Cl : systemic clearance	1.6 L/h/kg
V_c : apparent volume of distribution	1.6 L/kg
F : absolute bioavailability	0.64
τ : dosing interval	8 h
I_0 : initial 50% inhibitory concentration	0.013 mg/L
I_r : 50% inhibitory concentration after emergence of mutations	1.17 mg/L
t_r : time at which the resistant mutations dominate	84 days
φ : conversion factor between in vivo and in vitro studies	1

(from GlaxoSmithKline, Product Information for Retrovir®)

According to the prescribing information for Retrovir® (zidovudine), the relationship between the in vitro susceptibility of HIV to reverse transcriptase inhibitors and the one in vivo has not been established, that is why the value $\varphi = 1$ was assumed for the purpose of the study.

Even though most highly active antiretroviral therapy (HAART) nowadays consists of a combination of drugs, a drug efficacy function was used for a single antiretroviral agent, as assumed in the HIV dynamics model.

$$\gamma(t) = \frac{C(t)}{\varphi \cdot IC_{50}(t) + C(t)} \quad (2.7)$$

The simulations are given considering an individual weighing 70 kg, and assuming perfect adherence (the individual takes at the regular dosing interval the prescribed dose).

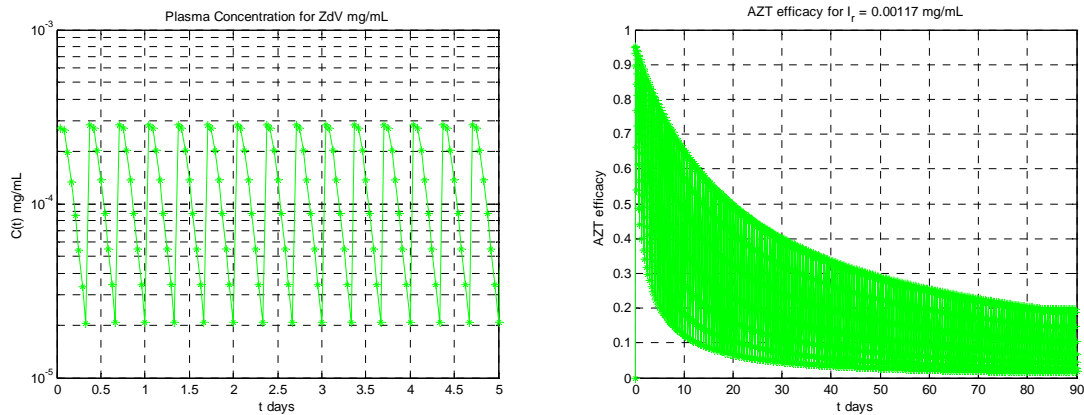


Figure 2.3 : simulation for normal AZT treatment regimen

2.3 Optimization method description

The proposed system-theoretic chemotherapy optimization method is based on a nonlinear, single-input / single-output model-based continuous time model predictive approach(Soroush and Kravaris, 1996).

An explicit analytical expression is derived for the optimal chemotherapy protocol, on the basis of the available model for HIV dynamics. One of the inherent assumptions of the proposed approach is that the nonlinear dynamic model needs to be stable. However, HIV natural disease progression can be approximated by a stable model, because of pseudo-steady state T cell levels.

Some preliminary concepts are stated before deriving the optimal chemotherapy protocol.

2.3.1 Lie derivatives

Given a nonlinear system of the following form:

$$\begin{aligned} \dot{x} &= f(x) + g(x) \cdot u \\ y &= h(x) \end{aligned} \tag{2.8}$$

$x \in \mathfrak{R}^n, \quad u \in \mathfrak{R}, \quad y \in \mathfrak{R}$

with $f = \begin{bmatrix} f_1(x_1, x_2, \dots, x_n) \\ f_2(x_1, x_2, \dots, x_n) \\ \dots \\ f_n(x_1, x_2, \dots, x_n) \end{bmatrix}, \quad g = \begin{bmatrix} g_1(x_1, x_2, \dots, x_n) \\ g_2(x_1, x_2, \dots, x_n) \\ \dots \\ g_n(x_1, x_2, \dots, x_n) \end{bmatrix}$ and $h = h(x_1, x_2, \dots, x_n)$.

The Lie derivative of h with respect to f is defined as follows:

$$L_f h = \sum_{i=1}^n \frac{\partial h}{\partial x_i} \cdot f_i = \frac{\partial h}{\partial x_1} f_1 + \frac{\partial h}{\partial x_2} f_2 + \dots + \frac{\partial h}{\partial x_n} f_n \tag{2.9}$$

In the same way, since the above definition produces a scalar quantity, higher order and mixed order derivatives can be defined recursively ($l = 1, 2, \dots$) as shown below:

Lie derivative of $L_f^l h$ with respect to f : $L_f^{l+1} h = L_f(L_f^l h)$ (2.10)

Lie derivative of $L_f^l h$ with respect to g : $L_g L_f^l h = L_g(L_f^l h)$

2.3.2 Relative degree

Consider a nonlinear input-driven dynamical system as in equation (2.8).

Define r as the minimum order of the output derivative.

The first order derivative of y with respect to time is expressed in terms of the Lie derivatives:

$$\begin{aligned}
 \frac{dy}{dt} &= \frac{\partial h}{\partial x_1} \frac{dx_1}{dt} + \frac{\partial h}{\partial x_2} \frac{dx_2}{dt} + \dots + \frac{\partial h}{\partial x_n} \frac{dx_n}{dt} \\
 \Leftrightarrow &= \frac{\partial h}{\partial x_1} [f_1(x) + g_1(x) \cdot u] + \frac{\partial h}{\partial x_2} [f_2(x) + g_2(x) \cdot u] + \dots + \frac{\partial h}{\partial x_n} [f_n(x) + g_n(x) \cdot u] \\
 \Leftrightarrow &= \left[\frac{\partial h}{\partial x_1} f_1 + \frac{\partial h}{\partial x_2} f_2 + \dots + \frac{\partial h}{\partial x_n} f_n \right] + \left[\frac{\partial h}{\partial x_1} g_1 + \frac{\partial h}{\partial x_2} g_2 + \dots + \frac{\partial h}{\partial x_n} g_n \right] \cdot u \\
 \Leftrightarrow &= L_f h + L_g h \cdot u
 \end{aligned} \tag{2.11}$$

From the above equations, it is clear that $L_g h$ determines whether or not the input u will affect dy/dt .

If $L_g h \neq 0$, the first order derivative of the system output is indeed affected by the input.

Thus, $r = 1$.

However, in the case where $L_g h = 0$, the first order derivative of the system output is not affected by the input.

Thus, the calculation of the second order derivative is required:

$$\begin{aligned}
 \frac{d^2 y}{dt^2} &= \frac{d}{dt} \left(\frac{dy}{dt} \right) = \frac{d}{dt} (L_f h + L_g h \cdot u) \\
 L_g h = 0 &\Rightarrow \frac{dy}{dt} = L_f h \\
 \frac{d^2 y}{dt^2} &= \frac{d}{dt} (L_f h) \\
 \Leftrightarrow &= L_f^2 h + L_g L_f h \cdot u
 \end{aligned} \tag{2.12}$$

In this case, the term $L_g L_f h$ determines whether or not the input u will affect $d^2 y/dt^2$.

If $L_g L_f h \neq 0$, then the relative degree of the system is $r = 2$.

If $L_g L_f h = 0$, the same procedure is performed until the r^{th} order output derivative is affected by the input : $L_g L_f^{r-1} h \neq 0$.

2.3.3 Description of the control law

The approach by Soroush and Kravaris (1996) allows to account for deadtime. However, in this study, the focus is on a delay-free system.

Consider a nonlinear dynamical system of the form: equation set (2.8)

$$\begin{aligned}\dot{x}(t) &= f(x(t)) + g(x(t)) \cdot u(t) \\ y(t) &= h(x(t)) \\ x &\in \mathfrak{R}^n, \quad u \in \mathfrak{R}, \quad y \in \mathfrak{R}\end{aligned}$$

Consider also that $L_g h \neq 0$ ($r = 1$) and y is desired to follow a specified trajectory y^d .

The speed of the output response, dy/dt , is affected by the input in such a way that it is possible to enforce a particular desirable trajectory on y .

For a given set point y_{sp} , y^d starts from the actual value of y at an arbitrary time t_0 and follows an exponential trajectory to the stated value of y_{sp} .

Considering a proportionality constant γ , this translates into the following equations:

$$\begin{aligned}\gamma \frac{dy^d}{dt} + y^d(t) &= y_{sp} \\ y^d(t_0) &= y(t_0)\end{aligned}\tag{2.13}$$

Developing the Taylor series expansion of y^d around t_0 and using the above equation:

$$y^d(t) = y^d(t_0) + \left(\frac{dy^d}{dt} \right)_{t_0} \cdot (t - t_0) + \left(\frac{d^2 y^d}{dt^2} \right)_{t_0} \cdot \frac{(t - t_0)^2}{2!} + \text{higher order terms}$$

$$y^d(t) = y^d(t_0) + \left[\frac{y_{sp} - y^d(t_0)}{\gamma} \right] \cdot (t - t_0) + \text{hot}$$
(2.14)

For “small” $\|t - t_0\|$, the above can be approximated as follows:

$$y^d(t) \approx y^d(t_0) + \left[\frac{y_{sp} - y^d(t_0)}{\gamma} \right] \cdot (t - t_0)$$
(2.15)

Also, it is possible to express the actual behavior of the output y by a Taylor-Lie series expansion, truncated for small values of $\|t - t_0\|$:

$$y(t) = y(t_0) + \left(\frac{dy}{dt} \right)_{t_0} \cdot (t - t_0) + \left(\frac{d^2 y}{dt^2} \right)_{t_0} \cdot \frac{(t - t_0)^2}{2!} + \text{higher order terms}$$

$$y(t) = y(t_0) + \left[L_f h(x(t_0)) + L_g h(x(t_0)) \cdot u(t_0) \right] \cdot (t - t_0) + \text{hot}$$

$$y(t) \approx y(t_0) + \left[L_f h(x(t_0)) + L_g h(x(t_0)) \cdot u(t_0) \right] \cdot (t - t_0)$$
(2.16)

The following pointwise optimization problem can be formulated:

$$J = \min_{u(t_0)} \left\| y^d(t) - y(t) \right\|^2 + q^2 \cdot \left\| u(t_0) \right\|^2$$
(2.17)

subject to the constraints : $u_{\min} \leq u \leq u_{\max}$

Using the expressions for $y^d(t)$ and $y(t)$ in the above performance index/criterion one obtains:

$$J = \min_{u(t_0)} \left\| \frac{y_{sp} - y^d(t_0)}{\gamma} - L_f h(x(t_0)) + L_g h(x(t_0)) \cdot u(t_0) \right\|^2 \cdot \|t - t_0\|^2 + q^2 \cdot \left\| u(t_0) \right\|^2$$
(2.18)

The value of $u(t_0)$ which minimizes J is obtained as follows:

$$\begin{aligned} \frac{dJ}{du(t_0)} = 0 = & 2q^2 \cdot \|u(t_0)\| + 2\left\{ [L_g h(x(t_0))]^2 \cdot u(t_0) \right\} \cdot \|t - t_0\|^2 + \\ & - 2L_g h(x(t_0)) \left[\frac{y_{sp} - y^d(t_0)}{\gamma} - L_f h(x(t_0)) \right] \cdot \|t - t_0\|^2 \end{aligned} \quad (2.19)$$

Solving for $u(t_0)$ and denoting $p^2 = \frac{q^2}{\|t - t_0\|^2}$ leads to the following chemotherapy protocol:

$$\begin{aligned} u(t_0) = S[\Psi(x(t_0), h(t_0))] \quad \text{where} \quad S[w] = \begin{cases} u_{\min} & \text{if } w < u_{\min} \\ w & \text{if } u_{\min} \leq w < u_{\max} \\ u_{\max} & \text{if } w \geq u_{\max} \end{cases} \\ \Psi(x(t_0), h(t_0)) = \frac{L_g h(x(t_0)) \cdot \left[\frac{y_{sp} - y(t_0)}{\gamma} - L_f h(x(t_0)) \right]}{p^2 + [L_g h(x(t_0))]^2} \end{aligned} \quad (2.20)$$

Since t_0 is completely arbitrary, the control law (2.20) can be written as :

$$\begin{aligned} u(t) = S[\Psi(x(t), h(t))] \quad \text{where} \quad S[w] = \begin{cases} u_{\min} & \text{if } w < u_{\min} \\ w & \text{if } u_{\min} \leq w < u_{\max} \\ u_{\max} & \text{if } w \geq u_{\max} \end{cases} \\ \Psi(x(t), h(t)) = \frac{L_g h(x(t)) \cdot \left[\frac{y_{sp} - y(t)}{\gamma} - L_f h(x(t)) \right]}{p^2 + [L_g h(x(t))]^2} \end{aligned} \quad (2.21)$$

The clinical interpretation of the tunable parameters introduced in the above expression for the optimal chemotherapy protocol is the following:

– γ is related to the speed of the response: if γ increases, the chemotherapy becomes more aggressive.

– p accounts for penalization of excessively high levels of the chemotherapy administered

Similarly, this procedure can be applied for processes for which $L_g h = 0$ i.e for $r \geq 2$. In general, for a system of relative order r , the following expression can be derived :

$$u(t) = S[\Psi(x(t), h(t))] \quad \text{where} \quad S[w] = \begin{cases} u_{\min} & \text{if } w < u_{\min} \\ w & \text{if } u_{\min} \leq w < u_{\max} \\ u_{\max} & \text{if } w \geq u_{\max} \end{cases} \quad (2.22)$$

$$\Psi(x(t), h(t)) = \frac{L_g L_f^{r-1} h(x(t)) \cdot \left[y_{sp} - h(x(t)) - \sum_{l=1}^r \gamma_l L_f^l h(x(t)) \right]}{\left\{ p^2 + [L_g L_f^{r-1} h(x(t))]^2 \right\} \cdot \gamma_r}$$

2.4 Derivation of the model optimization equations

Our simple model for HIV dynamics has been studied under 2 different minimization criteria.

2.4.1 Optimization A

Optimization A represents HIV chemotherapy optimization without minimization of liver cell depletion

Since, side effects are not included in this optimization, the dynamic model is the same as the set of equations (2.1).

$$\begin{aligned}
 \frac{dT}{dt} &= \frac{sV_b}{1 + V/V_b} - \mu_T T + rT \left(1 - \frac{T + T^* + T^{**}}{T_{\max}} \right) - \frac{K_1 VT}{V_b} + \frac{K_1 VT}{V_b} u(t) \\
 \frac{dT^*}{dt} &= -\mu_T T^* - K_2 T^* + \frac{K_1 VT}{V_b} - \frac{K_1 VT}{V_b} u(t) \\
 \frac{dT^{**}}{dt} &= K_2 T^* - \mu_b T^{**} \\
 \frac{dV}{dt} &= N\mu_b T^{**} - \mu_v V - \frac{K_1 VT}{V_b}
 \end{aligned} \tag{2.1}$$

The quadratic output function selected represents a meaningful quantifiable measure of the absolute deviation of T cells from the maximum T cell count.

$$y(t) = (T_{\max} - T)^2 \tag{2.23}$$

This way, the optimization aims at the minimization of the distance between y and y^d , forcing T to T_{\max} as fast as possible, and y_{sp} is set to 0.

Calculation of the Lie derivatives gives:

$$\begin{aligned}
 L_g h &= \sum_{i=1}^4 \frac{\partial h}{\partial x_i} \cdot g_i = \frac{\partial h}{\partial x_1} g_1 + \frac{\partial h}{\partial x_2} g_2 + \frac{\partial h}{\partial x_3} g_3 + \frac{\partial h}{\partial x_4} g_4 \\
 &= 2 \cdot (T - T_{\max}) \cdot \left[\frac{K_1 V T}{V_b} \right]
 \end{aligned} \tag{2.24}$$

$$\begin{aligned}
 L_f h &= \sum_{i=1}^4 \frac{\partial h}{\partial x_i} \cdot f_i = \frac{\partial h}{\partial x_1} f_1 + \frac{\partial h}{\partial x_2} f_2 + \frac{\partial h}{\partial x_3} f_3 + \frac{\partial h}{\partial x_4} f_4 \\
 &= 2 \cdot (T - T_{\max}) \cdot \left[\frac{s \cdot V_b}{1 + V/V_b} - \mu_T T + r T \left(1 - \frac{T + T^* + T^{**}}{T_{\max}} \right) - \frac{K_1 V T}{V_b} \right]
 \end{aligned} \tag{2.25}$$

Since, $L_g h \neq 0$ for arbitrary values of the state variables, the relative order is $r = 1$.

These equations are placed in the derived optimal chemotherapy expression, appropriately modified to accommodate clinically meaningful units.

$$\begin{aligned}
 u(t) &= S[\Psi(x(t), h(t))] \quad \text{where} \quad S[w] = \begin{cases} u_{\min} & \text{if } w < u_{\min} \\ w & \text{if } u_{\min} \leq w < u_{\max} \\ u_{\max} & \text{if } w \geq u_{\max} \end{cases} \\
 \Psi(x(t), h(t)) &= \frac{L_g h(x(t)) \cdot \left[\frac{y_{sp} - y(t)}{\gamma} - L_f h(x(t)) \right]}{(p \cdot V_b^2)^2 + [L_g h(x(t))]^2}
 \end{aligned} \tag{2.26}$$

Please notice, that as expected in actual practice, the chemotherapy variable u is subject to hard constraints that reflect actual technical and physical limitations encountered during the chemotherapy administration cycle.

2.4.2 Optimization B

Optimization B stands for HIV chemotherapy optimization with concurrent minimization of liver cell depletion.

A fifth differential equation is added to the four differential equations of the postulated model for HIV in order to account for the liver side effects.

$$\begin{aligned}
 \frac{dT}{dt} &= \frac{sV_b}{1 + V/V_b} - \mu_T T + rT \left(1 - \frac{T + T^* + T^{**}}{T_{\max}} \right) - \frac{K_1 VT}{V_b} + \frac{K_1 VT}{V_b} u(t) \\
 \frac{dT^*}{dt} &= -\mu_T T^* - K_2 T^* + \frac{K_1 VT}{V_b} - \frac{K_1 VT}{V_b} u(t) \\
 \frac{dT^{**}}{dt} &= K_2 T^* - \mu_b T^{**} \\
 \frac{dV}{dt} &= N\mu_b T^{**} - \mu_v V - \frac{K_1 VT}{V_b} \\
 \frac{dX}{dt} &= -k_{se} X C_{\max} \cdot u(t) + (1 - u(t)) \cdot k_r (X_{\max} - X)
 \end{aligned} \tag{2.27}$$

$$\text{with } k_r = \frac{X_{\max}}{10(X_{\max} - X) + 5X_{\max}}$$

The output is defined as:

$$y(t) = (T_{\max} - T)^2 + (X_{\max} - X)^2 \tag{2.28}$$

The distance from the actual to the desired output is minimized, so that the actual T cell count is driven to its maximum value T_{\max} , while at the same time, the actual number of functional liver cells is also driven to its maximum X_{\max} .

A simple calculation of the associated Lie derivatives gives:

$$\begin{aligned}
 L_g h &= \sum_{i=1}^5 \frac{\partial h}{\partial x_i} \cdot g_i = \frac{\partial h}{\partial x_1} g_1 + \frac{\partial h}{\partial x_2} g_2 + \frac{\partial h}{\partial x_3} g_3 + \frac{\partial h}{\partial x_4} g_4 + \frac{\partial h}{\partial x_5} g_5 \\
 &= 2 \cdot (T - T_{\max}) \cdot \left[\frac{K_1 VT}{V_b} \right] + 2 \cdot (X - X_{\max}) \cdot \left[-k_{se} X C_{\max} - k_r (X_{\max} - X) \right]
 \end{aligned} \tag{2.29}$$

$$\begin{aligned}
 L_f h &= \sum_{i=1}^4 \frac{\partial h}{\partial x_i} \cdot f_i = \frac{\partial h}{\partial x_1} f_1 + \frac{\partial h}{\partial x_2} f_2 + \frac{\partial h}{\partial x_3} f_3 + \frac{\partial h}{\partial x_4} f_4 + \frac{\partial h}{\partial x_5} f_5 \\
 &= 2 \cdot (T - T_{\max}) \cdot \left[\frac{s \cdot V_b}{1 + V/V_b} - \mu_T T + rT \left(1 - \frac{T + T^* + T^{**}}{T_{\max}} \right) - \frac{K_1 VT}{V_b} \right] + \\
 &\quad + 2 \cdot (X - X_{\max}) \cdot [k_r (X_{\max} - X)]
 \end{aligned} \tag{2.30}$$

Since, $L_g h \neq 0$, the relative order is $r = 1$ and the control law is formalistically identical to the one developed earlier.

$$\begin{aligned}
 u(t) &= S[\Psi(x(t), h(t))] \quad \text{where} \quad S[w] = \begin{cases} u_{\min} & \text{if } w < u_{\min} \\ w & \text{if } u_{\min} \leq w < u_{\max} \\ u_{\max} & \text{if } w \geq u_{\max} \end{cases} \\
 \Psi(x(t), h(t)) &= \frac{L_g h(x(t)) \cdot \left[\frac{y_{sp} - y(t)}{\gamma} - L_f h(x(t)) \right]}{(p \cdot V_b^2)^2 + [L_g h(x(t))]^2}
 \end{aligned} \tag{2.26}$$

In this case, parameter p is now understood as an additional penalization attempt for high values of u , since side effects are now explicitly constrained by the presence of liver cells in the output function.

2.5 Simulations

The numerical simulation results were obtained using a MATLAB code.

The initial conditions used are : $T(0) = 700V_b$ cells, $T^*(0) = 20 V_b$ cells, $T^{**}(0) = 0.2 V_b$ cells $V(0) = 50 V_b$ virions and $X(0) = 10^9$ cells.

On the plots, the following notation is used:

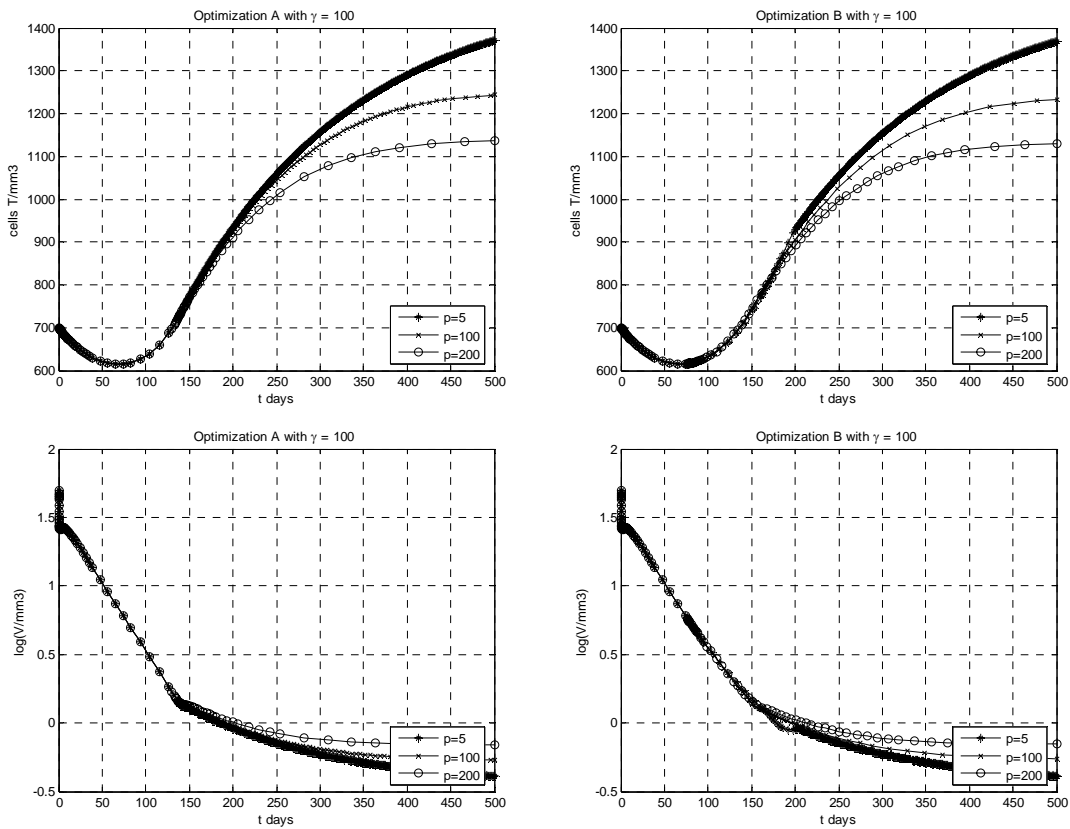
Optimization A = HIV chemotherapy optimization without minimization of liver cell depletion

Optimization B= HIV chemotherapy optimization with minimization of liver cell depletion

2.5.1 Behavior of HIV model with therapy optimization

2.5.1.1 Influence of the parameters p and γ

The graphs below represent the results obtained for the optimizations A (left) and B (right) for varying values of p at $\gamma=100$.



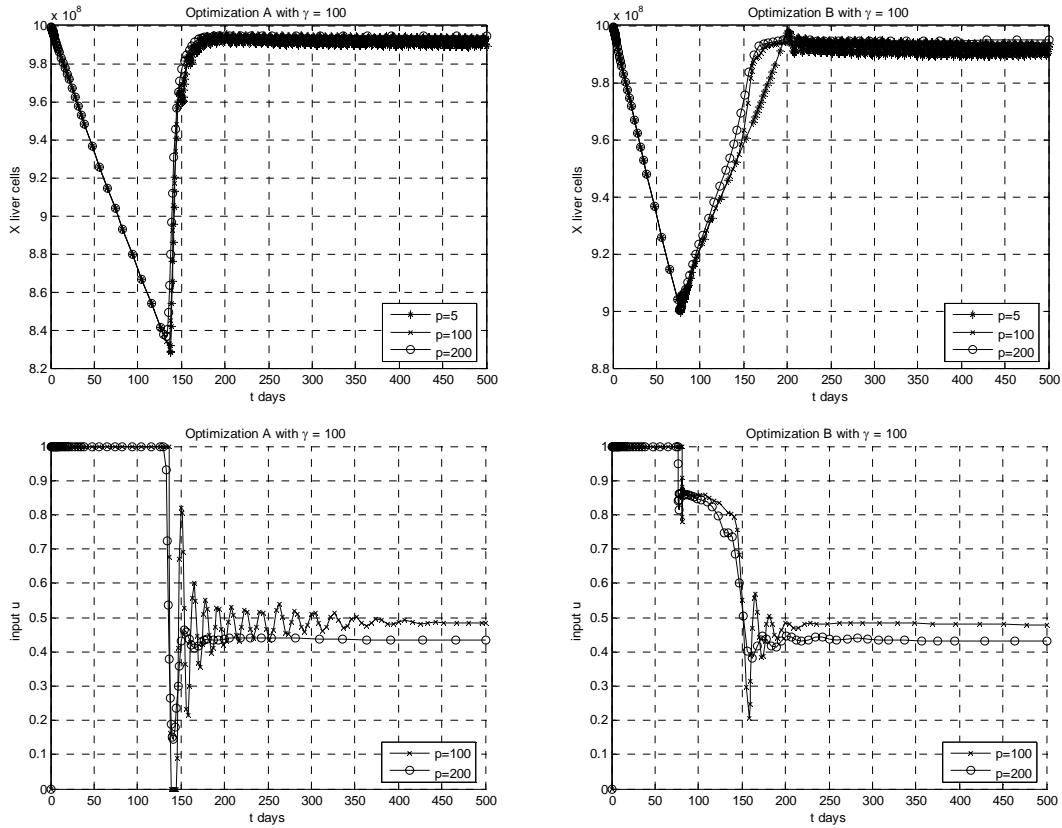


Figure 2.4: comparison of optimizations A and B for varying values of p at $\gamma=100$.

On the last two graphs of Figure 2.4, those which represent the input, $p = 5$ was not represented, since the resulting chemotherapy pattern was unacceptably aggressive. This issue will be discussed later.

The graphs (Figure 2.5) below represent the results obtained for the optimizations A (left) and B (right) for varying values of γ at $p = 200$.

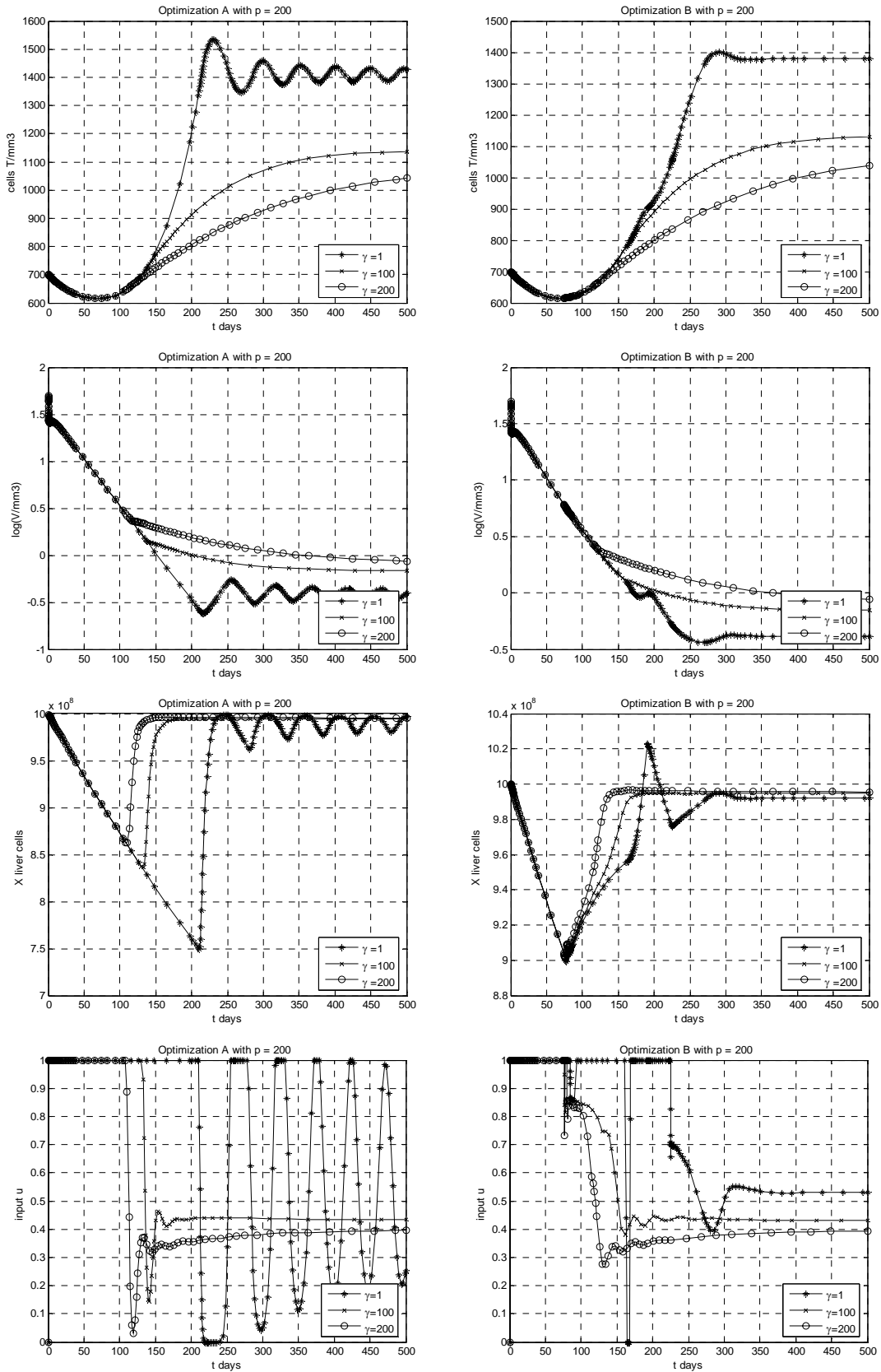


Figure 2.5: comparison of optimizations A and B for varying values of γ at $p=200$.

2.5.1.2 Saturation function : $0 \leq u \leq 1$

In this case, the constraints chosen for u naturally reflect its intrinsic meaning: effectiveness should be constrained between 0 and 100%.

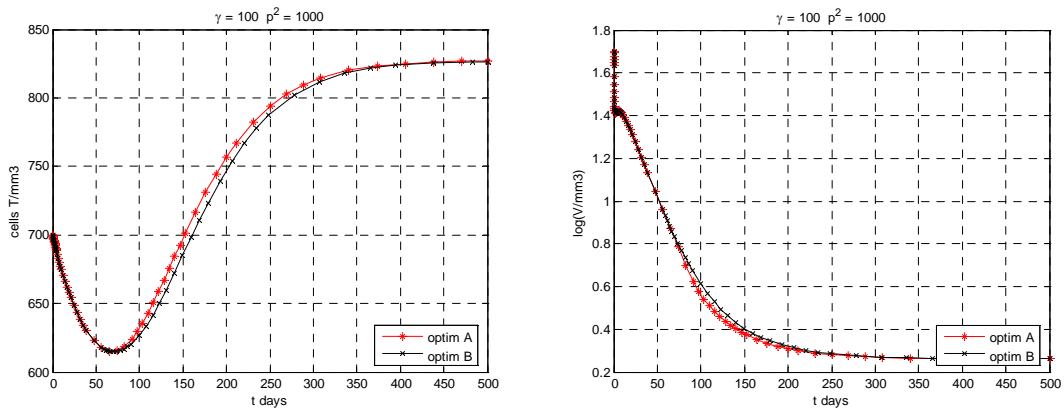
The proposed chemotherapy pattern becomes:

$$u(t) = S[\Psi(x(t), h(t))] \quad \text{where} \quad S[w] = \begin{cases} 0 & \text{if } w < 0 \\ w & \text{if } 0 \leq w < 1 \\ 1 & \text{if } w \geq 1 \end{cases} \quad (2.31)$$

$$\Psi(x(t), h(t)) = \frac{L_g h(t) \cdot \left[\frac{y_{sp} - y(t)}{\gamma} - L_f h(t) \right]}{(p \cdot V_b^2)^2 + [L_g h(t)]^2}$$

Here, a first comparison between the two optimization criteria is realized for a given set of parameters (γ and p).

On the same graph and for the same set of parameters the dynamics of the states of interest (T , V , u and X) are plotted for Optimizations A and B, as shown in Figure 2.6.



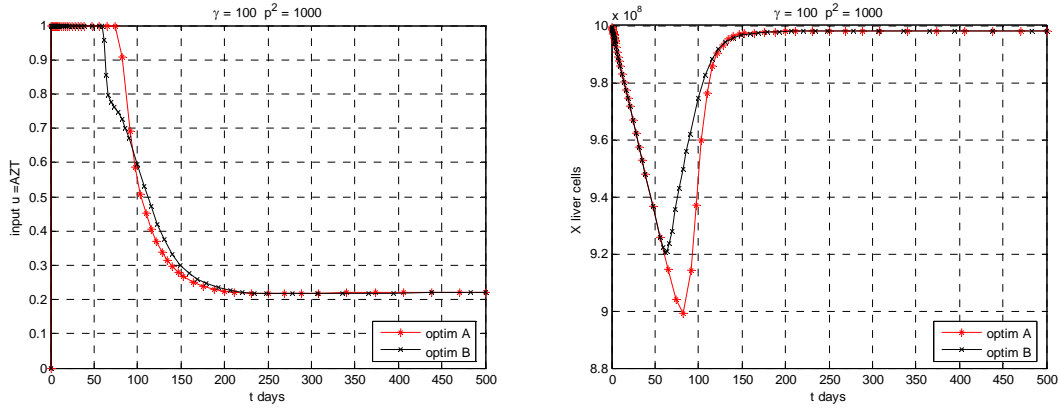


Figure 2.6: Comparison of optimizations A and B for $0 \leq u \leq 1$

It can already be seen that the difference between the two optimization criteria is small. The difference lies in the length of time for which $u = 1$. Optimization B accounts for side effects, thus a high drug regimen can not be administered for too long. This results in a smaller largest deviation of X from its maximum value X_{max} : 8% instead of 10%.

2.5.1.3 Saturation function: $0.3 \leq u \leq 0.9$

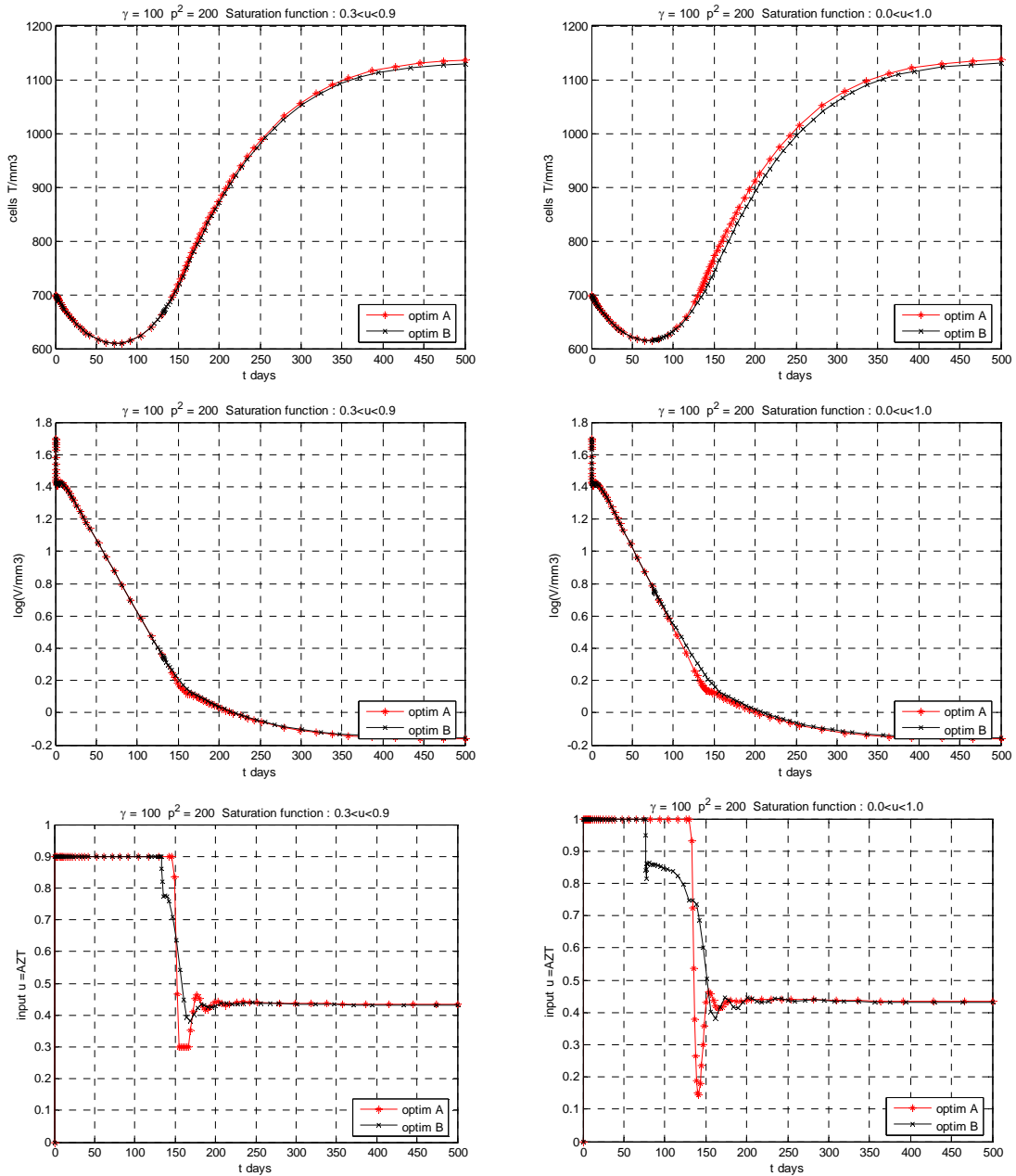
$$u(t) = S[\Psi(x(t), h(t))] \quad \text{where} \quad S[w] = \begin{cases} 0.3 & \text{if } w < 0.3 \\ w & \text{if } 0.3 \leq w < 0.9 \\ 0.9 & \text{if } w \geq 0.9 \end{cases} \tag{2.32}$$

$$\Psi(x(t), h(t)) = \frac{L_g h(t) \cdot \left[\frac{y_{sp} - y(t)}{\gamma} - L_f h(t) \right]}{(p \cdot V_b^2)^2 + [L_g h(t)]^2}$$

For a given set of parameters (γ and p), the graphs below (Figure 2.7) show the difference between the 2 types of optimization considered. On the same graph and for the same set of parameters the dynamics of each state for optimizations A and B are plotted.

On the left, the plots are for the control law including a more severely constrained u in the saturation function applied, namely: $0.3 \leq u \leq 0.9$.

The plots on the right are given for comparison: chemotherapy patterns including a saturation function with: $0.0 \leq u \leq 1.0$.



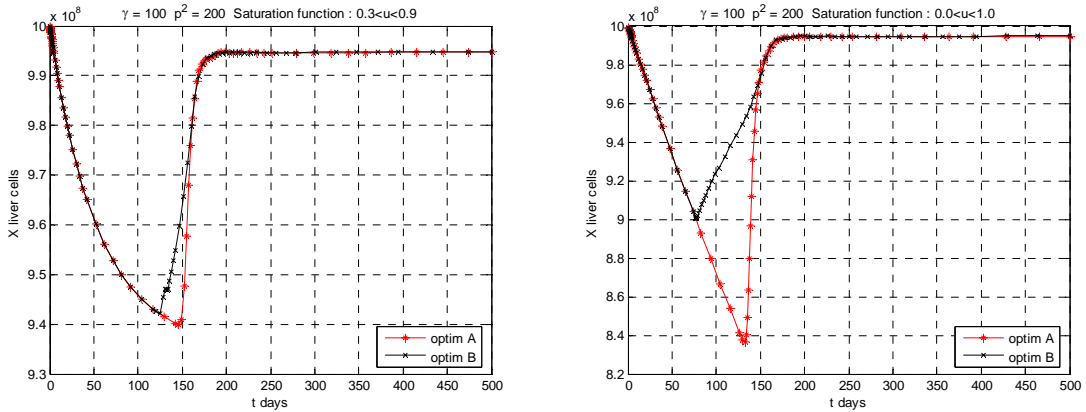


Figure 2.7: comparison of optimizations A and B for different saturation functions.

]

As seen in the case of $0.0 \leq u \leq 1.0$, the difference between the two types of optimization considered is small. The difference when $0.3 \leq u \leq 0.9$ is even smaller: the difference in the deviation of X from its maximum value X_{max} for A and B is not significant, because the applied chemotherapy is more severely constrained. However, when $0.3 \leq u \leq 0.9$ the largest deviation of X from its maximum value X_{max} (regardless of A or B approaches) is smaller than the one observed for $0.0 \leq u \leq 1.0$.

2.6 Conclusions

The simulation results presented in the previous section helped to illustrate the relevant behavior features of the optimization methods A and B, and also the effect of the associated chemotherapy parameters.

By taking a look at Figure 2.4, it can be demonstrated that an increase in the value of the penalty input parameter p causes a lower final T cell count but a higher final viral load. This is due to the fact that if p increases, high chemotherapy strength is penalized. Thus, the value of u is maintained at $u = 1$ for a shorter period of time. This is equivalent to a less aggressive therapy: even though there is a slight decline in the T cell count levels and a boost in the viral load, liver cell counts are slightly higher.

By taking a look at Figure 2.5, it can be shown that an increase in the value of the parameter γ also causes a decline in the T cell count levels as well as a boost in the viral load. Furthermore, high liver cell counts are reached faster. This is due to the fact that the speed of the response is forced to approach the set point at a speed with proportionality constant $1/\gamma$. Consequently, greater values of γ will slow the response, driving the system further from the desired optimal values. This is equivalent to a less aggressive therapy: there is a decrease in the T cell count levels, an increase in the viral load, and liver cell counts are slightly higher.

The different approaches for the optimization of the drug schedule (A and B) illustrate the general behavior of the model and allow for several conclusions with respect to the specific problem of interest.

Because the optimization criteria in the optimization B account for side effects, liver cell counts (representing the drug toxicity) will reach regeneration in a faster way than in the approach A.

It can already be seen that the difference between the two optimization criteria is small. The difference lies in the length of time for which $u = 1$. Optimization B accounts for side effects, thus a high drug regimen can not be administered for too long. This results in a smaller largest deviation of X from its maximum value X_{max} : 8% instead of 10% as it can be seen on Figure 2.6 .

So, the optimization criteria used for the optimization B clearly limit liver cell depletion within a narrower range, and force liver cell dynamics to its original level, irrespective of the values of the parameters (input penalty p and speed γ).

This illustrate that it is possible to envisage drug regimen which would be efficient towards the disease, but which would minimize serious side effects.

Another interesting feature of the present study was to investigate the influence of the constraints on the proposed chemotherapy pattern. The choice for u to be constrained between 0 and 1.0 was dictated by its physical meaning: an efficacy is constrained between 0 and 100%. The choice for u to be constrained between 0.3 and 0.9 was dictated by pharmacokinetic studies.

A benefit of having a narrower range for u is that u is always related to the drug dose administered, as seen in the pharmacokinetic model section. This means that the fluctuations in the drug dosage regimen will be less dramatic, and easier to administer for a specific patient.

Considering Figure 2.7, it can be seen that there is no significant difference in the results obtained using the different saturation functions (in the constraints: $0.0 \leq u \leq 1.0$ and $0.3 \leq u \leq 0.9$), especially for T cell counts and viral load . However, there is definitely a

difference for the liver cell counts. When more drastic constraints are used in the derivation of the control law, liver cell depletion becomes less important:

_ For optimization A: the largest deviation of X from its maximum value X_{max} is of 6% when $0.3 \leq u \leq 0.9$, compared to 16% when $0.0 \leq u \leq 1.0$.

_ For optimization B : the largest deviation of X from its maximum value X_{max} is less than 6% when $0.3 \leq u \leq 0.9$, compared to 10% when $0.0 \leq u \leq 1.0$.

A slightly less aggressive drug regimen leads to the same performances in terms of slowing the progression of the disease, but generates less side effects.

2.7 Discussion

The global picture presents a tradeoff between efficiency towards the progression of the disease and side effects due to drug administration, as it was first presented by Camilo Velez Vega in 2002.

The question which arises is when is it more important to maintain slightly higher levels of uninfected T cells than high number of functional liver cells?

Indeed, this question arises for the practitioner as one of the reasons why there is a need to change a drug regimen: drug toxicity creates side effects that make it difficult for a patient to take the drugs, and regimen failure, which means that the drugs are not working well enough.

A useful strategy for graphical observation of the tradeoff between increased T cell levels and increased liver cell counts can be implemented following the methodology presented

by Kazantzis et al. (1999) : calculating a performance index $ISE = \int_0^{\infty} [y_{sp} - h(x(t))]^2 \cdot dt$

and infinity input norm $\|u\|_{\infty} = \sup_{t \in [0, \infty)} |u(t)|$ for each selection of p and γ . This analysis is

not developed here, since additional improvements need to be done on the model.

The practitioner criterion would reflect the question stated above, and dictate the drug regimen for a patient accordingly by manipulation of the tunable chemotherapy parameters. The optimal schedule suggested could be an optimization of type B with rather low p and γ , and $0.3 \leq u \leq 0.9$, so that liver cell counts are maintained within 10% of the maximum level, while T cell counts and viral load exhibit behaviors very close to a continuous maximum chemotherapy schedule.

However, the model which was used to represent HIV dynamics is rather simple compared to the more detailed and refined models developed recently, which account for

time varying parameters (Huang et al, 2003) or intracellular delays (Banks et al, 2002 or Nelson and Perelson, 2002)

The choice of this model for the study was motivated by simplicity, and it has also been studied previously by Denise Kirschner and her group for the purposes of developing an optimal chemotherapy strategy. However, some extra features were added, namely the incorporation of a side effect model and the idea of time-varying drug exposures.

The analysis presented using this model provides a simple framework for the testing and the development of an optimal chemotherapy strategy. However, its simplicity and a lack of an explicit integration of a variability factor amongst patients makes the model appropriate only for an insightful unraveling of basic trends during the administration stage of chemotherapy protocols, and should only be viewed as such from a clinical point standpoint. Further studies need to be conducted using a more sophisticated (mechanism, classes of drugs used...) model to represent HIV dynamics under antiretroviral therapy.

Also, a more realistic side effect model should be developed in order to account for other serious sources of drug toxicity which should be taken into account in such a chemotherapy optimization attempt.

The more complex the model is (HIV dynamics, side effects), the better the representation of the actual course of the disease is (more accurate). However, this represents a challenge since more sophisticated models contain a lot of parameters which need to be calibrated by the clinical practitioner since each patient has a particular sensitivity to drug administration.

REFERENCES

AIDSInfo Fact Sheets and Booklets , October 2004
from <http://www.aidsinfo.nih.gov/other/factsheet.asp>

Banks, H.T., Bortz, D.M., Holte, S.E. (2002) Incorporation of variability into the modeling of viral delays in HIV infection dynamics, *Mathematical Biosciences* 183 (2002) 63-91.

Highleyman Liz (April 1998), Side Effects associated with Anti-HIV drugs, *Bulletin of Experimental Treatments for AIDS*, April 1998
from: <http://www.sfaf.org/treatment/beta/b36/b36adverse.html>

Carr, Andrew and Cooper, David (2000), Adverse effects of antiretroviral therapy, *THE LANCET* **356** (October 21, 2000)

Dixit, N.M and Perelson, A.S. (2004), Complex patterns of viral load decay under antiretroviral therapy: influence of pharmacokinetics and intracellular delay, *Journal of Theoretical Biology* **226** (2004) 95-109.

Fister, K Renee, Lenhart, Suzanne and McNally, Joseph Scott (1998), Optimizing chemotherapy in an HIV model, *Electronic Journal of Differential Equations* **1998-32** (1998) 1-12

GlaxoSmithKline, Product Information for Retrovir® Oral. Website:
http://www.gsk.com/products/retrovir_us.htm

Huang, Y., Rosenkrantz, S.L. and Wu, H. (2003), Modeling HIV dynamics and antiviral response with consideration of time-varying drug exposures, adherence and phenotypic sensitivity, *Mathematical Biosciences* **184** (2003) 165-186.

Johns Hopkins University Division of Infectious Diseases and AIDS Service. R. Gandhi, J. G. Bartlett, M. Linkinhoker, May 1999

http://www.hopkins-aids.edu/hiv_lifecycle/hivcycle_txt.html

Kazantzis, N. and Kravaris, C. (1999). Energy-predictive control: a new synthesis approach for nonlinear process control, *Chemical Engineering Science* **54** (1999), 1697-1709.

Kirschner, D. and Webb, G.F. (1996), A model for treatment strategy in the chemotherapy of AIDS, *Bulletin of Mathematical Biology* **58-2** (1996) 367-390

Kirschner, D., Lenhart, S. and Serbin, S. (1997), Optimal control of the chemotherapy of HIV, *Journal of Mathematical Biology* (1997) **35**: 775-792.

Nelson, Patrick W., Perelson, Alan S. (2002) Mathematical analysis of delay differential equation models of HIV-1 infection, *Mathematical Biosciences* 179 (2002) 73-94.

Perelson, A., Kirschner D. and Deboer, R (1993), The dynamics of HIV infection of CD4⁺ T Cells, *Mathematical Biosciences* **114** (1993) 81-125.

Perelson, A.S. and Nelson, P.W. (1999), Mathematical Analysis of HIV-1 Dynamics in Vivo, *Society for Industrial and Applied Mathematics* **41-1** (1999) 3-44

Project Inform (1998), PI Perspective 25: Therapy Side Effects Update *Project Inform - September, 1998* from <http://www.aegis.com/pubs/projinform/1998/PI980906.html>

Velez Vega, C., (2002) *Optimization of antiretroviral therapy for HIV infected patients by simultaneous analysis of immune restoration and serious side effects*. Unpublished Masters thesis, Texas A&M University, Texas, USA.

NOMENCLATURE

C_{max}	Maximum allowable drug concentration
Cl	Systemic clearance
D_l	Doses
F	Absolute bioavailability
$f(x), g(x)$	Vector fields in standard state – space description of a continuous-time nonlinear system.
I_0, I_r	50% inhibitory concentrations (initial and after emergence of mutations)
K_1, K_2	Reaction Rates associated with HIV dynamics
k_{se}, k_r	Reaction rates associated with the side effects model
k_a, k_e	Reaction rates associated with the pharmacokinetics model
$L_f h(x)$	Lie derivative of the scalar field h with respect to the vector field f
N	Number of virions produced by T^{**}
r	Rate of T cell growth
s	Source term for T
T	Uninfected $CD4^+$ T Cells
T^*	Latently infected T cells
T^{**}	Actively infected T cells
T_{max}	Maximum T cell level
t_r	Time at which the resistant mutations dominate
u	Manipulated input
V	Viral load.
V_b	Blood volume
V_c	Apparent volume of distribution
X_{max}	Maximum number of liver cells

Greek letters:

μ_T	Death rate of T cells, unassociated with viral infection.
μ_b	Death rate of T cells associated with viral induced cell lysis
μ_v	Death rate of V
τ	Dosing interval
φ	Conversion factor between in vivo and in vitro studies

3 NONLINEAR DIGITAL CONTROL SYSTEMS FOR COMPLEX CHEMICAL PROCESSES

3.1 Introduction

Most textbooks about process control focus mainly on continuous systems although, in practice, controllers are implemented digitally (Bequette, 2003). The physical inputs and outputs are continuous, but manipulated input changes are made at discrete time intervals, and measured outputs are available at discrete sample times.

Two alternative approaches could be followed in the design of digital computer-control systems (Kazantzis and Kravaris, 1999) :

1. From a continuous-time model, synthesize a continuous-time controller in accordance to established methodologies. Then, discretize the developed controller, and implement it digitally through fast sampling, by applying the methodological principles of the discrete-equivalent design. (Franklin et al. ,1992)
This method is extensively used by control engineers.
2. From a continuous-time model, obtain a discrete-time process model. Then, synthesize a discrete-time controller (Franklin et al. ,1992, Soroush and Kravaris, 1992, Hernandez and Arkun, 1993).

The last approach deals right at the beginning with the issue of sampling. Furthermore, notice that both approaches introduce time-discretization at a certain stage, as Figure 3.1 illustrates.

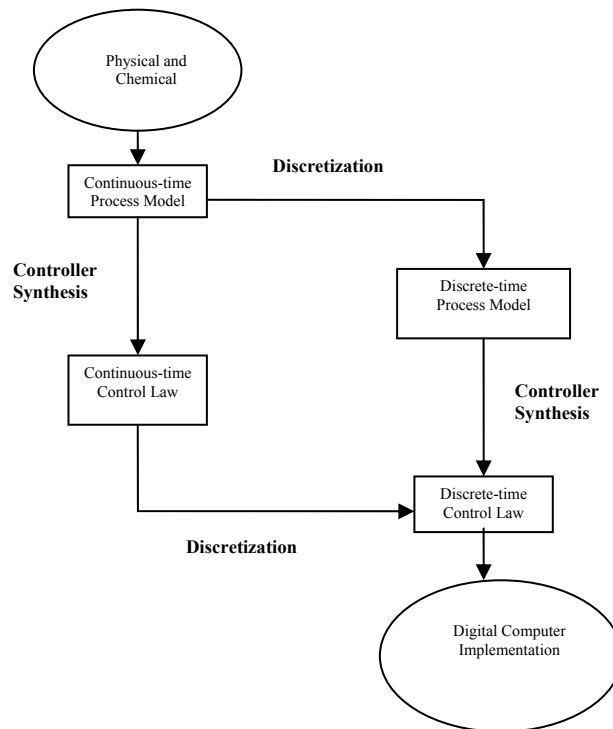


Figure 3.1 : Alternative approaches for the design of digital control systems.

(Kazantzis and Kravaris, 1999)

Time-discretization is a particularly challenging problem in the field of nonlinear systems. Traditional methods involve numerical simulation techniques such as Euler or Runge-Kutta, but the accuracy of the resulting approximate discrete-time system depends on the sampling period (Kazantzis and Kravaris, 1999).

The popularity of the Euler approximate discrete-time model for controller design can be attributed to the fact that it is the simplest approximate model that preserves the structure of the original continuous-time model (Nešić and Teel, 2004).

This however requires fast sampling, which can eventually become a problem since it may lead to nonminimum-phase behavior in discrete-time. On the other end of the sampling spectrum, large sampling periods may arise in many industrial control problems as either a technical or physical limitation on the system under consideration (Kazantzis and Kravaris, 1999, Nešić and Teel, 2004).

The proposed digital controller design methodology is a two-step one: first a discrete-time model is obtained using Euler's discretization method, and in a second step, a nonlinear controller is synthesized in the discrete-time domain. In particular, two approaches are followed and presented, that are both based on the methodological principles of Lyapunov design and relying on a short-horizon model-based prediction and optimization of the rate of "energy dissipation" of the system, as it is realized through the time derivative of an appropriately selected Lyapunov function. First, the Lyapunov function is computed by solving the discrete Lyapunov matrix equation (in a discrete-time analogy of Kazantzis and Kravaris, 1999). In the second approach, it is computed by solving a Zubov-like functional equation based on the system's drift vector field (in a discrete-time analogy of Dubljević and Kazantzis, 2002).

Two examples are considered that illustrate the proposed approach: a Van de Vusse chemical reaction system in a continuous-stirred tank reactor (CSTR), and a biochemical reaction scheme taking place in a biological CSTR.

3.2 Mathematical preliminaries

A comprehensive presentation of the subsequent theoretical developments requires a review of basic notions and techniques associated with Lyapunov stability analysis for nonlinear autonomous systems. In particular, the background presented here involves the application of Lyapunov's direct method to analyze the asymptotic stability characteristics around a reference equilibrium point as well as how to estimate the size of the stability region (Kazantzis and Kravaris, 1999).

3.2.1 Euler discretization

Consider the single input - single output nonlinear process with a state space description of the form:

$$\begin{aligned}\dot{x} &= f(x) + g(x) \cdot u \\ y &= h(x)\end{aligned}\tag{3.1}$$

where $x \in \mathfrak{R}^n$ is the vector of state variables, $u \in \mathfrak{R}$ is the manipulated input and $y \in \mathfrak{R}$ is the (controlled) output variable.

It is assumed that $f(x)$, $g(x)$ are smooth vector fields on \mathfrak{R}^n and $h(x)$ a smooth scalar field on \mathfrak{R}^n . For a fixed value of the output setpoint, y_{sp} , a reference equilibrium point (x_o, u_o) may now be defined:

$$\begin{aligned}0 &= f(x_o) + g(x_o) \cdot u_o \\ y_{sp} &= h(x_o)\end{aligned}\tag{3.2}$$

A sampled-data representation of system (1) can be obtained using Euler's discretization method and expressed in the following form:

$$\begin{aligned}x(k+1) &= x(k) + \delta \cdot [f(x(k)) + g(x(k)) \cdot u(k)] = \varphi(x(k), u(k)) \\ y(k) &= h(x(k))\end{aligned}\tag{3.3}$$

where δ is the sampling period. Please notice, that in order to ensure numerical stability and accuracy of the above discretization scheme, a typical value of δ selected is assumed to be between five and ten times smaller than the process dynamic constant:

$$\delta = \frac{1}{10 \cdot |\lambda_{\max}(A)|}, \text{ with } A \text{ being the Jacobian matrix at } (x_o, u_o).$$

It is easy to prove that the continuous-time system and the resulting discrete-time system have the same equilibrium characteristics, and therefore the same equilibrium manifold.

It is moreover assumed, that for the autonomous open-loop discrete system:

$$\begin{aligned}x(k+1) &= x(k) + \delta \cdot [f(x(k)) + g(x(k)) \cdot u_o] = \varphi(x(k)) \\ y(k) &= h(x(k))\end{aligned}\tag{3.4}$$

all the eigenvalues of the discrete Jacobian Matrix, $A_d = I + A \cdot \delta$, have magnitudes less than one, $|\lambda_i| < 1$ with $i=1..n$, where $A = \frac{\partial f(x_o)}{\partial x} + \frac{\partial g(x_o)}{\partial x} \cdot u_o$ and I is the identity matrix.

This is mathematically guaranteed if A is Hurwitz (stable process) and the discretization step small enough. It should be pointed out, that the above does not pose a restriction, since for an unstable process a pre-stabilizing controller can be used to render A Hurwitz. (Slotine and Li, 1991).

3.2.2 Quadratic Lyapunov function

Since A is assumed Hurwitz, one can invoke standard converse Lyapunov Theorems to prove the existence of a Lyapunov function $V(x)$ (Kazantzis and Kravaris, 1999).

Consider now the discrete quadratic Lyapunov function:

$$V(x(k)) = \frac{1}{2} (x(k) - x_o)^T \cdot P \cdot (x(k) - x_o)\tag{3.5}$$

where P is a positive definite symmetric matrix and the unique solution of the discrete Lyapunov equation (Elaydi, 1999):

$$A_d^T \cdot P \cdot A_d - P = -Q\tag{3.6}$$

with Q being a positive definite symmetric matrix.

The choice of Q is at this point arbitrary, but it may be proven that for any $\gamma > 0$, there exists $\delta > 0$ such that the rate of change of the discrete Lyapunov function along the trajectory of the unforced system (3.4) satisfies the following inequality:

$$\Delta V(x(k)) \leq \left(-\lambda_{\min}(Q) + \gamma^2 \cdot \lambda_{\max}(P) + 2\gamma \cdot \|P \cdot A_d\| \right) \cdot \|x - x_o\|_2^2 \quad (3.7)$$

$$\text{Choosing: } -\lambda_{\min}(Q) + \gamma^2 \cdot \lambda_{\max}(P) + 2\gamma \cdot \|P \cdot A_d\| < 0 \quad (3.8)$$

it is ensured that $\Delta V(x(k))$ is negative definite for all x in : $\|x - x_o\|_2 < \delta$, and according to Lyapunov's direct method, the equilibrium point x_o is locally asymptotically stable.

Typically, as in the present study, we choose $Q^* = I$ (Khalil, 2001).

3.2.3 Zubov's method

Consider now the following functional equation:

$$\begin{aligned} V(x(k+1)) - V(x(k)) &= -Q(x(k)) \Leftrightarrow V(\varphi(x)) - V(x) = -Q(x) \\ V(x_o) &= 0 \end{aligned} \quad (3.9)$$

where $V : \mathfrak{R}^n \rightarrow \mathfrak{R}$ is the unknown solution, and $Q(x)$ is a positive definite real analytic scalar function defined on \mathfrak{R}^n with $Q(x_o) = 0$ and $\left(\frac{\partial Q}{\partial x} \right)_{x_o} = 0$.

Notice that, by construction, the rate of change $\Delta V(x(k))$ is negative definite since $Q(x)$ is positive definite:

$$\Delta V(x(k)) = V(x(k+1)) - V(x(k)) = V(\varphi(x(k))) - V(x(k)) = -Q(x(k)) < 0 \quad (3.10)$$

Therefore, $V(x)$ is a suitable Lyapunov function candidate for the autonomous system (3.4). In such a case, the stability property of dynamics (3.4) and standard converse Lyapunov stability theorems for nonlinear discrete dynamical systems imply the existence of a Lyapunov function that satisfies the functional equation (3.9).

It should be emphasized that the above construction represents exactly the discrete-time analog of Zubov's PDE, which was developed for the explicit computation of Lyapunov functions for nonlinear dynamical systems modeled through ODEs in the continuous-time domain.

3.2.3.1 Existence and uniqueness of solution

Theorems (O'Shea, 1964, Kazantzis, 2001, Kazantzis & Kravaris, 2001 and Kazantzis, 2002) guarantee the existence and uniqueness of a locally analytic solution $V(x)$ of the functional equation (3.9) in the vicinity of the reference equilibrium point x_o .

3.2.3.2 Solution method

Since $\varphi(x)$, $Q(x)$ and the solution $V(x)$ are locally analytic, it is possible to calculate the solution $V(x)$ as a multivariate Taylor series around the equilibrium point of interest $x=x_o$.

The proposed solution method can be realized through the following steps (as a discrete-time analogy of Kazantzis et al., 2005):

- _ Expand $\varphi(x)$, $Q(x)$ and the unknown solution $V(x)$ in multivariate Taylor series and insert them into functional equation (3.9).
- _ Equate the Taylor coefficients of the same order of both sides of functional equation (3.9).
- _ Derive a hierarchy of linear recursion formulas through which it is possible to calculate the N^{th} order coefficient of $V(x)$ given the Taylor coefficients up to order $N-1$ that have been computed in previous recursive steps.

It is possible to explicitly derive the aforementioned recursive formulas and present them in a mathematically compact form if tensorial notation is used:

- _ the partial derivatives of the μ -th component $f_\mu(x)$ of a vector function $f(x)$ evaluated at $x=x_o$ are denoted as follows:

$$\begin{aligned}
 f_{\mu}^i &= \frac{\partial f_{\mu}}{\partial x_i}(x_0) \\
 f_{\mu}^{ij} &= \frac{\partial^2 f_{\mu}}{\partial x_i \partial x_j}(x_0) \\
 f_{\mu}^{ijk} &= \frac{\partial^3 f_{\mu}}{\partial x_i \partial x_j \partial x_k}(x_0) \quad , \text{ etc....}
 \end{aligned}
 \tag{3.11}$$

_ the standard summation convention where repeated upper and lower tensorial indices are summed up.

Under the above notation, the unknown solution $V(x)$ of the functional equation (3.9) represented as a multivariate Taylor series has the following form:

$$\begin{aligned}
 V(x) &= \frac{1}{1!} V^{i_1}(x_{i_1} - x_{i_{1,0}}) + \frac{1}{2!} V^{i_1 i_2}(x_{i_1} - x_{i_{1,0}})(x_{i_2} - x_{i_{2,0}}) + \dots + \\
 &+ \frac{1}{N!} V^{i_1 i_2 \dots i_N}(x_{i_1} - x_{i_{1,0}}) \dots (x_{i_N} - x_{i_{N,0}})
 \end{aligned}
 \tag{3.12}$$

As mentioned above, the Taylor series expansions of $\varphi(x)$, $Q(x)$ and $V(x)$ are inserted into functional equation, and the coefficients of the same order are equated.

Since $Q(x_0) = \frac{\partial Q}{\partial x}(x_0) = 0$, $V(x)$ does not have linear terms in x : $\frac{\partial V}{\partial x}(x_0) = 0$, or equivalently : $V^{i_1} = 0$ for $i_1 = 1, \dots, n$.

Furthermore, the following relation for the N -th order coefficients can be obtained:

$$\sum_{L=1}^N \sum_{\substack{0 \leq m_1 \leq \dots \leq m_L \\ m_1 + m_2 + \dots + m_L = N}} V^{j_1 \dots j_L} \varphi_{j_1}^{m_1} \dots \varphi_{j_L}^{m_L} = -Q^{i_1 \dots i_L}
 \tag{3.13}$$

where $i_1, \dots, i_N = 1, \dots, n$ and $N \geq 2$.

Note that the second summation symbol in the above expression means summing up the

relevant quantities over the $\frac{N!}{m_1! \dots m_L!}$ possible combinations to assign the N indices

(i_1, \dots, i_N) as upper indices to the L positions $\varphi_{j_1} \dots \varphi_{j_L}$ with m_l of them being put in the

first position, m_2 of them in the second position, etc $\left(\sum_{i=1}^L m_i = N \right)$.

It is important to notice that the above expression represents a set of linear algebraic equations in the unknown coefficients V^{i_1, \dots, i_N} . This is precisely the mathematical reason that enables the proposed method to be easily implemented using a symbolic software package.

Indeed, a MAPLE code has been developed to automatically compute the Taylor coefficients of the unknown solution $V(x)$ of the Zubov-like functional equation (3.9) for the examples studied later.

3.2.3.3 Local positive-definiteness of the solution $V(x)$

Let:

$$\begin{aligned}\varphi(x) &= x_0 + A \cdot (x - x_0) + \bar{\varphi}(x) \\ Q(x) &= (x - x_0)^T \cdot Q \cdot (x - x_0) + \bar{Q}(x)\end{aligned}\tag{3.14}$$

with $\bar{\varphi}(x)$ and $\bar{Q}(x)$ real analytic and : $\bar{\varphi}(x_0) = \bar{Q}(x_0) = \frac{\partial \bar{\varphi}}{\partial x}(x_0) = \frac{\partial \bar{Q}}{\partial x}(x_0) = 0$

Furthermore, the solution $V(x)$ can be represented as follows:

$$V(x) = (x - x_0)^T \cdot P \cdot (x - x_0) + \bar{V}(x)\tag{3.15}$$

$$\text{where } \bar{V}(x_0) = \frac{\partial \bar{V}}{\partial x}(x_0) = \frac{\partial^2 \bar{V}}{\partial x^2}(x_0) = 0\tag{3.16}$$

Thus, that matrix P satisfies the following Lyapunov matrix equation:

$$A^T \cdot P \cdot A - P = -Q\tag{3.6}$$

This coincides with the one encountered in the linear case. Under the assumptions stated, the above matrix equation admits a unique, positive-definite and symmetric solution P , and therefore, $V(x)$ is locally positive definite and a Lyapunov function for the controlled system dynamics.

3.2.4 Quadratic estimates of the stability region

It has already been shown that in a small neighborhood of the equilibrium point x_o , $\Delta V(x(k))$ is a negative definite quadratic function. Note that if $\Delta V(x(k)) < 0$ in the entire state-space, then global asymptotic stability is established for system (3.4). Assuming that $\Delta V(x(k))$ is a continuous function that changes sign at certain points in state-space, we may conclude that there will be a set of points M_{ol} , where $\Delta V(x(k))$ vanishes:

$$M_{ol} = \{x \in \mathfrak{R}^n \mid \Delta V(x(k)) = 0\} \quad (3.17)$$

Moreover, it is assumed that the change of sign for $\Delta V(x(k))$ occurs at the above set of points. Consider now a point \hat{x} in M_{ol} with its distance from x_o being minimum:

$$\min_{x \in M_{ol}} \|x - x_o\|_2 = \|\hat{x} - x_o\| = d_{\min} \quad (3.18)$$

Points having this property can be found either:

- (i) by numerically solving the following nonlinear programming problem:

$$\min_{x \in M_{ol}} \|x - x_o\|_2 \text{ subject to the following set of constraints } \Delta V(x(k)) = 0, \quad x \neq x_o$$

or:

- (ii) for a 2-dimensional system, by plotting the $\Delta V(x(k)) = 0$ and $V(x(k)) \leq c$ surfaces and graphically extracting the necessary information.

The largest ball $B(d_{\min})$ in which $\Delta V(x(k))$ is negative definite, is tangent to the $\Delta V(x(k)) = 0$ surface at \hat{x} (Perlmutter, 1972):

$$B(d_{\min}) = \{x \in \mathfrak{R}^n \mid \|x - x_o\|_2 \leq d_{\min}\} \quad (3.19)$$

A positively invariant set Ω_c is now sought, in order to provide a simple estimate of the stability region. For a quadratic Lyapunov function (3.5), a set that exhibits the desired properties is:

$$\Omega_c = \{x \in \mathfrak{R}^n \mid V(x(k)) \leq c\} \quad (3.20)$$

whenever Ω_c is constrained in $B(d_{\min})$.

$$\text{For } \Omega_c \text{ to be a subset of } B(d_{\min}), \text{ one can choose: } c < \lambda_{\min}(P) \cdot d_{\min}^2 \quad (3.21)$$

(Khalil, 2001).

We conclude that for a selection of the matrix $Q^* = I$ and the corresponding matrix P , solution of the discrete Lyapunov matrix equation, a simple quadratic estimate of the stability region can be provided by the set Ω_c , with c satisfying the inequality (3.21).

Remark: The results in this section have been presented in reference to the open-loop system. Because this analysis is generic in nature, it will also be used later on for the closed-loop system resulting from the application of the control law, which will be derived in the next section.

3.3 Formulation of the energy-predictive control problem and derivation of the control law

Soroush and Kravaris addressed the derivation of a continuous-time, nonlinear control law for an open-loop single-input single-output process through a model predictive approach which minimizes an appropriate quadratic performance index, which contains both an error term accounting for the mismatch between the predicted output and a desired reference trajectory, as well as an input penalty term (Soroush & Kravaris, 1996).

Similar ideas will influence the development of a digital energy-predictive control scheme in our approach.

The discrete Lyapunov function $V(x(k))$ is associated with the "unforced" autonomous system (3.4). The field of mechanics postulates that the energy content of a mechanical system driven by an external frictional force can be realized through an energy function that corresponds to its autonomous dynamics and it is a monotonically decreasing function of time (Goldstein, 1980). In our case, the frictional force is the input variable: unexpected disturbances drive the system far from the design steady state conditions, and the objective is to derive a control law driving the system back to the desired steady state in a smooth, fast and reliable fashion.

In light of the above considerations and within a similar in spirit framework of analysis to the one presented in (Kazantzis, N. and Kravaris, C. 1999), the ensuing theoretical developments are feasible.

Assuming that the full state-vector is measurable and $L_g V(x) \neq 0$ (relative degree $r = 1$), the derivation of a simple and explicit short-horizon prediction equation for $V(x(k))$ can be obtained by using Taylor series.

In particular, the following prediction equation for $V(x(k))$ is valid for the small time interval $[t_o, t]$, with $t_o = k_o \delta$ and $t = (k_o + 1)\delta$ such that the sampling period $\delta = |t - t_o| \ll 1.0$.

$$V(x(k_o + 1)) = V(x(k_o)) + [L_f V(x(k_o)) + u(k_o) \cdot L_g V(x(k_o))] \cdot \delta + o(\delta^2) \quad (3.22)$$

Eq (14) implies that:

$$\Delta V(x(k)) = V(x(k_o + 1)) - V(x(k_o)) = [L_f V(x(k_o)) + u(k_o) \cdot L_g V(x(k_o))] \cdot \delta \quad (3.23)$$

As the above equation indicates, for a given point $t_o = k_o \delta$, the manipulated input $u(k_o)$ directly affects the speed of evolution of $V(x(k))$. Keeping in mind that a quadratic

Lyapunov function can be viewed as a suitable measure of the distance between the current position of the system in state-space and the equilibrium point x_o , the speed of its evolution in time can provide a measure of the speed of the system's response as it approaches x_o . Since the manipulated input u directly influences the speed of the evolution of $V(x(k))$, an optimization problem can be formulated in order to synthesize an optimal control law that enforces the system's Lyapunov function to evolve according to a prescribed dynamic fashion, such that the desired trajectory is postulated as follows:

$$\begin{cases} \frac{dV_d(t)}{dt} = -a^2 V_d(t) \\ V_d(t_o) = V(x(t_o)) \end{cases} \Rightarrow \begin{cases} V_d(x(k_o + 1)) = V_d(x(k_o)) \cdot (1 - a^2 \delta) + o(|\delta^2|) \\ V_d(x(k_o)) = V(x(k_o)) = V(x(k_o)) \end{cases} \quad (3.24)$$

where $V_d(x(k))$ is a reference trajectory, evolving with a speed of a^2 . Using appropriate terminology from the field of mechanics, the dynamic equation (3.24) essentially describes the desirable rate of energy dissipation of the system.

The $o(|\delta^2|)$ truncation of equation (3.24) leads to:

$$V_d(x(k_o + 1)) = V(x(k_o)) \cdot (1 - a^2 \delta) \quad (3.25)$$

A quadratic performance index that consists of an error term accounting for the mismatch between the predicted behavior of $V(x(k))$ and the reference trajectory $V_d(x(k))$, as well as an input penalty term is proposed. The optimization problem has the following simple structure:

$$\min_{u(k_o) \in \mathfrak{R}} \left\{ \|V(x(k_o + 1)) - V_d(x(k_o + 1))\|^2 + q^2 \|u(k_o) - u_o\|^2 \right\} \quad (3.26)$$

subject to the constraints: $u_{\min} \leq u \leq u_{\max}$

where $\|\bullet\|$ is any function norm over a finite and small time interval for which the short-horizon prediction equation (3.22) is fairly accurate. Note that u_o is the equilibrium value of the manipulated input, which is determined by the set point $y_{sp} : u_o = u_o(y_{sp})$.

Inserting expressions (3.22) and (3.25) for $V(x(k))$ and $V_d(x(k))$ respectively into (3.26) gives:

$$\begin{aligned}
 & \min_{u(k_o) \in \mathfrak{R}} \left\{ \|V(k_o + 1) - V_d(k_o + 1)\|^2 + q^2 \|u(k_o) - u_o\|^2 \right\} \\
 &= \min_{u(k_o) \in \mathfrak{R}} \left\{ \left\| (1 - a^2 \delta)V(k_o) - V(k_o) - [L_f V(k_o) + u(k_o)L_g V(k_o)] \cdot \delta \right\|^2 + q^2 \|u(k_o) - u_o\|^2 \right\} \\
 &= \min_{u(k_o) \in \mathfrak{R}} \left\{ \left\| -a^2 \delta \cdot V(k_o) - [L_f V(k_o) + u(k_o)L_g V(k_o)] \cdot \delta \right\|^2 + q^2 \|u(k_o) - u_o\|^2 \right\} \\
 &= \min_{u(k_o) \in \mathfrak{R}} \left\{ \left\| a^2 \delta \cdot V(k_o) + [L_f V(k_o) + u(k_o)L_g V(k_o)] \cdot \delta \right\|^2 + q^2 \|u(k_o) - u_o\|^2 \right\} \\
 &= \min_{u(k_o) \in \mathfrak{R}} \left\{ \left\| \delta \cdot (a^2 \cdot V(k_o) + [L_f V(k_o) + u(k_o)L_g V(k_o)]) \right\|^2 + q^2 \|u(k_o) - u_o\|^2 \right\} \\
 &= \min_{u(k_o) \in \mathfrak{R}} \left\{ \|\delta\|^2 \cdot \left\| a^2 \cdot V(k_o) + [L_f V(k_o) + u(k_o)L_g V(k_o)] \right\|^2 + q^2 \|u(k_o) - u_o\|^2 \right\} \\
 &= \min_{u(k_o) \in \mathfrak{R}} \left\{ \left\| a^2 \cdot V(k_o) + [L_f V(k_o) + u(k_o)L_g V(k_o)] \right\|^2 + q^2 / \|\delta\|^2 \|u(k_o) - u_o\|^2 \right\}
 \end{aligned}$$

The optimization problem takes the form:

$$\min_{u(k_o) \in \mathfrak{R}} \left\{ \left\| a^2 V(x(k_o)) + L_f V(x(k_o)) + u_o \cdot L_g V(x(k_o)) \right\|^2 + p^2 \|u(k_o) - u_o\|^2 \right\} \quad (3.27)$$

where $p^2 = q^2 / \delta^2$.

The above one-dimensional quadratic minimization problem is trivially solvable, with a solution of the following form:

$$u(k_o) = S[\Psi(x(k_o), V(x(k_o)))] \quad \text{where} \quad S[w] = \begin{cases} u_{\min} & \text{if } w < u_{\min} \\ w & \text{if } u_{\min} \leq w < u_{\max} \\ u_{\max} & \text{if } w \geq u_{\max} \end{cases} \quad (3.28)$$

$$\Psi(x(k_o), V(x(k_o))) = \frac{p^2 u_o(y_{sp}) - L_g V(x(k_o)) \cdot [L_f V(x(k_o)) + a^2 V(x(k_o))]}{p^2 + [L_g V(x(k_o))]^2}$$

$S[w]$ is called the saturation function.

Since the initial point $k_o = k$ is completely arbitrary, the following control law is then obtained, which will be applied at every time instant:

$$u(k) = S[\Psi(x(k), V(x(k)))] \quad \text{where} \quad S[w] = \begin{cases} u_{\min} & \text{if } w < u_{\min} \\ w & \text{if } u_{\min} \leq w < u_{\max} \\ u_{\max} & \text{if } w \geq u_{\max} \end{cases} \quad (3.29)$$

$$\Psi(x(k), V(x(k))) = \frac{p^2 u_o (y_{sp}) - L_g V(x(k)) \cdot [L_f V(x(k)) + a^2 V(x(k))]}{p^2 + [L_g V(x(k))]^2}$$

The above control law is a static feedback control law and contains two adjustable design parameters:

– a^2 that is associated with the rate of energy dissipation or the speed of the closed loop response, and

– p^2 that is associated with the size of the input excursion from the equilibrium value u_o .

Including input constraints in the control law may lead to a performance loss if the controller is not tuned appropriately. However, it allows the control law to take into account inherent technical and/or physical limitations of the process, and thus make it more meaningful.

In the absence of input constraints, the saturation function can be omitted. The resulting controller attains the following simpler form:

$$u(k) = \frac{p^2 u_o (y_{sp}) - L_g V(x(k)) \cdot [L_f V(x(k)) + a^2 V(x(k))]}{p^2 + [L_g V(x(k))]^2} \quad (3.30)$$

The effect of both tunable parameters on the closed-loop performance characteristics will be illustrated and discussed in a later section.

3.4 Properties of the control law

The investigation of the basic properties of the derived control law is presented in the absence of input constraints, that is omitting the saturation function.

3.4.1 Continuity property

Eq. (3.30) implies that the presence of p^2 in the denominator prevents the input variable $u(x(k))$ from becoming unbounded. This property distinguishes the proposed control law from the one based on exact input/output linearization or model predictive control without input penalty. Notice, that this property holds true even in the presence of input constraints.

3.4.2 Equilibrium properties of the closed-loop system

Under the control law (3.30), the closed-loop system is:

$$\begin{aligned} x(k+1) &= x(k) + \delta \cdot \left[f(x(k)) + g(x(k)) \cdot \frac{p^2 u_o(y_{sp}) - L_g V(x(k)) \cdot [L_f V(x(k)) + a^2 V(x(k))]}{p^2 + [L_g V(x(k))]^2} \right] \\ y(k) &= h(x(k)) \end{aligned} \quad (3.31)$$

And in particular for $V(x(k))$ given in Eq (3.5):

$$\begin{aligned}
 x(k+1) &= x(k) + \delta \cdot [f(x(k)) + g(x(k)) \cdot u(k)] \\
 u(k) &= \frac{p^2 u_o(y_{sp}) - 0.5(x(k) - x_o)^T \cdot P \cdot g(x(k)) \cdot [0.5(x(k) - x_o)^T \cdot P \cdot f(x(k)) + 0.5a^2(x(k) - x_o)^T \cdot P \cdot (x(k) - x_o)]}{p^2 + [0.5(x(k) - x_o)^T \cdot P \cdot g(x(k))]^2} \\
 y(k) &= h(x(k))
 \end{aligned}$$

It is seen that the point (x_o, u_o) is still an equilibrium point for the closed-loop system, and therefore, the control law (3.30) induces unity static gain at equilibrium $y = y_{sp}$. Furthermore, it can be easily shown, that this property holds true even in the presence of input constraints.

3.4.3 Local asymptotic stability of the closed-loop system

The rate of change of the scalar function $V(x(k))$ in the discrete-time domain along the trajectories of the closed-loop system (3.31) is given by:

$$\begin{aligned}
 \Delta V(x(k)) &= V(x(k+1)) - V(x(k)) \\
 &= \left[L_f V(x(k)) + \frac{p^2 u_o(y_{sp}) - L_g V(x(k)) \cdot [L_f V(x(k)) + a^2 V(x(k))]}{p^2 + [L_g V(x(k))]^2} \cdot L_g V(x(k)) \right] \cdot \delta \\
 &= \left[L_f V(x(k)) + u_o L_g V(x(k)) - \frac{[L_g V(x(k))]^2}{p^2 + [L_g V(x(k))]^2} [L_f V(x(k)) + u_o L_g V(x(k)) + a^2 V(x(k))] \right] \cdot \delta
 \end{aligned} \tag{3.32}$$

Recall that stability analysis performed on the open-loop system indicated that for sufficiently small $\|x - x_o\|_2 \ll 1$ and $\delta \ll 1$, $L_f V(x(k)) + u_o \cdot L_g V(x(k))$ behaves as a negative definite quadratic function.

Since $\frac{[L_g V(x(k))]^2}{p^2 + [L_g V(x(k))]^2}$ is a smooth scalar field on \mathfrak{R}^n that vanishes at $x = x_o$, the quantity:

$$\frac{[L_g V(x(k))]^2}{p^2 + [L_g V(x(k))]^2} [L_f V(x(k)) + u_o L_g V(x(k)) + a^2 V(x(k))] \text{ is of the order of } o(\|x - x_o\|_2^3).$$

Therefore, for sufficiently small $\|x - x_o\|_2 \ll 1$ and $\delta \ll 1$, $\Delta V(x(k))$ is negative definite, and locally, internal asymptotic for the closed-loop system is established.

Since, closed-loop internal stability considerations play the key role in the development of efficient nonminimum-phase compensation methods, the proposed control law can be implemented efficiently to digital control systems. The above stabilization property becomes particularly important for the (digital) nonminimum-phase compensation problem in the discrete-time domain, due to the well-known effect of sampling on the stability characteristics of zero-dynamics, and thus, the possibility of a continuous-time minimum-phase process to become nonminimum-phase under fast sampling and within a digital control system design framework .

3.4.4 Enlargement of the stability region in closed-loop

Evaluating the rate of change of the scalar function $V(x(k)), \Delta V(x(k))$, in the discrete-time domain along a trajectory of the closed-loop system, it was shown that in a small neighborhood of x_o , $\Delta V(x(k))$ behaves as a negative definite quadratic function. If $\Delta V(x(k))$ does not change sign in the entire state-space, then the control law enforces asymptotic stability in the large.

It is now assumed that $\Delta V(x(k))$ is a continuous function that changes sign at certain points in state-space.

A new set M_{cl} may now be defined for the closed-loop system, containing the points at

$$\text{which } \Delta V_{cl}(x(k)) \text{ vanishes: } M_{cl} = \{x \in \mathfrak{R}^n \mid \Delta V_{cl}(x(k)) = 0\} \quad (3.33)$$

It is moreover assumed that at the points contained in M_{cl} , $\Delta V_{cl}(x(k))$ changes sign.

The analysis that follows will prove that the distance of any point of the set M_{cl} from x_o (closed-loop system), is larger than the corresponding distance of any point in M_{ol} (open-loop system).

According to the methodology developed in Section II, this will lead to the conclusion that the proposed control law possesses the property of enlarging the quadratic estimates of the stability region.

As it was previously shown, the zero points of $\Delta V(x(k))$ for the open-loop system are given by:

$$\begin{aligned} \Delta V_{ol}(x) = 0 &\Rightarrow \frac{\Delta V_{ol}(x)}{\delta} = 0 \\ M_{ol} &= \left\{ x \in \mathfrak{R}^n \mid \frac{\Delta V_{ol}(x)}{\delta} = L_f V(x) + u_o L_g V(x) = 0 \right\} \end{aligned} \quad (3.34)$$

For the closed-loop system, the points at which $\Delta V(x(k))$ vanishes are given by:

$$\begin{aligned} \Delta V_{cl}(x) = 0 &\Rightarrow \frac{\Delta V_{cl}(x)}{\delta} = L_f V(x) + u_o L_g V(x) - \frac{a^2}{p^2} [L_g V(x)]^2 \cdot V(x) = 0 \\ &= M_{ol}(x) - \Theta_r(x) = 0 \\ M_{cl} &= \left\{ x \in \mathfrak{R}^n \mid M_{ol}(x) - \Theta_r(x) = 0 \right\} \end{aligned} \quad (3.35)$$

where $\Theta_r(x) = \frac{a^2}{p^2} [L_g V(x)]^2 \cdot V(x) = \frac{1}{r_d} [L_g V(x)]^2 \cdot V(x) > 0$ and $r_d = \left(\frac{p}{a}\right)^2 = \left(\frac{q}{a \cdot \delta}\right)^2 = \frac{r_c}{\delta^2}$

Let a be a zero of $M_{ol}(x)$: $M_{ol}(a) = 0$

Since $\Theta_r(x) > 0$, it can be easily deduced that: $M_{cl}(x) = M_{ol}(x) - \Theta_r(x) < 0$ for any x that satisfies $\|x - x_o\|_2 < \|a - x_o\|_2$. Then, the control law (3.29) leads to global asymptotic stability for the closed-loop system.

If for some c with $\|c - x_o\|_2 > \|a - x_o\|_2$, $M_{cl}(c) = M_{ol}(c) - \Theta_r(c) > 0$,

then there exists a point b which satisfies: $M_{cl}(b) = M_{ol}(b) - \Theta_r(b) = 0$ with $\|c - x_o\|_2 > \|b - x_o\|_2 > \|a - x_o\|_2$.

As a result, the control law (3.30) causes in this case an enlargement of the quadratic estimate of the stability region.

Remark: Note that if for the open-loop system, x_o is globally asymptotically stable: $M_{ol}(x) < 0$ for any $x \in \mathfrak{R}^n$, it is also globally asymptotically stable for the closed-loop system under the control law (3.30), since $\Theta_r(x) > 0$.

Eq. (3.34) indicates that the ratio of the two adjustable parameters of the control law (3.30), $r_d = \left(\frac{p}{a}\right)^2$, influences the quadratic estimate of the closed-loop stability region.

As the ratio r_d decreases, the magnitude of the negative term ($-\Theta_r(x) < 0$) in Eq. (3.35) increases, leading to an increase of the size of the quadratic estimate of the stability region.

Indeed, let $r' < r$ and

$$M_{cl}(b) = M_{ol}(b) - \Theta_r(b) = 0, \quad (3.36)$$

$$M_{cl}(c) = M_{ol}(c) - \Theta_{r'}(c) = 0 \quad (3.37)$$

with $b \neq c$. Suppose that $\|c - x_o\|_2 < \|b - x_o\|_2$. This would imply that:

$$M_{cl}(c) = M_{ol}(c) - \Theta_r(c) < 0. \quad (3.38)$$

$$\text{Since } \Theta_r(c) < \Theta_{r'}(c), \text{ inequality (3.37) yields: } M_{cl}(c) = M_{ol}(c) - \Theta_{r'}(c) < 0. \quad (3.39)$$

The latter result is in contradiction with Eq. (3.37). Therefore, $\|c - x_o\|_2 > \|b - x_o\|_2$, resulting in a larger quadratic estimate of the stability region.

3.4.5 Synthesis of a dynamic output feedback controller

The synthesis of output feedback controllers for open-loop stable processes can be realized as a combination of state feedback control laws and open-loop state observers. Indeed, all states variables are rarely available for direct online measurement.

For the case of an open-loop stable process, the unmeasurable states can be reliably estimated through online simulation of the process dynamics:

$$w(k+1) = w(k) + [f(w(k)) + g(w(k)) \cdot u(w(k))] \cdot \delta \quad (3.40)$$

By combining the state feedback control law (3.30) with the observer dynamics (3.40) that reconstructs possibly unmeasurable states, a realization for a dynamic output feedback controller is obtainable:

$$\begin{aligned} w(k+1) &= w(k+1) + \delta \cdot [f(w(k)) + g(w(k)) \cdot u(k)] \\ u(k) &= \frac{p^2 u_o(e + h(w(k))) - L_g V(w(k)) \cdot [L_f V(w(k)) + a^2 V(w(k))]}{p^2 + [L_g V(w(k))]^2} \\ e &= y_{sp} - y = y_{sp} - h(w(k)) \end{aligned} \quad (3.41)$$

The closed-loop system under the controller (3.41) takes the form:

$$\begin{aligned} x(k+1) &= x(k+1) + \delta \cdot \left[f(x(k)) + g(x(k)) \cdot \frac{p^2 u_o(y_{sp} - h(x(k)) + h(w(k))) - L_g V(w(k)) \cdot [L_f V(w(k)) + a^2 V(w(k))]}{p^2 + [L_g V(w(k))]^2} \right] \\ w(k+1) &= w(k+1) + \delta \cdot \left[f(w(k)) + g(w(k)) \cdot \frac{p^2 u_o(y_{sp} - h(x(k)) + h(w(k))) - L_g V(w(k)) \cdot [L_f V(w(k)) + a^2 V(w(k))]}{p^2 + [L_g V(w(k))]^2} \right] \\ y &= h(x(k)) \end{aligned} \quad (3.42)$$

Employing standard linear stability analysis, it is straightforward to show that the unforced closed-loop system ($y_{sp} = \text{constant}$) under the controller (3.41) is locally asymptotic stable. Algebraic details are omitted for brevity.

Notice that the controller (3.41) is a model-state feedback controller depicted in Fig. 3.2.

The main features and properties of the aforementioned controller structure have been identified and discussed in Coulibaly et al. (1992) and Kravaris et al. (1997).

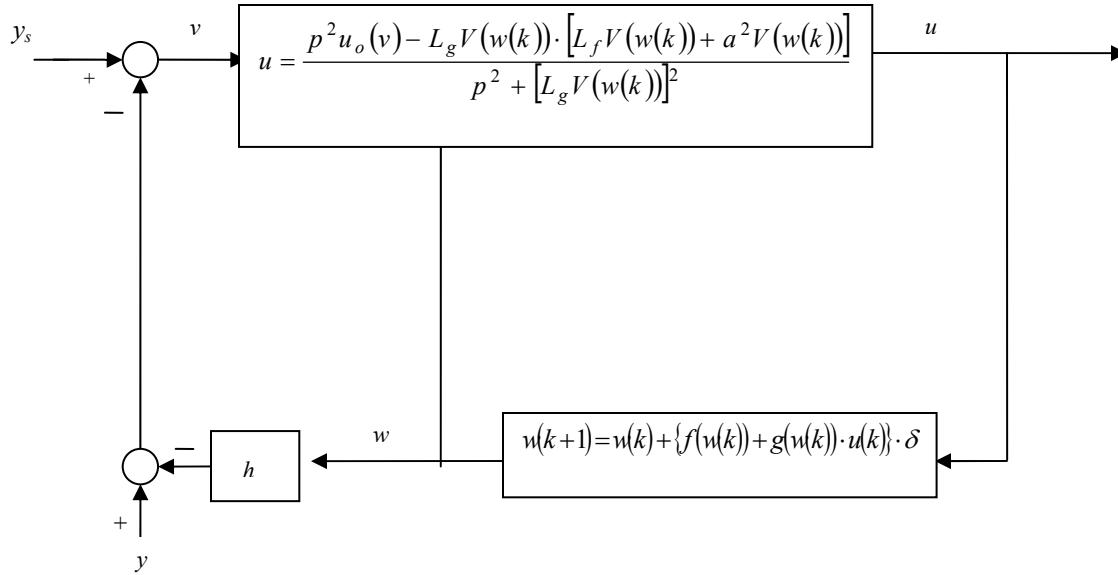


Figure 3.2: Model state feedback controller.
(adapted from Kazantzis and Kravaris, 1999)

3.5 Illustrative Example I: Van de Vusse Reaction in a CSTR

Consider a continuous stirred tank reactor, where the isothermal series/parallel Van de Vusse reaction (Wright and Kravaris, 1992) is taking place:

$$\begin{cases} A \xrightarrow{k_1} B \xrightarrow{k_2} C \\ 2A \xrightarrow{k_3} D \end{cases}$$

The desired product is the component B, the intermediate component in the series reaction. Klatt and Engel (1998) note that the production of cyclopentanol from cyclopentadiene is based on such a reaction scheme A = cyclopentadiene, B = cyclopentanol, C= cyclopentanediol, and D = dycyclopentadiene.

The rates of formation of species A and B are assumed to be:

$$\begin{aligned} r_a &= -k_1 C_a - k_3 C_a^2 \quad \text{where } k_1 = 50h^{-1} \quad k_2 = 100h^{-1} \quad k_3 = 10l(mol \cdot h)^{-1} \\ r_b &= k_1 C_b - k_2 C_b \end{aligned}$$

The feed stream consists of pure A. The mass balances for species A and B are given by:

$$\begin{aligned}
 V \frac{dC_a}{dt} &= F(C_{a0} - C_a) + V(-k_1 C_a - k_3 C_a^2) \\
 V \frac{dC_b}{dt} &= F(-C_b) + V(k_1 C_b - k_2 C_b)
 \end{aligned}
 \tag{3.43}$$

where F is the inlet flowrate of A, V is the reactor volume which is considered to be constant during the operation, C_a and C_b are the concentrations of the species A and B inside the reactor and $C_{a0} = 10 \text{ mol.l}^{-1}$ is the concentration of A in the feed stream.

We wish to maintain C_b at its set point, by manipulating the dilution rate F/V .

By letting:

$$x_1 = C_a, \quad x_2 = C_b, \quad u = F/V, \quad y = C_b$$

$$\begin{aligned}
 \frac{dx_1}{dt} &= -k_1 \cdot x_1 - k_3 \cdot x_1^2 + (x_{10} - x_1) \cdot u = f_1(x_1, x_2) + g_1(x_1, x_2) \cdot u \\
 \frac{dx_2}{dt} &= k_1 \cdot x_1 - k_2 \cdot x_2 - x_2 \cdot u = f_2(x_1, x_2) + g_2(x_1, x_2) \cdot u \\
 y &= x_2
 \end{aligned}
 \tag{3.44}$$

The system is initially at steady state with $x_{1,s} = 3.0 \text{ mol/l}$, $x_{2,s} = 1.117 \text{ mol/l}$, $u_s = 34.28 \text{ h}^{-1}$.

It is now assumed that the system is subjected to a negative step change in the set point value from 1.117 to 1.05 mol/l .

Accordingly, the new steady-state values are: $x_{10} = 2.697 \text{ mol/l}$, $x_{20} = y_{sp} = 1.05 \text{ mol/l}$, $u_0 = 28.4228 \text{ h}^{-1}$.

Furthermore, it can be shown that for the chosen set of process parameters and steady-state values the system is in the nonminimum-phase region (Wright & Kravaris, 1992).

For the unforced system ($u = u_0$), the Jacobian matrix A evaluated at $x = x_0$, is:

$$A = \begin{bmatrix} -132.3629 & 0.0 \\ 50.0 & -128.4229 \end{bmatrix}$$

The eigenvalues of A are: $\lambda = \begin{pmatrix} -128.4229 \\ -132.3629 \end{pmatrix}$,

which would lead to $\delta = \frac{1}{50|\lambda_{\max}(A)|} = 0.0001511 \text{ h}$.

For convenience, we select the discretization step to be: $\delta = 0.0001 h$.

In order to check if the sampling period δ is small enough to guaranty numerical stability and high accuracy of the resulting sampled-data representation, we will compare the open-loop responses of the original continuous-time system with the ones based on the sampled-data representation obtained using Euler's discretization method.

3.5.1 Open-loop Responses

A Matlab code (Matlab 7.0) was used for this comparison: the built-in ODE solver *ode15s* was used for the simulation using the continuous-time system.

$$\begin{aligned}\frac{dx_1}{dt} &= -k_1 \cdot x_1 - k_3 \cdot x_1^2 + (x_{1o} - x_1) \cdot u_0 = f_1(x_1, x_2) + g_1(x_1, x_2) \cdot u_0 \\ \frac{dx_2}{dt} &= k_1 \cdot x_1 - k_2 \cdot x_2 - x_2 \cdot u_0 = f_2(x_1, x_2) + g_2(x_1, x_2) \cdot u_0 \\ y &= x_2\end{aligned}\tag{3.45}$$

$$\begin{aligned}x(k+1) &= x(k) + \delta \cdot [f(x(k)) + g(x(k)) \cdot u_0] \\ y(k) &= h(x(k))\end{aligned}\tag{3.46}$$

In the case of an open-loop system, we chose the input to be equal to $u_0 = 28.4228 h^{-1}$.

The sampling period δ has been assumed to be less than fifty times smaller than the process dynamic constant, so that numerical stability is guaranteed.

$$\delta = \frac{1}{50 \cdot |\lambda_{\max}(A)|} = 0.00015 h \Rightarrow \delta = 0.0001 h.$$

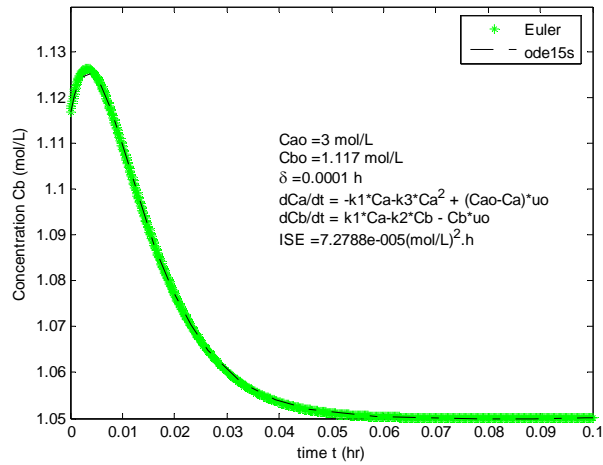


Figure 3.3. : Open-loop response: check for the sampling period of the discretization

The sampling period δ being small enough for the purposes of our study, will be considered in the sequel constant ($\delta = 0.0001 h$).

Table 3.1 summarizes the numerical values of the parameters which will be used in the present study.

Table 3.1: Numerical values of the Van de Vusse reaction in a CSTR

Parameter	Value
k_1	$50 h^{-1}$
k_2	$100 h^{-1}$
k_3	$10 l.(mol . h)^{-1}$
C_a^0 (inlet concentration of A)	$10 mol.l^{-1}$
y_{sp}	$1.05 mol.l^{-1}$
x_{10}	$2.697 mol.l^{-1}$
x_{20}	$1.05 mol.l^{-1}$
u_0	$28.4228 h^{-1}$
δ	$0.0001 h$

3.5.2 Estimation of the stability region size:

For $Q^* = I$, the discrete Lyapunov matrix equation (3.6) was solved in order to obtain the matrix P :

$$P = \begin{bmatrix} 40.86586 & 7.46553 \\ 7.46553 & 39.18495 \end{bmatrix}$$

The eigenvalues of P are: $\lambda(P) = \begin{pmatrix} 47.53809 \\ 32.51272 \end{pmatrix}$

P is indeed a symmetric, positive definite matrix.

The proposed quadratic Lyapunov function V is:

$$V(x) = 20.43293 \cdot (x_1 - 2.6969)^2 + 7.46553 \cdot (x_1 - 2.6969)(x_2 - 1.05) + 19.59248 \cdot (x_2 - 1.05)^2 \quad (3.47)$$

In Fig. 3.4., the variation of the size of the stability region with respect to the ratio r is graphically presented. The stability region estimates have been evaluated by following the standard methodology presented in section II.

A Maple code was used to graphically represent both the $\Delta V(x(k)) = 0$ and $V(x(k)) \leq c$ surfaces.

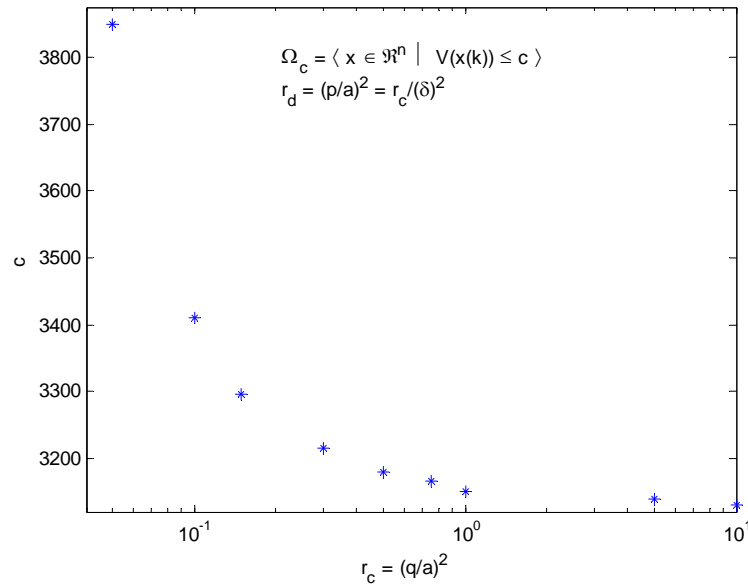


Figure 3.4: Variation of the size of the stability region with r.

As it is evident, the control law leads to an enlargement of the quadratic estimate of the size of the stability region, using the quadratic Lyapunov (3.47) and for decreasing values

of the ratio $r_d = \left(\frac{p}{a}\right)^2$.

3.5.3 Closed-loop Responses: The effect of the controller parameters a^2 and p^2

Let us now examine the closed-loop performance characteristics for the system under consideration, when the control law (3.29) is implemented and how they are influenced by the design parameters a^2 and p^2 .

The input constraints of the Saturation function in the controller (3.29) are defined as follows : $u_{\min} = 0$ and no u_{\max} . This leads to the following controller to be implemented in our system:

$$\begin{aligned}
 u(k) &= S[\Psi(x(k), V(x(k)))] \quad \text{where} \quad S[w] = \begin{cases} u_{\min} = 0 & \text{if } w < u_{\min} \\ w & \text{if } u_{\min} \leq w \end{cases} \\
 \Psi(x(k), V(x(k))) &= \frac{p^2 u_o (y_{sp}) - L_g V(x(k)) \cdot [L_f V(x(k)) + a^2 V(x(k))]}{p^2 + [L_g V(x(k))]^2}
 \end{aligned} \tag{3.48}$$

In the formulation of the optimization problem in Section III, the parameters a^2 and p^2 were associated with two main performance characteristics:

– a^2 : associated with the rate of energy dissipation or the speed of the closed loop response, that could be quantified through the ISE performance index:

$$ISE = \sum_{k=0}^{\infty} [y_{sp} - h(x(k))]^2 \cdot \delta \tag{3.49}$$

– p^2 : associated with the size of the input excursion from the equilibrium u_o , that could be quantified as follows:

$$\|u(k) - u_o\|_{\infty} = \sup_{k \in [0, \infty)} |u(k) - u_o| \tag{3.50}$$

As a^2 increases, the speed of the closed-loop response increases and the value of the ISE-index decreases. Moreover, since the increase of parameter a^2 leads to a more aggressive controller, one intuitively expects larger input excursions from the value u_o . With regard to the p^2 parameter, an increase of p^2 would penalize input deviations from u_o more severely and lead to larger value of the ISE-index, due to a more sluggish controller. Moreover, the augmentation of the closed-loop stability region favors the selection of a relatively large a^2 and/or a relatively small p^2 . It is therefore apparent that the conflicting nature of the effect of a^2 and p^2 on the closed-loop performance characteristics results in a trade-off type of decision making concerning the values of the parameters.

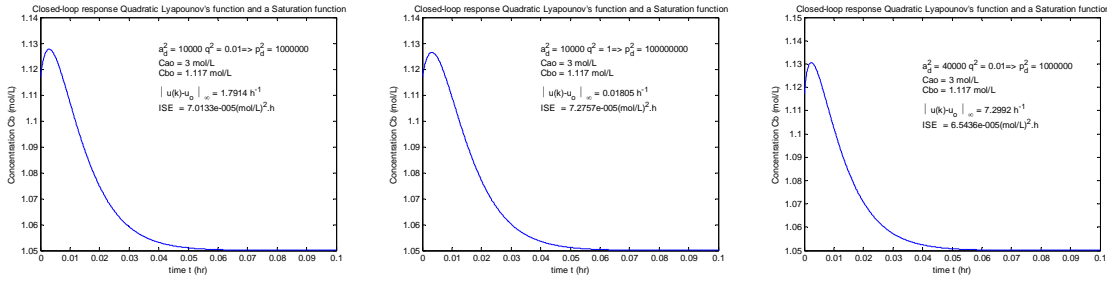


Figure 3.5: Closed-loop responses for different values of a^2 and p^2 .

Notice the manifestation of the nonminimum phase behavior as it is realized through the display of inverse response characteristics in Fig. 3.5.

The graphs in Fig. 5 depict the closed-loop responses for $a^2 = 10000$ and $q^2 = 0.01$, ($p^2 = q^2 / \delta^2$), $a^2 = 10000$ and $q^2 = 0.1$ and $a^2 = 40000$ and $q^2 = 0.01$ respectively.

As a^2 increases, the controller becomes more aggressive and consequently the ISE-index decreases, while input deviations from u_o become larger. If a larger value of p^2 were chosen, that would penalize deviations of u from u_o more severely, a more aggressive controller could be then tolerated and therefore an increase of the speed of the response by increasing a^2 could be sought.

As a result, there are alternate points in the parameter space (a^2, p^2) that entail similar closed-loop performance characteristics.

Now, the influence of the addition of the saturation function in the derivation of the controller will be investigated.

Consider now the input constraints of the saturation function in the controller (3.29) are as follows : $u_{\min} = 0$ and $u_{\max} = 60 \text{ h}^{-1} (\approx 2u_o)$. This leads to the following controller to be implemented in our system:

$$u(k) = S[\Psi(x(k), V(x(k)))] \quad \text{where} \quad S[w] = \begin{cases} 0 & \text{if } w < 0 \\ w & \text{if } u_{\min} \leq w < u_{\max} \\ 60 & \text{if } w \geq 60 \end{cases} \quad (3.51)$$

$$\Psi(x(k), V(x(k))) = \frac{p^2 u_o(y_{sp}) - L_g V(x(k)) \cdot [L_f V(x(k)) + a^2 V(x(k))]}{p^2 + [L_g V(x(k))]^2}$$

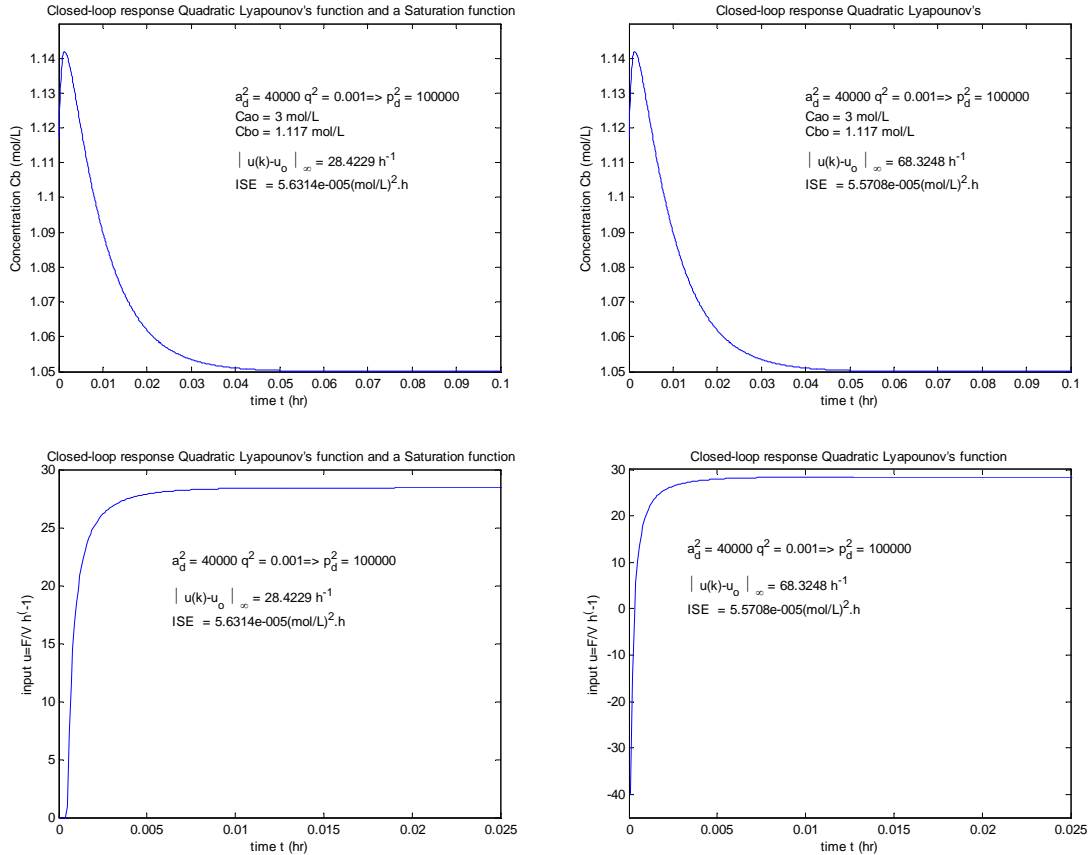


Figure 3.6: Comparison between two controllers: with and without input constraints.

The difference between the two graphs in Fig. 3.6 ($a^2=40000$, $q^2=0.001$) for the same values of the control parameters is the addition of input constraints in the formulation of the control law: the graphs on the left hand-side were obtained using the controller (3.51) with $u_{\min} = 0$ and $u_{\max} = 60 \text{ h}^{-1}$, whereas the ones on the right hand-side were obtained with the controller (3.30).

The input, u , can't be negative. Without this constraint, with ($a^2=40000$, $q^2=0.001$), we had $\|u(k)-u_o\|_{\infty} = 68.3248 \text{ h}^{-1}$, which means $u(k)$ being negative at some point.

This illustrates the point that including input constraints in the derivation of the control law allows to take into account limitations of the process.

However, as described in Fig. 3.7, including input constraints, especially drastic ones, can lead to a loss of performance when an aggressive controller is applied, since the input will hit the constraints.

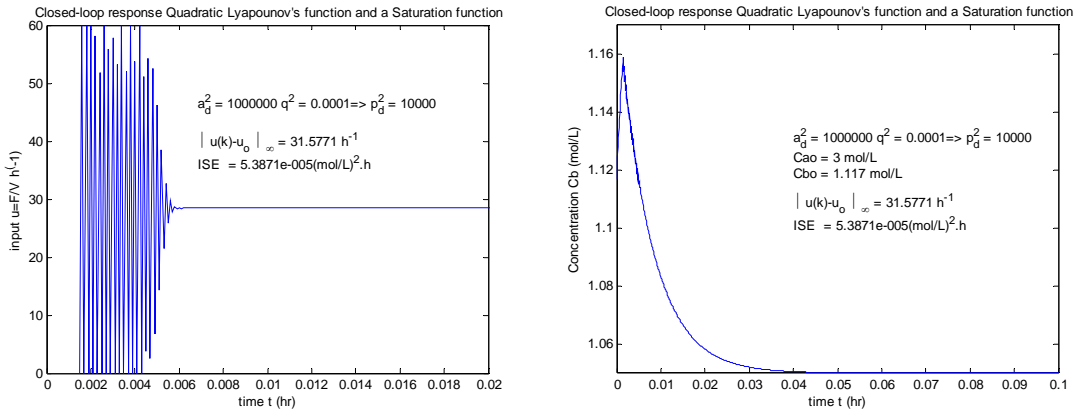


Figure 3.7: Influence of the Saturation function on the performance characteristics.

Including input constraints in the control law may lead to a loss in performance, particularly when the controller is not properly tuned. However, it allows the control law to take into account some limitations of the process, and thus make it more meaningful.

3.5.4 Results obtained using Zubov's method

In Fig. 3.8., the variation of the size of the stability region with the ratio r are graphically presented. They have been evaluated by following the standard methodology presented in section II.

A Maple code was used to graphically represent $\Delta V(x(k)) = 0$ and $V(x(k)) \leq c$ surfaces, the same method which was used to estimates the size of the stability region with the quadratic Lyapunov function.

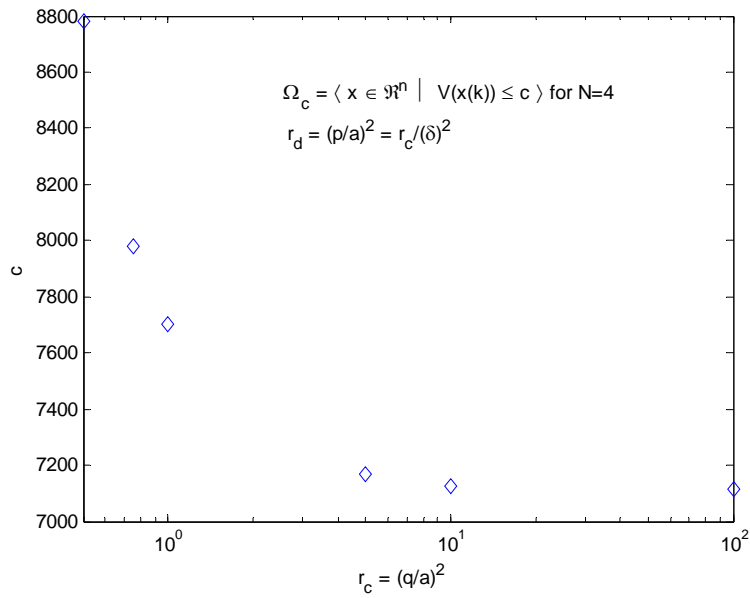


Figure 3.8: Estimates of the stability region as r varies for the 4th order approximation of V

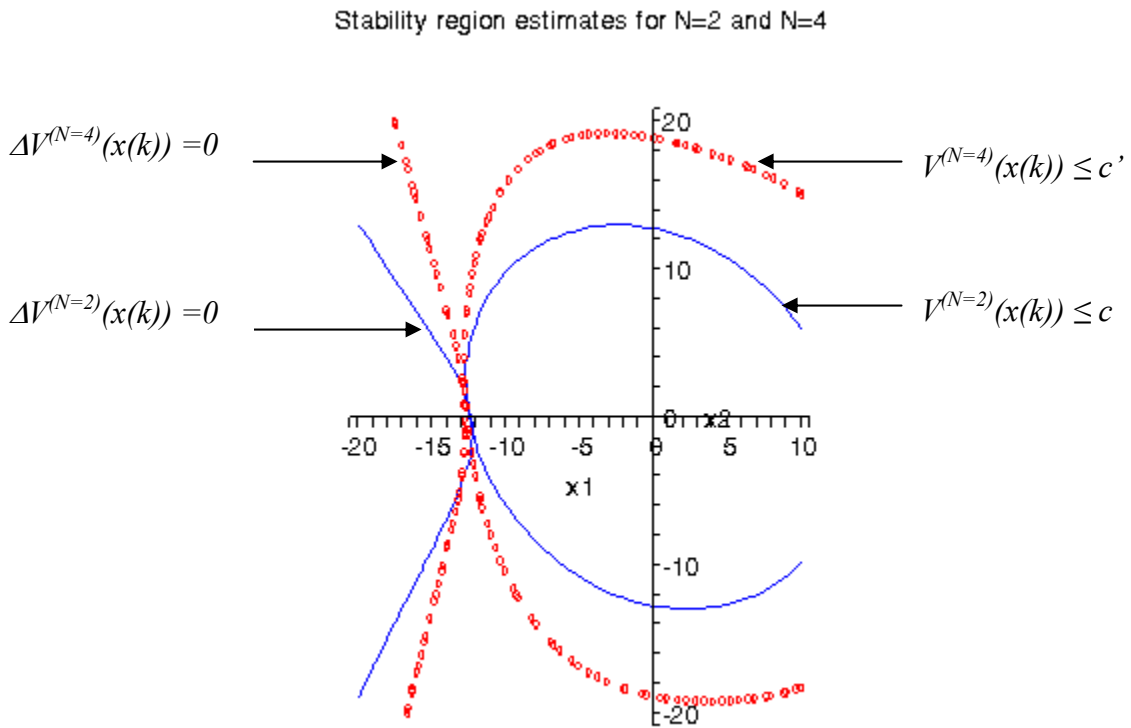


Figure 3.9: Stability region size estimates for different orders of the Taylor approximation of V

As it is evident, the control law using the 4th-order Taylor series truncation (N=4) for the Lyapunov function leads to a significant enlargement of the estimate of the size of the stability region in comparison to the values obtained using the quadratic Lyapunov function Eq. 3.47.

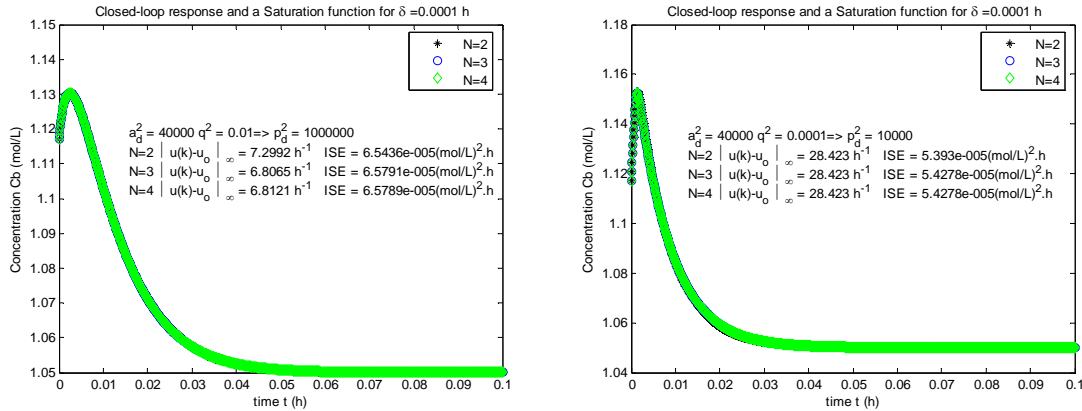


Figure 3.10: Comparison of the results obtained for different orders of the Taylor approximation of V

However, there is no significant difference in the performance characteristics obtained with the controllers derived using different truncation orders for the Taylor series. This is probably due to the mild process nonlinearity, which suggests, that even a lower truncation order would suffice to ensure acceptable closed-loop operation. Figure 3.10 represents the performance characteristics for the controllers derived for $N = 2, 3$ and 4 , for different sets of initial conditions than those defined earlier.

In order to better illustrate the interests of the Zubov-like method, another example is addressed.

3.6 Illustrative Example II: A Biological Reactor

Biochemical reactors are used in a wide variety of processes, from waste treatment to alcohol fermentation. Moreover, bioreactors represent challenging control problems, even in the case studied here with only a few variables, because of the nonlinearity related to their kinetics. Some interesting studies of controller design for bioreactors were conducted by Brengel and Seider (1989) Harris and Palazoğlu (1998) or Efe, Abadoglu and Kaynak (1999).

The example considered here has already been studied because of its educational interest (Bequette, 2003).

The specific growth rate chosen for the purpose of this study introduces substrate

inhibition kinetics:
$$\mu = \frac{\mu_{\max} \cdot S}{k_m + S + k_1 \cdot S^2}$$

Within a standard bioreactor modeling framework, biomass consumes substrate to produce more cells. Under standard assumptions, the mass balances for the biomass and substrate are given by:

$$\begin{aligned} \frac{dX}{dt} &= -D \cdot X + \frac{\mu_{\max} \cdot X \cdot S}{k_m + S + k_1 \cdot S^2} \\ \frac{dS}{dt} &= D \cdot (S_f - S) - \frac{\mu_{\max} \cdot X \cdot S}{Y[k_m + S + k_1 \cdot S^2]} \end{aligned} \quad (3.52)$$

where D is the dilution rate, X and S are the concentrations of the biomass and the substrate inside the reactor and S_f is the concentration of substrate in the feed stream.

Different control strategies have been used to control continuous bioreactors. Here, we wish to maintain X at its set point (output), by manipulating the dilution rate D

(manipulated input). The interesting feature with working with the dilution rate as the manipulated input is that the resulting dynamic model is independent of scale.

By letting:

$$x_1 = X, \quad x_2 = S, \quad u = F/V = D, \quad y = X$$

the above dynamic process equations become:

$$\begin{aligned} \frac{dx_1}{dt} &= \frac{\mu_{\max} \cdot x_1 \cdot x_2}{k_m + x_2 + k_1 \cdot x_2^2} - x_1 \cdot u = f_1(x_1, x_2) + g_1(x_1, x_2) \cdot u \\ \frac{dx_2}{dt} &= -\frac{\mu_{\max} \cdot x_1 \cdot x_2}{Y[k_m + x_2 + k_1 \cdot x_2^2]} + (x_{2f} - x_2) \cdot u = f_2(x_1, x_2) + g_2(x_1, x_2) \cdot u \\ y &= x_2 \end{aligned} \quad (3.53)$$

The system is initially at steady state with $x_{1,s}=1.530163\text{g/l}$, $x_{2,s}=0.174593\text{ g/l}$, $u_s=0.3\text{ h}^{-1}$. It is now assumed that the system is subjected to a positive step change in the set point value from 1.530163 to 1.58 g/l .

Accordingly, the new steady-state values are: $x_{10}=1.58\text{ mol/l}$, $x_{20}=y_{sp}=0.05\text{ mol/l}$, $u_0=0.154847\text{ h}^{-1}$.

For the unforced system ($u = u_o$), the Jacobian matrix A evaluated at $x = x_o$, is:

$$A = \begin{bmatrix} 0 & 3.3986 \\ -0.3871 & -8.6513 \end{bmatrix}$$

The eigenvalues of A are: $\lambda = \begin{pmatrix} -0.1548 \\ -8.4965 \end{pmatrix}$, which would lead to

$$\delta = \frac{1}{10|\lambda_{\max}(A)|} = 0.01176\text{ h} .$$

For convenience, we assume now: $\delta = 0.01\text{ h}$.

In order to check if the sampling period δ is small enough to guarantee asymptotic stability, we will numerically compare the open-loop responses of the continuous-time

system with the ones generated by its sampled-data representation obtained using Euler's discretization method.

3.6.1 Open-loop Responses

A Matlab code (Matlab 7.0) was used for this comparison. In particular, the built-in ODE solver *ode15s* was used for the simulation of the dynamics of the continuous-time system.

$$\begin{aligned} \frac{dx_1}{dt} &= \frac{\mu_{\max} \cdot x_1 \cdot x_2}{k_m + x_2 + k_1 \cdot x_2^2} - x_1 \cdot u_0 = f_1(x_1, x_2) + g_1(x_1, x_2) \cdot u_0 \\ \frac{dx_2}{dt} &= -\frac{\mu_{\max} \cdot x_1 \cdot x_2}{Y[k_m + x_2 + k_1 \cdot x_2^2]} + (x_{2f} - x_2) \cdot u_0 = f_2(x_1, x_2) + g_2(x_1, x_2) \cdot u_0 \end{aligned} \quad (3.54)$$

$y = x_2$

On the same graph, the response of the discrete-time process model is also shown:

$$\begin{aligned} x(k+1) &= x(k) + \delta \cdot [f(x(k)) + g(x(k)) \cdot u_o] \\ y(k) &= h(x(k)) \end{aligned} \quad (3.55)$$

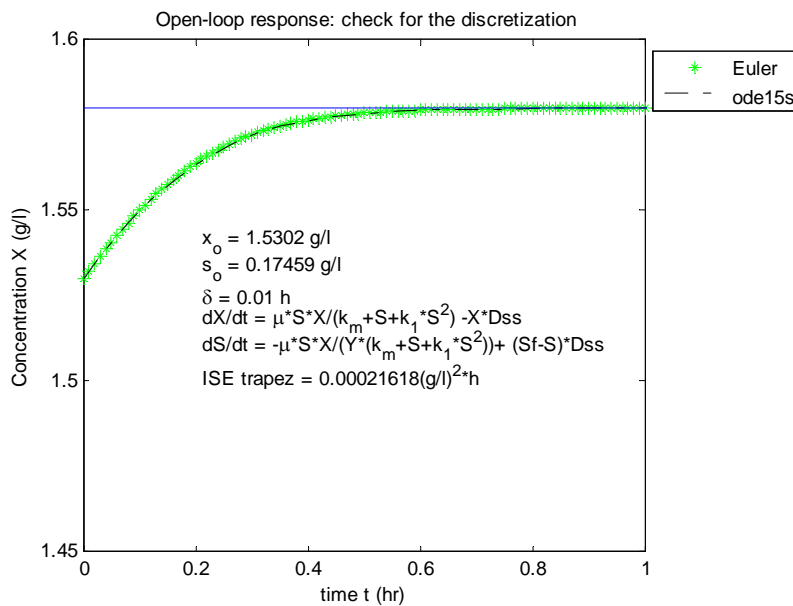


Figure 3.11: Open-loop response: check for the sampling period of the discretization

Figure 3.11 shows that the sampling period determined previously is small enough. Therefore, a value of $\delta = 0.01 h$ is chosen for convenience.

Table 3.2 summarizes the numerical values of the parameters which will be used in this study.

Table 3.2: Numerical values of the bioreactor example

Parameter	Value
k_1	$0.4545 L.g^{-1}$
k_m	$0.12 g.L^{-1}$
μ_{max}	$0.53 h^{-1}$
S_f (feed substrate concentration)	$4.0 g.l^{-1}$
Y (yield coefficient)	0.4
y_{sp}	$1.05 gl.l^{-1}$
x_{10}	$1.58 g.l^{-1}$
x_{20}	$0.05 g.l^{-1}$
u_0	$0.154847 h^{-1}$
δ	0.01 h

Here, only the Zubov-like method will be demonstrated, as it is relevant towards the purpose of our study.

3.6.2 Results obtained using Zubov's method

This example is expected to better illustrate the importance of Zubov's method, because of the stronger process nonlinearity.

Consider now the input constraints of the saturation function in the controller (3.29) which are as follows : $u_{min} = 0$ and no u_{max} . This leads to the following controller to be implemented in our system: (equivalent to Eq. 3.48)

$$\begin{aligned}
 u(k) &= S[\Psi(x(k), V(x(k)))] \quad \text{where} \quad S[w] = \begin{cases} u_{\min} = 0 & \text{if } w < u_{\min} \\ w & \text{if } u_{\min} \leq w \end{cases} \\
 \Psi(x(k), V(x(k))) &= \frac{p^2 u_o(y_{sp}) - L_g V(x(k)) \cdot [L_f V(x(k)) + a^2 V(x(k))]}{p^2 + [L_g V(x(k))]^2}
 \end{aligned} \tag{3.56}$$

A MAPLE code (given in Annex) was used to automatically compute the Taylor coefficients of the unknown solution $V(x)$ of the Zubov-like functional equation (3.9).

$$V_2(x_1, x_2) = 167.740573 \cdot (x_1 - 1.58)^2 + 129.269491 \cdot (x_1 - 1.58)(x_2 - 0.05) + 28.433921 \cdot (x_2 - 0.05)^2 \tag{3.57}$$

$$\begin{aligned}
 V_4(x_1, x_2) &= 167.740573 \cdot (x_1 - 1.58)^2 + 129.269491 \cdot (x_1 - 1.58)(x_2 - 0.05) + 28.433921 \cdot (x_2 - 0.05)^2 \\
 &\quad - 3.919351 \cdot (x_1 - 1.58)^3 - 0.069863 \cdot (x_1 - 1.58)^2 (x_2 - 0.05) \\
 &\quad - 18.015423 \cdot (x_1 - 1.58)(x_2 - 0.05)^2 + 8.086482 \cdot (x_2 - 0.05)^3 \\
 &\quad + 2.790416 \cdot (x_1 - 1.58)^4 + 0.064053 \cdot (x_1 - 1.58)^3 (x_2 - 0.05) + 16.520301 \cdot (x_1 - 1.58)^2 (x_2 - 0.05)^2 \\
 &\quad - 6.676026 \cdot (x_1 - 1.58)(x_2 - 0.05)^3 + 1.592616 \cdot (x_2 - 0.05)^4
 \end{aligned} \tag{3.58}$$

A Matlab code (Matlab 7.0) was used for evaluating the performance of the proposed digital controller (obtained using Equations 3.57 (N=2) and 3.58 (N=4) and the associated Lyapunov functions appearing in the proposed nonlinear controller 3.56) when implemented in the discrete-time model:

$$\begin{aligned}
 x(k+1) &= x(k) + \delta \cdot [f(x(k)) + g(x(k)) \cdot u] \\
 y(k) &= h(x(k))
 \end{aligned} \tag{3.59}$$

Figure 3.12 represents the performance characteristics for the controllers derived for $N = 2$ and 4 as truncation orders for the Taylor series, and for different sets of parameter values a^2 and q^2 .

On the left: $a^2 = 40$ and $q^2 = 0.1$. On the right, $a^2 = 400$ and $q^2 = 0.1$, which represents a more aggressive controller, as seen previously.

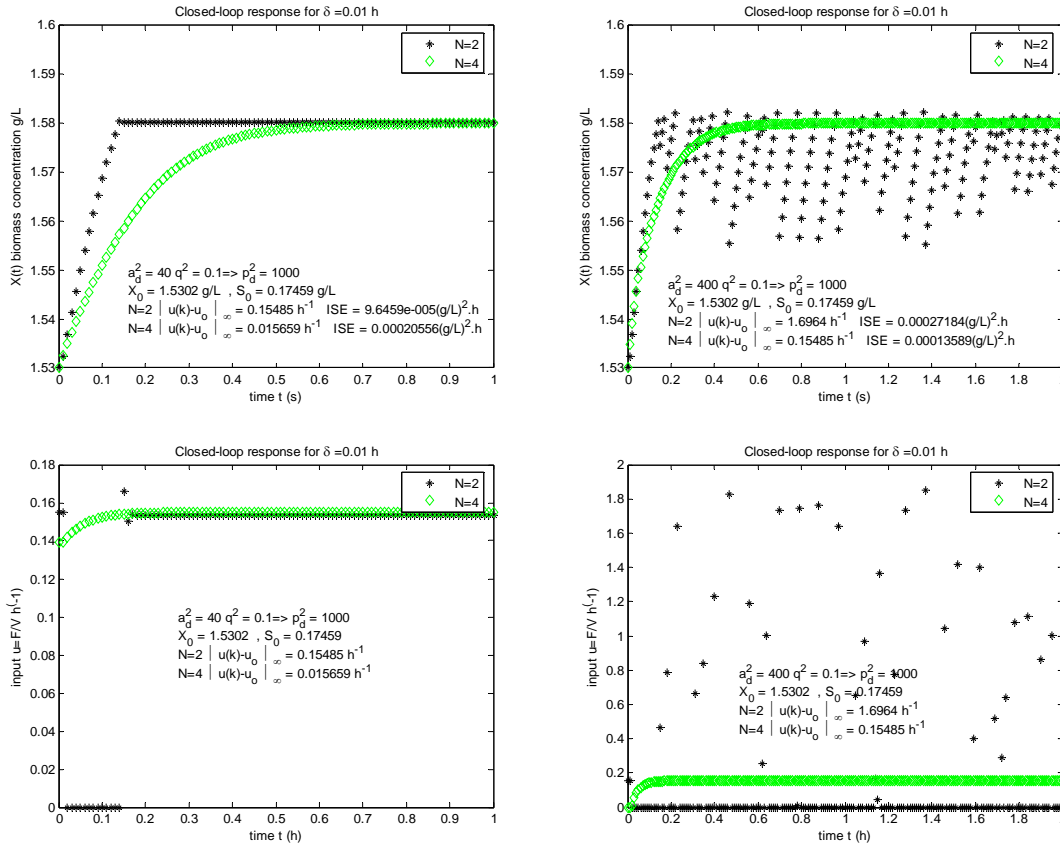


Figure 3.12: Comparison of the results obtained for different truncation orders of the Taylor series approximation of V

It is important to notice that for a more aggressive controller (right hand side of Figure 3.12), the controller designed for $N=2$ does not exhibit operationally acceptable performance characteristics. The loss in terms of performance is such that the desired output set point value for X is not achieved.

The manipulated input, in this case, constantly hits the constraint $u_{\min} = 0$. On the other hand, the controller designed using $N=4$ enables the system to reach the desired set point value y_{sp} .

However, the results obtained with a less aggressive controller (left hand side of Figure 3.12) also help drawing some interesting conclusions.

The performance characteristics, as reflected upon the value of the ISE and $\|u(k) - u_o\|_{\infty}$, support the claim that the controller designed for $N=2$ is better than the one designed

using $N=4$ as the truncation order: y_{sp} is reached faster (lower value of the *ISE* index, for a value of $\|u(k)-u_o\|_\infty$ which seems reasonable).

Nevertheless, the behavior of the manipulated input is smoother when $N=4$: it does not hit the constraint, and the value of $\|u(k)-u_o\|_\infty$ is small. Indeed, for $N=2$, the input oscillates between the constraint $u_{\min} = 0$ and other values, closer to u_o . One can notice that the behavior tends to be the one observed in the case of a more aggressive controller. But here, the controller manages to achieve the goal $X = y_{sp}$.

In a real process, it is impossible for the actuator to be able to follow the control moves generated by controller using the second order truncation of the Taylor series expansion of V .

In this case, it appears that a higher order of the Taylor series approximation for V does definitely matter.

3.7 Conclusions

A general framework for the development of a new synthesis approach for nonlinear process control, based on a notion of short-horizon energy-predictive control, was presented.

The approach that was followed in the design of digital computer-control systems was to obtain the discrete-time process model directly from process model identification methods or via time-discretization of a continuous-time process model and then directly synthesize a discrete-time controller.

The proposed approach, starting from a continuous-time process model that is discretized to obtain a discrete-time process model, follows the methodological principles of Lyapunov design and optimization of the rate of energy dissipation of the system, as it is realized through a suitably selected control Lyapunov function.

The latter is computed either by solving the Lyapunov matrix equation, or for enhanced accuracy when coping with severe process nonlinearities, by solving a Zubov-like functional equation for the system's drift vector field.

A state feedback control law with two tunable parameters was derived as the solution of an optimization problem, formulated on the basis of the Lyapunov function and closed-loop performance considerations.

Even though a systematic methodology was presented responding to the needs of optimizing the digitally controlled process dynamics, it should be emphasized that the responsibility of the process control engineer is not trivial. The choice of the tunable parameters as well as the choice of the input constraints of the saturation function included into the control law are important and should reflect the design objectives, as well as the restrictions of the process.

NOMENCLATURE

A^T	Transpose of Matrix A
$B(d_{\min})$	Set defined by Eq. (3.19)
C_a	Concentration of species A (Van de Vusse Example)
C_{a_0}	Inlet concentration of species A (Van de Vusse Example)
D	Dilution rate (Biological reactor Example)
d_{\min}	Quantity defined by Eq. (3.18)
$e = y_{sp} - y$	Error signal
F	Flowrate (Van de Vusse Example)
$f(x), g(x)$	Vector fields in standard state – space description of a continuous-time nonlinear system.
$h(x)$	Scalar fields that determine the output map
I	n -dimensional Identity matrix
k	Iteration
k_i	Reaction rate constant (Van de Vusse and Biological reactor Examples)
$L_f h(x)$	Lie derivative of the scalar field h with respect to the vector field f
M_{ol}	Set defined by Eq. (3.17)
M_{cl}	Set defined by Eq. (3.33)
r_a	Reaction rate of species A (Van de Vusse Example)
S_f	Feed substrate concentration (Biological reactor Example)
t	Time
u	Manipulated input
V	Lyapunov function
x	Vector of state variables
y	Process output

Y Yield coefficient (Biological reactor Example)

Greek letters:

δ Sampling period

$\lambda(P)$ Eigenvalue of matrix P

Ω_c Set defined by Eq. (3.20)

$\mu = \frac{\mu_{\max} S}{k_m + S + k_1 S^2}$ Specific growth rate (Biological reactor Example)

Other symbols:

\in Belongs to

\Re Real line

\Re^n n-dimensional Euclidian space

$\|\bullet\|_2$ Euclidian norm in \Re^n

$\|\bullet\|_\infty$ Max- norm in \Re^n

Subscripts:

min Minimum

max Supremum

sp Set point value

REFERENCES

Bequette, B. Wayne, (2003) *Process control: modeling, design and simulation*, Prentice Hall, 2003.

Bregel, D.D. and Seider, W.D. (1989) Multistep nonlinear predictive controller, *Industrial & Engineering Chemistry Research* **28** (1989), 1812-1822.

Corriou, J. P. , (1996) *Commande des procédés*, Technique et Documentation, 1996.

Coulibaly, E.S., Maiti, S. and Brosilow, C. (1992), Internal model predictive control (IMPC), *AIChE Annual Meeting*, Miami Beach, FL.

Dubljević, S. and Kazantzis, N. (2002), A new Lyapunov design approach for nonlinear systems based on Zubov's method, *Automatica* **38** (2002), 1999-2007.

Efe, M. O., Abadoğlu, E and Kaynak, O. (1999), A novel analysis and design of a neural network assisted nonlinear controller for a bioreactor, *International Journal of Robust and Nonlinear Control* **9** (1999), 799-815.

Elaydi, S.N., (1999). *An Introduction to Difference Equations*, Springer Verlag, 1999.

Franklin, G.F., Powell, J.D. and Workman, M.L. (1992) *Digital control of dynamic systems*. New York, Addison Wesley, 1992.

Goldstein, H. (1980). *Classical mechanics* Reading, MA: Addison-Wesley, 1980.

Harris, K.R. and Palazoğlu, A. (1998), Studies on the analysis of nonlinear processes via functional expansions –III: controller design, *Chemical Engineering Science* **53-23** (1998), 4005-4022.

Hernandez, E. and Arkun, Y. (1993), Control of nonlinear systems using polynomial ARMA models, *AIChE Journal* **39** (1993), 446-460.

Isidori, A.,(1989), *Nonlinear control systems: An introduction*, Springer Verlag, New York, 1989.

Kazantzis, N., Kravaris, C., Tseronis, C. and Wright, R. (2005), Optimal controller tuning for nonlinear processes, *Automatica* **41** (2005) 79-86.

Kazantzis, N (2002), On the existence and uniqueness of locally analytic invertible solutions of a system of nonlinear functional equations , *Journal of Computational and Applied Mathematics*, **146-2** (2002), 301-308 .

Kazantzis, N (2001), On invariant manifolds of nonlinear discrete-time input-driven dynamical systems , *Physics Letters A*, **292**, Issues 1-2, 24 (2001), 107-114 .

Kazantzis, N. and Kravaris, C. (2001). Discrete-time nonlinear observer design using functional equations, *Systems & Control Letters*, **42-2** (2001), 81-94 .

Kazantzis, N. and Kravaris, C. (1999). Energy-predictive control: a new synthesis approach for nonlinear process control, *Chemical Engineering Science* **54** (1999), 1697-1709.

Kazantzis, N. and Kravaris, C. (1999). Time-discretization of nonlinear control systems via Taylor methods, *Computers and Chemical Engineering* **23** (1999), 763-784.

Khalil, H.K. (2001) *Nonlinear systems* (3rd ed.), Englewood Cliffs, New Jersey, Prentice-Hall (2001).

Klatt, K.U. and Engell, S. (1998), Gain-scheduling trajectory control of a Continuous Stirred Tank Reactor, *Computers & Chemical Engineering*, **22** 4-5 (1998) 491-502

Kravaris, C., Niemiec, M., Berber, R., & Brosilow, C. (1997). *Nonlinear model based control of nonminimum phase processes*. In R. Berber & C. Kravaris, (eds.), *Nonlinear Model Based Process Control*, Kluwer Academic Publishers, 1998, 115–141.

Nešić, D. , Teel, A.R. and Kokotović, P.V. (1999), Sufficient conditions for stabilization of sampled-data nonlinear systems via discrete-time approximations, *Systems & Control Letters* **38** (1999) 259-270.

Nešić, D. and Teel, A.R (2004), A framework for stabilization of nonlinear sampled-data systems based on their approximate discrete-time models, *IEEE Transactions on Automatic Control* **49-7** (2004).

O’Shea, P.R. (1964), The extension of Zubov’s method to sampled data control systems described by nonlinear autonomous difference equations, *IEEE Transactions on Automatic Control* **9** (1964), 62.

Perlmutter, D.D. (1972) *Stability of Chemical reactors*. Englewood Cliffs, NJ. Prentice Hall, 1972.

Slotine, J. and Li, W. (1991) *Applied Nonlinear Control*. Englewood Cliffs, NJ. Prentice Hall, 1972.

Soroush, M. and Kravaris, C. (1996). A continuous-time formulation of nonlinear model predictive control. *Int. J. Control*, **63**, 121-146

Soroush, M. and Kravaris, C. (1992). Discrete-time nonlinear controller synthesis by input/output linearization, *AIChE Journal* **38** (1992), 1935.

Wright, R.A. and C. Kravaris, C., (1992) Nonminimum-phase compensation for nonlinear processes, *A.I.Ch.E. Journal* **38** (1992), p. 26

APPENDICES

MAPLE Code for the Van de Vusse Example

```

> k1:=50:
> k2:=100:
> k3:=10:
> Cao:=10:
> ysp:=1.05:
System of differential Equations
> diff_x1:=-k1*x1-k3*x1^2+(Cao-x1)*u;
      diff_x1 := -50 x1 - 10 x12 + (10 - x1) u
> diff_x2:=k1*x1-k2*x2-x2*u;
      diff_x2 := 50 x1 - 100 x2 - x2 u
> desired_y:=x2;
      desired_y := x2
> solve({diff_x1=0, diff_x2=0, desired_y=ysp});
{u = 28.42287502, x2 = 1.050000000, x1 = 2.696880376}, {x2 = 1.050000000, x1 = 6.435351029, u = 206.4452871}
> x1o:=2.69688:
> x2o:=1.0500:
> uo:=28.42288:
> f1:=proc(x1,x2) -k1*x1-k3*x1^2 end proc:
> f2:=proc(x1,x2) k1*x1-k2*x2 end proc:
> g1:=proc(x1,x2) (Cao-x1) end proc:
> g2:=proc(x1,x2) -x2 end proc:
> df1x1:=proc(x1,x2) D[1](f1)(x1,x2) end proc:
> df1x2:=proc(x1,x2) D[2](f1)(x1,x2) end proc:
> df2x1:=proc(x1,x2) D[1](f2)(x1,x2) end proc:
> df2x2:=proc(x1,x2) D[2](f2)(x1,x2) end proc:
> dg1x1:=proc(x1,x2) D[1](g1)(x1,x2) end proc:
> dg1x2:=proc(x1,x2) D[2](g1)(x1,x2) end proc:
> dg2x1:=proc(x1,x2) D[1](g2)(x1,x2) end proc:
> dg2x2:=proc(x1,x2) D[2](g2)(x1,x2) end proc:
> with(LinearAlgebra):
For the unforced system (u = uo), the Jacobian Matrix evaluated at x = xo :
> Jacobian:=
Matrix([[df1x1(x1o,x2o),df1x2(x1o,x2o)], [df2x1(x1o,x2o),df2
x2(x1o,x2o)]])+uo*Matrix([[dg1x1(x1o,x2o),dg1x2(x1o,x2o)], [
dg2x1(x1o,x2o),dg2x2(x1o,x2o)]]);

```

$$Jacobian := \begin{bmatrix} -132.360479999999996 & 0. \\ 50. & -128.422879999999992 \end{bmatrix}$$

```
> with(LinearAlgebra):Eigenvalues(Jacobian);
```

$$\begin{bmatrix} -128.422879999999992 + 0. I \\ -132.360479999999996 + 0. I \end{bmatrix}$$

```
> Id:=Matrix(2,2, shape=identity):
```

Lyapounov's Matrix Equation

```
> A:=Matrix([[ -132.360479999999996, 0.], [50., -128.422879999999992]]);
```

$$A := \begin{bmatrix} -132.360479999999996 & 0. \\ 50. & -128.422879999999992 \end{bmatrix}$$

```
> At:=Transpose(A):
```

```
> P:=Matrix(2,2, symbol=p, shape=symmetric):
```

```
> P . A + At . P;
```

$$\begin{bmatrix} -264.7209600 p_{1,1} + 100. p_{1,2} & -260.7833600 p_{1,2} + 50. p_{2,2} \\ -260.7833600 p_{1,2} + 50. p_{2,2} & -256.8457600 p_{2,2} \end{bmatrix}$$

```
> solve({-264.72096*p[1, 1]+100.*p[1, 2]=-1, -260.78336*p[1, 2]+50.*p[2, 2]=0, -256.84576*p[2, 2]=-1});
{p1,1 = 0.004059549810, p1,2 = 0.0007464792274, p2,2 = 0.003893387222}
```

```
> P := Matrix([[0.00405955, 0.0007465], [0.0007465, 0.0038934]]);
```

$$P := \begin{bmatrix} 0.00405955 & 0.0007465 \\ 0.0007465 & 0.0038934 \end{bmatrix}$$

```
> Eigenvalues(P);
```

$$\begin{bmatrix} 0.00472758331817055549 + 0. I \\ 0.00322536668182944481 + 0. I \end{bmatrix}$$

deviation variables: x1= Ca-Cass, x2=Cb-Cbss

```
> V_Lyap:=proc(x1,x2) 0.5*Vector [row] ([x1,x2]) .P
.Vector([x1,x2]) end proc:
```

```
> V_Lyap(x1,x2);
```

$$x1(0.002029775 x1 + 0.00037325 x2) + x2(0.00037325 x1 + 0.00194670 x2)$$

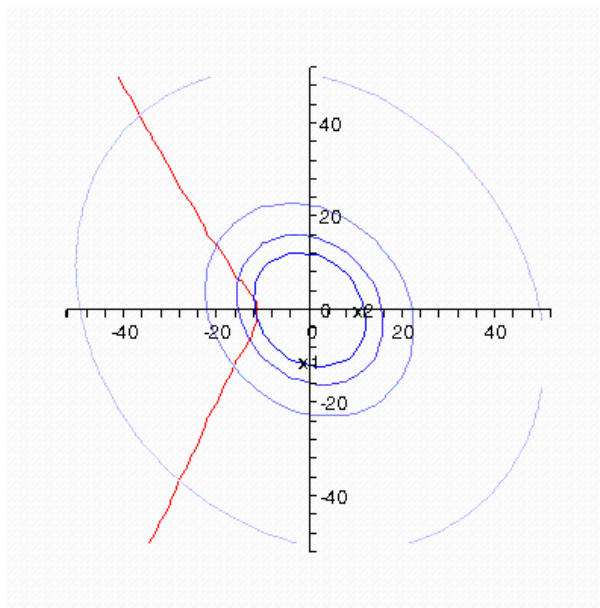
```
> Lyap:=proc(x1,x2) x1*(0.2029775e-2*x1+0.37325e-3*x2)+x2*(0.37325e-3*x1+0.194670e-2*x2) end proc:
```

```
> expand(x1*(0.2029775e-2*x1+0.37325e-3*x2)+x2*(0.37325e-3*x1+0.194670e-2*x2));
```

```

0.002029775 x12 + 0.00074650 x1 x2 + 0.00194670 x23
> dVdx1:=proc(x1,x2) D[1](Lyap)(x1,x2) end proc:
> dVdx2:=proc(x1,x2) D[2](Lyap)(x1,x2) end proc:
> LfV:= proc(x1,x2) (dVdx1(x1,x2))*(-k1*(x1+x1o)-
k3*(x1+x1o)^2)+(dVdx2(x1,x2))*(k1*(x1+x1o)-k2*(x2+x2o)) end
proc:
> LfV(x1,x2);
(0.004059550 x1 + 0.00074650 x2) (-50 x1 - 134.84400 - 10 (x1 + 2.69688)2)
+ (0.00074650 x1 + 0.00389340 x2) (50 x1 + 29.84400 - 100 x2)
> LgV:= proc(x1,x2) (dVdx1(x1,x2))*(Cao-
(x1+x1o))+(dVdx2(x1,x2))*(-(x2+x2o)) end proc:
> LgV(x1,x2);
(0.004059550 x1 + 0.00074650 x2) (7.30312 - x1) + (0.00074650 x1 + 0.00389340 x2) (-x2 - 1.0500)
> Mol:= proc(x1,x2) LfV(x1,x2)+uo*LgV(x1,x2)end proc:
> Mcl:= proc(x1,x2,r) Mol(x1,x2)-
(1/r)*(LgV(x1,x2))^2*v_Lyap(x1,x2) end proc:
> with(plots):
> display({contourplot(Lyap(x1,x2),x1=-100..50,x2=-
50..50,contours=[0.3,0.5,1,5],coloring=[blue,white]),contou
rplot(Mcl(x1,x2,10),x1=-100..50,x2=-50..50,contours=[0])});

```



The code for the Zubov-like method is not included for the Van de Vusse Reaction in a CSTR example. It is given for the Biological Reactor example.

MAPLE Code for the Biological Reactor Example

```

> km:=0.12:
> k1:=0.4545:
> mu:=0.53:
> Y:=0.4:
> x2f:=4.0:
> ysp:=1.58:
System of differential Equations
> diff_x1:=mu*x2*x1/(km+x2+k1*x2^2)-x1*u;
      diff_x1 :=  $\frac{0.53 x_2 x_1}{0.12 + x_2 + 0.4545 x_2^2} - x_1 u$ 
> diff_x2:=-mu*x1*x2/(Y*(km+x2+k1*x2^2))+(x2f-x2)*u;
      diff_x2 :=  $-\frac{1.325000000 x_2 x_1}{0.12 + x_2 + 0.4545 x_2^2} + (4.0 - x_2) u$ 
> desired_y:=x1;
      desired_y := x1
> solve({diff_x1=0, diff_x2=0, desired_y=ysp});
      {x2 = 0., u = 0., x1 = 1.580000000}, {x2 = 0.05000000000, u = 0.1548473804, x1 = 1.580000000}
> x1o:=1.58:
> x2o:=0.05:
> uo:=0.1548474:

> f1:=proc(x1,x2) mu*x2*x1/(km+x2+k1*x2^2) end proc:
> f2:=proc(x1,x2) -mu*x1*x2/(Y*(km+x2+k1*x2^2)) end proc:
> g1:=proc(x1,x2) -x1 end proc:
> g2:=proc(x1,x2) (x2f-x2) end proc:
> df1x1:=proc(x1,x2) D[1](f1)(x1,x2) end proc:
> df1x2:=proc(x1,x2) D[2](f1)(x1,x2) end proc:
> df2x1:=proc(x1,x2) D[1](f2)(x1,x2) end proc:
> df2x2:=proc(x1,x2) D[2](f2)(x1,x2) end proc:
> dg1x1:=proc(x1,x2) D[1](g1)(x1,x2) end proc:
> dg1x2:=proc(x1,x2) D[2](g1)(x1,x2) end proc:
> dg2x1:=proc(x1,x2) D[1](g2)(x1,x2) end proc:
> dg2x2:=proc(x1,x2) D[2](g2)(x1,x2) end proc:

```

For the unforced system ($u = u_o$), the Jacobian Matrix evaluated at $x = x_o$:

```

> Jacobian:=
Matrix([[df1x1(x1o,x2o), df1x2(x1o,x2o)], [df2x1(x1o,x2o), df2x2(x1o,x2o)]])+uo*Matrix([[dg1x1(x1o,x2o), dg1x2(x1o,x2o)], [dg2x1(x1o,x2o), dg2x2(x1o,x2o)]]);

```

$$Jacobian := \begin{bmatrix} -1.95999999841323102 \cdot 10^{-8} & 3.398586761999999986 \\ -0.387118450900000022 & -8.651314304999999966 \end{bmatrix}$$

```
> with(LinearAlgebra):Eigenvalues(Jacobian);
```

$$\begin{bmatrix} -0.154847399959257004 + 0. I \\ -8.49646692464074248 + 0. I \end{bmatrix}$$

```
> Id:=Matrix(2,2, shape=identity):
```

```
> delta_vrai:=1/(10*8.5);
```

$$\delta_{vrai} := 0.01176470588$$

```
> delta:=0.01;
```

$$\delta := 0.01$$

Lyapounov's Matrix Equation

```
> A:=Jacobian:
```

```
> Ad:=Id+delta*A;
```

$$Ad := \begin{bmatrix} 0.99999999980400000 & 0.0339858676199999988 \\ -0.00387118450900000030 & 0.913486856949999981 \end{bmatrix}$$

```
> with(LinearAlgebra):Adt:=Transpose(Ad):
```

```
>
```

```
> Pd:=Matrix(2,2, symbol=pi, shape=symmetric):
```

```
> Adt . Pd . Ad - Pd ;
```

$$\begin{bmatrix} -4 \cdot 10^{-10} \pi_{1,1} - 0.007742369016 \pi_{1,2} + 0.00001498606950 \pi_{2,2}, & 0.03398586761 \pi_{1,1} - 0.0866447089 \pi_{1,2} - 0.003536276170 \pi_{2,2} \\ [0.03398586761 \pi_{1,1} - 0.0866447089 \pi_{1,2} - 0.003536276170 \pi_{2,2}, & 0.001155039198 \pi_{1,1} + 0.06209128678 \pi_{1,2} - 0.1655417623 \pi_{2,2}] \end{bmatrix}$$

```
> solve({-0.4e-9*pi[1, 1]-0.7742369016e-2*pi[1, 2]+0.1498606950e-4*pi[2, 2]=-1, 0.3398586761e-1*pi[1, 1]-0.866447089e-1*pi[1, 2]-0.3536276170e-2*pi[2, 2]=0, 0.1155039198e-2*pi[1, 1]+0.6209128678e-1*pi[1, 2]-.1655417623*pi[2, 2]=-1});
```

$$\{\pi_{2,2} = 56.86784224, \pi_{1,2} = 129.2694896, \pi_{1,1} = 335.4811425\}$$

```
> Pd := Matrix([[ 335.4811425, 129.2694896], [129.2694896, 56.86784224]]);
```

$$Pd := \begin{bmatrix} 335.4811425 & 129.2694896 \\ 129.2694896 & 56.86784224 \end{bmatrix}$$

```
> with(LinearAlgebra):Eigenvalues(Pd);
```

$$\begin{bmatrix} 386.219075854735876 + 0. j \\ 6.12990888526415745 + 0. j \end{bmatrix}$$

```
> V_Lyap:=proc(x1,x2) 0.5*Vector [row] ([x1-x1o,x2-x2o])
.Pd .Vector([x1-x1o,x2-x2o]) end proc:
```

```
> V_Lyap(x1,x2);
```

```
(x1 - 1.58) (167.7405712 x1 - 268.2618398 + 64.63474480 x2) + (x2 - 0.05) (64.63474480 x1 - 103.5445929 + 28.43392112 x2)
```

```
> Lyap:=proc(x1,x2) (x1-1.530163)*(112.4046883*x1-
177.8314793+33.41476578*x2)+(x2-.174593)*(33.41476578*x1-
54.92118770+21.71421222*x2) end proc:
```

```
> dVdx1:=proc(x1,x2) D[1](Lyap)(x1,x2) end proc:
```

```
> dVdx2:=proc(x1,x2) D[2](Lyap)(x1,x2) end proc:
```

```
> LfV:= proc(x1,x2)
```

```
(dVdx1(x1,x2))*(f1(x1,x2))+(dVdx2(x1,x2))*(f2(x1,x2)) end
proc:
```

```
> LfV(x1,x2);
```

```
0.53 (-355.6629586 + 224.8093766 x1 + 66.82953156 x2) x2 x1
```

```
0.12 + x2 + 0.4545 x22
```

```
1.325000000 (-109.8423754 + 66.82953156 x1 + 43.42842444 x2) x2 x1
```

```
0.12 + x2 + 0.4545 x22
```

```
> LgV:= proc(x1,x2)
```

```
(dVdx1(x1,x2))*(g1(x1,x2))+(dVdx2(x1,x2))*(g2(x1,x2)) end
proc:
```

```
> LgV(x1,x2);
```

```
(-355.6629586 + 224.8093766 x1 + 66.82953156 x2) x1 + (-109.8423754 + 66.82953156 x1 +
```

Zubov functional equation

```
>
```

```
> x1s:=x1o:
```

```
> x2s:=x2o:
```

```
> fvs:=uo:
```

```
> delta:=0.01:
```

```
> readlib(mtaylor):
```

```
> readlib(coeftayl):
```

```
> with(LinearAlgebra):
```

```
> x10:=0:x20:=0:
```

```
> Q:=0.5*(x1^2+x2^2):
```

```
F1:=x1+delta*(mu*(x2+x2s)*(x1+x1s)/(km+(x2+x2s)+k1*(x2+x2s)
^2)-(x1+x1s)*fvs):F2:=x2+delta*(-
mu*(x2+x2s)*(x1+x1s)/(Y*(km+(x2+x2s)+k1*(x2+x2s)^2))+(x2f-
x2-x2s)*fvs):
```

```
>
```

```
> N:=5:
```

```

> s:=mtaylor(V(x1,x2)-V(x10,x20)-D[1](V)(x10,x20)*x1-
D[2](V)(x10,x20)*x2,[x1=x10,x2=x20],N):
> sp:=subs([x1=F1,x2=F2],s):
> d:={}:q(1):={}:
>
> for j from 2 to N-1 do
  for i from 0 to j do
    p[i,j-i]:=(i!*(j-
i)!)*coeftayl(s,[x1,x2]=[x10,x20],[i,j-i]):
    q(j):=q(j-1) union {p[i,j-i]}:
    d:=d union q(j):
  od:
od:

> pde:=mtaylor(sp-s+Q,[x1=x10,x2=x20],N):c:={}:r(1):={}:
> for j from 2 to N-1 do
  for i from 0 to j do
    t[i,j-i]:=coeftayl(pde,[x1,x2]=[x10,x20],[i,j-i]):
    r(j):=r(j-1) union {t[i,j-i]}:
    c:=c union r(j):
  od:
od:
> fin:=solve(c,d):
> fin;
>
{D1,1,1,1(V)(0,0) = 66.96998161, D2,2,2(V)(0,0) = 48.51889251, D1,1,2,2(V)(0,0) = 66.08120420,
  D1,2,2,2(V)(0,0) = -40.05615398, D1,1,1,2(V)(0,0) = 0.3843165256, D1,2(V)(0,0) = 129.2694906,
  D1,2,2(V)(0,0) = -36.03084504, D2,2,2(V)(0,0) = 56.86784297, D1,1,1(V)(0,0) = -23.51610814,
  D2,2,2,2(V)(0,0) = 38.22278055, D1,1(V)(0,0) = 335.4811454,
  D1,1,2(V)(0,0) = -.1397250168}

> mtaylor(f(x,y), [x,y], 5);
f(0,0)+D1,f(0,0)x+D2,f(0,0)y+1/2D1,1,f(0,0)x^2+xD1,2,f(0,0)y+1/2D2,2,f(0,0)y^2+1/6x^3D1,1,1,f(0,0)
+1/2x^2D1,1,2,f(0,0)y+1/2xy^2D1,2,2,f(0,0)+1/6y^3D2,2,2,f(0,0)+1/24x^4D1,1,1,1,f(0,0)+1/6x^3D1,1,1,2,f(0,0)y
+1/4x^2y^2D1,1,2,2,f(0,0)+1/6xy^3D1,2,2,2,f(0,0)+1/24y^4D2,2,2,2,f(0,0)

>
deviation variables:
2nd order truncation
> Vdev_quad:=proc(x1,x2) 0.5*335.4811454*x1^2
+129.2694906*x1*x2 +0.5*56.86784297*x2^2 end proc:
> Vdev_quad(x1-x1s,x2-x2s);

```

```

167.7405727 (x1 - 1.58)3 + 129.2694906 (x1 - 1.58) (x2 - 0.05) + 28.43392148 (x2 - 0.05)2
> dVdx1_2:=proc(x1,x2) D[1](Vdev_quad)(x1,x2) end proc:
> dVdx2_2:=proc(x1,x2) D[2](Vdev_quad)(x1,x2) end proc:
> LfV_2:= proc(x1,x2)
(dVdx1_2(x1,x2))*(mu*(x2+x2s)*(x1+x1s)/(km+(x2+x2s)+k1*(x2+
x2s)^2))+(dVdx2_2(x1,x2))*(-
mu*(x2+x2s)*(x1+x1s)/(Y*(km+(x2+x2s)+k1*(x2+x2s)^2))) end
proc:
> LgV_2:= proc(x1,x2) (dVdx1_2(x1,x2))*(-x1-
x1s)+(dVdx2_2(x1,x2))*(x2f-x2-x2s) end proc:
>
>
4th order truncation
> Vdev_4:=proc(x1,x2) 0.5*335.4811454*x1^2
+129.2694906*x1*x2 + 0.5*56.86784297*x2^2 + 1/6*(-
23.51610814)*x1^3+1/2*(-.1397250168)*x1^2*x2+1/2*(-
36.03084504)*x1*x2^2 +1/6*(48.51889251)*x2^3 +
1/24*(66.96998161)*x1^4+
1/6*(.3843165256)*x1^3*x2+1/4*(66.08120420)*x1^2*x2^2
+1/6*(-40.05615398)*x1*x2^3 +1/24*(38.22278055)*x2^4 end
proc:
> Vdev_4(x1-x1s,x2-x2s);
167.7405727 (x1 - 1.58)2 + 129.2694906 (x1 - 1.58) (x2 - 0.05) + 28.43392148 (x2 - 0.05)2 - 3.919351357 (x1 - 1.58)3
- 0.06986250840 (x1 - 1.58)2 (x2 - 0.05) - 18.01542252 (x1 - 1.58) (x2 - 0.05)2 + 8.086482085 (x2 - 0.05)3
+ 2.790415900 (x1 - 1.58)4 + 0.06405275427 (x1 - 1.58)3 (x2 - 0.05) + 16.52030105 (x1 - 1.58)2 (x2 - 0.05)2
- 6.676025663 (x1 - 1.58) (x2 - 0.05)3 + 1.592615856 (x2 - 0.05)4
> dVdx1_4:=proc(x1,x2) D[1](Vdev_4)(x1,x2) end proc:
> dVdx2_4:=proc(x1,x2) D[2](Vdev_4)(x1,x2) end proc:
> LfV_4:= proc(x1,x2)
(dVdx1_4(x1,x2))*(mu*(x2+x2s)*(x1+x1s)/(km+(x2+x2s)+k1*(x2+
x2s)^2))+(dVdx2_4(x1,x2))*(-
mu*(x2+x2s)*(x1+x1s)/(Y*(km+(x2+x2s)+k1*(x2+x2s)^2))) end
proc:
> LgV_4:= proc(x1,x2) (dVdx1_4(x1,x2))*(-x1-
x1s)+(dVdx2_4(x1,x2))*(x2f-x2-x2s) end proc:
>
>
>
> with(plots):
Warning, the name changecoords has been redefined

> display({contourplot(Vdev_quad(x1,x2),x1=-20..10,x2=-
20..20,contours=[1000,5000],coloring=[blue,white]),contourp

```

```
plot(Vdev_4(x1,x2),x1=-20..10,x2=-  
20..20,contours=[1000,5000],coloring=[red,white]));
```

